THE
PHYSICAL REVIEW
A Journal of Experimental and Theoretical Physics Established by E. L. Nichols in 1893
VOL. 55, NO. 9 MAY 1, 1939 SECOND SERIES

The Stopping Power of Mercury and of Nitrogen for Cosmic-Ray Electrons

JAMES H. BARTLETT, JR.
Department of Physics, University of Illinois, Urbana, Illinois
(Received April 4, 1939)

Form factors have been found for nitrogen (with the analytic wave functions of Brown, Bartlett and Dunn) and for mercury (with a Hartree field). For nitrogen, the form factors so found differ appreciably from those computed with a Thomas-Fermi field. For mercury, there is not much difference.

The formula for the cross section for impact radiation due to high energy electrons has been revised. There is still a quadratic dependence of $k\varphi_k/E_0\overline{p}$ on the energy, but the coefficients have been changed, so that this quantity is increased by about ten percent for small values of k/E_0.

WHEN cosmic rays diffuse through and are absorbed in various substances, the principal processes involved are impact radiation and pair production. The cross sections for these processes depend upon the magnitude of the nuclear charge, and upon the amount of screening by the atomic electrons. They have been calculated by Bethe for a Thomas-Fermi atom,[1] and the results for lead are displayed by Bethe and Heitler[2] and by Heitler.[3]

In the atmosphere one wishes to know the number of electrons at sea level as compared with the number of primaries entering at the top. This result, according to present theory,[4, 5] is somewhat sensitive to the character of the elementary processes. Since fairly accurate wave functions are known for nitrogen[6] and for mercury,[7] it was thought interesting to see what modifications in the above results would be occasioned by the introduction of these functions.

[1] H. A. Bethe, Proc. Camb. Phil. Soc. **30**, 524 (1934).
[2] H. A. Bethe and W. Heitler, Proc. Roy. Soc. **A146**, 83 (1934), Figs. 2 and 5.
[3] W. Heitler, *The Quantum Theory of Radiation* (Oxford, 1936), pp. 170 and 199.
[4] J. F. Carlson and J. R. Oppenheimer, Phys. Rev. **51**, 220 (1937).
[5] Verbal communication from Professor Oppenheimer.
[6] Brown, Bartlett and Dunn, Phys. Rev. **44**, 236 (1933).

THEORY[1]

Notation

E_0 = initial energy
E = final energy
$(\mathbf{p}_0/c)$ = initial momentum
$(\mathbf{p}/c)$ = final momentum
$k = h\nu = E_0 - E$
$(\mathbf{k}/c)$ = momentum of light quantum emitted
$\mathbf{q} = \mathbf{p}_0 - \mathbf{p} - \mathbf{k} = c \times$ momentum transferred to atom

$$\theta = \angle(p, k), \qquad \theta_0 = \angle(p_0, k),$$

$$\varphi = \angle(\overline{pk}, \overline{p_0 k}), \quad \mu = m_0 c^2, \quad q' = (q/hc),$$

$$\delta = q_{\min} = E - p - (E_0 - p_0)$$

$$\cong (\mu^2 k/2E_0E) \text{ if } E \gg \mu, \ E_0 \gg \mu, \quad (1)$$

[7] D. R. Hartree, Phys. Rev. **46**, 738 (1934).

$$F(q')=(1/Z)\int\rho(r)\exp[i(q\cdot r)/\hbar c]d\tau$$

$$=(1/Z)[\overline{(\sin q'r)/q'r}],$$

$$p_\perp=p\sin\theta,\quad \bar{\rho}=(Z^2r_0^2/137),\quad r_0=e^2/m_0c^2.$$

(In atomic units, $\hbar=1$ and $c=137$, so that $137\,q'=q$.)

Cross section

The differential cross section for emission of a light quantum k by an electron of initial energy E_0, momentum $\mathbf{p}_0/c$, is

$$d\Phi=\{Z^2e^4[1-F(q)]^2pdk/274\pi q^4kp_0\}$$
$$\times\sin\theta_0d\theta_0\sin\theta d\theta d\varphi$$
$$\times\left\{\left(\frac{p_\perp}{E-p\cos\theta}\right)^2(4E_0^2-q^2)\right.$$
$$+\left(\frac{p_{0\perp}}{E_0-p_0\cos\theta_0}\right)^2(4E^2-q^2)$$
$$-\frac{2p_{0\perp}p_\perp\cos\varphi}{(E-p\cos\theta)(E_0-p_0\cos\theta_0)}(4E_0E-q^2)$$
$$\left.+\frac{2k^2(\mathbf{p}_\perp-\mathbf{p}_{0\perp})^2}{(E-p\cos\theta)(E_0-p_0\cos\theta_0)}\right\}. \quad (2)$$

Bethe substitutes as follows:

$$x=(2p_0\sin\tfrac{1}{2}\theta_0)^2+(2p\sin\tfrac{1}{2}\theta)^2,$$
$$y=(2p_0\sin\tfrac{1}{2}\theta_0)^2-(2p\sin\tfrac{1}{2}\theta)^2,$$
$$z=q^2-\delta^2,$$
$$w^2=2xz-z^2-(k^2/8p_0^2p^2)x^2(4\mu^2+x).$$

If $\mu\ll E_0$, E and k, then the result is obtained that

$$\Phi(\nu)d\nu=\frac{Z^2e^4}{137\times2\pi}\frac{dk}{k}\frac{p}{p_0}\frac{16}{E_0E}$$
$$\times\int_\delta^\infty\frac{d(q^2)}{q^4}[1-F(q)]^2\int_{\frac{1}{2}(q^2-\delta^2)}^{2\mu^2(q-\delta)/\delta}dx$$
$$\times\int_0^w\frac{dy}{(w^2-y^2)^{\frac{1}{2}}}\left\{\frac{E_0^2+E^2}{s^2-y^2}(q^2-\delta^2)\right.$$
$$\left.-\frac{k^2(E_0^2+E^2)}{16E_0^2E^2}\frac{s^2-4\mu^2}{s^2}-\frac{8E_0E\mu^2y^2}{(s^2-y^2)^2}\right\}, \quad (3)$$

where $s=2\mu^2+x$. We may write the integral with respect to x and y as the sum of three parts, and so must find

$$y_1=\int dx\int_0^w\frac{dy}{(s^2-y^2)(w^2-y^2)^{\frac{1}{2}}}=\frac{\pi}{2}\int dx\frac{1}{s(s^2-w^2)^{\frac{1}{2}}},$$

$$y_2=\int\frac{s^2-4\mu^2}{s^2}ds\int_0^w\frac{dy}{(w^2-y^2)^{\frac{1}{2}}},$$

$$y_3=\int dx\int_0^w\frac{y^2dy}{(s^2-y^2)^2(w^2-y^2)^{\frac{1}{2}}}.$$

Let $\xi=s/2\mu^2$ and $\zeta=z/4\mu^2$. Then

$$y_1\leqq\frac{\pi}{4\mu^2}\int_{1+\zeta}^{q/\delta}\frac{d\xi}{\xi\{\xi^2-4(\xi-1)\zeta+4\zeta^2\}^{\frac{1}{2}}}$$
$$=\frac{\pi}{4\mu^2}\int_{1+\zeta}^{q/\delta}\frac{d\xi}{\xi(X)^{\frac{1}{2}}}=-\frac{\pi}{4\mu^2}\frac{1}{(4\zeta^2+4\zeta)^{\frac{1}{2}}}$$
$$\times\log\left\{\frac{X^{\frac{1}{2}}+(4\zeta^2+4\zeta)^{\frac{1}{2}}}{x}-\frac{4\zeta}{(4\zeta^2+4\zeta)^{\frac{1}{2}}}\right\}\Bigg|_{1+\zeta}^{q/\delta}.$$

Now k, E_0 and E are all supposed (for these

TABLE I. *F(q') for Thomas-Fermi atom.*

β	ξ	$(q')_N$	$(q')_{Hg}$	F	β	ξ	$(q')_N$	$(q')_{Hg}$	F
0				1.00	1.1	0.154	3.699	8.331	0.284
0.1	0.014	0.3363	0.7574	0.922	1.2	0.168	4.035	9.089	0.264
0.2	0.028	0.6726	1.515	0.796	1.3	0.182	4.372	9.846	0.240
0.3	0.042	1.009	2.272	0.684	1.4	0.196	4.708	10.60	0.224
0.4	0.056	1.345	3.030	0.589	1.5	0.210	5.044	11.36	0.205
0.5	0.070	1.681	3.787	0.522	1.6	0.224	5.380	12.12	0.189
0.6	0.084	2.018	4.544	0.469	1.7	0.238	5.72	12.88	0.175
0.7	0.098	2.354	5.302	0.422	1.8	0.252	6.05	13.63	0.167
0.8	0.112	2.690	6.059	0.378	1.9	0.266	6.39	14.39	0.156
0.9	0.126	3.027	6.817	0.342	2.0	0.280	6.73	15.15	0.147
1.0	0.140	3.363	7.574	0.309	2.90	0.407	9.77	22	0.095
					3.70	0.518	12.43	28	0.073
					6.60	0.924	22.20	50	0.033
					13.20	1.85	44.40	100	0.012

calculations) to be of the same order of magnitude, and so δ is generally to be neglected compared with μ. The terms in $E_0^2+E^2$ can then be shown to have the multiplier

$$(\pi/4\mu^2)(q-\delta)^2 \quad (q^2\ll\mu^2). \quad \text{[Bethe (42)]}$$

Let us now evaluate y_3

$$y_3=\frac{\pi}{8\mu^2}\int_{1+\zeta}^{q/\delta}\left\{\frac{\xi d\xi}{[(\xi-2\zeta)^2+4\zeta]^{\frac{1}{2}}}-\frac{d\xi}{\xi[(\xi-2\zeta)^2+4\zeta]^{\frac{1}{2}}}\right\}.$$

For q comparable with δ, ζ is small with respect to 1, and therefore with respect to ξ over the range of integration.

$$y_3=\frac{\pi}{8\mu^2}\int_{1+\zeta}^{q/\delta}\frac{-(4\zeta^2+4\zeta)+4\xi\zeta}{\xi[(\xi-2\zeta)^2+4\zeta]^{\frac{1}{2}}}d\xi$$

$$\leqq\frac{\pi}{8\mu^2}\cdot 4\zeta\int_1^{q/\delta}\left(-\frac{1}{\xi^4}+\frac{1}{\xi^3}\right)d\xi$$

$$=\frac{\pi}{8\mu^2}\frac{q^2-\delta^2}{\mu^2}\frac{1}{6\xi^3}(2-3\xi)\Big|_1^{q/\delta}$$

$$=\frac{\pi}{8\mu^2}\frac{q^2-\delta^2}{6\mu^2}\left(2\frac{\delta^3}{q^3}-3\frac{\delta^2}{q^2}+1\right).$$

This differs from Bethe's formula (45), in that we do not obtain any logarithmic terms.

We shall interest ourselves in the region where $F(q)$ is appreciable, and shall find what the contributions from this region are, with and without screening. The total unscreened cross section is known, and one has only to subtract off the difference of the above contributions, to find the total screened cross section.

TABLE II. *$F(q')$ for mercury, Hartree field. (For small values of q', $1-F(q')=0.147q'^2$).*

q'	$F(q')$	q'	$F(q')$	q'	$F(q')$
0.0	1.00	0.9	0.904	7.0	0.325
0.1	0.997	1.0	0.889	8.0	0.284
0.2	0.994	1.5	0.796	9.0	0.254
0.3	0.986	2.0	0.729	10.0	0.223
0.4	0.976	2.5	0.667	16.0	0.141
0.5	0.964	3.0	0.601	22.0	0.091
0.6	0.950	4.0	0.517	28.0	0.070
0.7	0.936	5.0	0.441	50	0.033
0.8	0.921	6.0	0.383	100	0.012

TABLE III. *$F(q')$ for nitrogen (analytic wave functions).*

q'	$F(q')$	q'	$F(q')$
0	1	4	0.239
0.25	0.976	5	0.214
0.5	0.915	7	0.175
1	0.735	10	0.121
1.5	0.568	12.5	0.085
2	0.445	15	0.058
3	0.303	20	0.028

Form-factors

Bragg and West[8] have tabulated $ZF(q')$, for $Z=55$, against $\beta=(1/\lambda)\sin\frac{1}{2}\theta\times10^{-8}$, *where* λ *is measured in cm.* If $\lambda=\lambda'\times0.532\times10^{-8}$, $(1/\lambda')\sin\frac{1}{2}\theta=0.532\beta$. Now $q_{Cs}'=(4\pi/\lambda')\sin\frac{1}{2}\theta=4\pi\times0.532\beta$. The corresponding q' for any other element is found by multiplying this by $(Z/55)^{\frac{1}{2}}$. For mercury, $q'=7.574\beta$, and for nitrogen, $q'=3.363\beta$. Bethe[9] has defined a quantity $\xi=(1/\lambda')(\sin\frac{1}{2}\theta)Z^{-\frac{1}{2}}=0.532\beta(55)^{-\frac{1}{2}}=0.14\beta$. At $\xi=0.098$, *Bragg and West give* $F(q')=0.422$, *whereas according to Bethe it is* $\leqq0.61$. *We* have calculated values of $F(q')$ with Hartree functions, and *find approximate agreement with Bragg and West.* Also, we have used the Thomas-Fermi field for $q'_{H_2}=28$, and the $F(q')$ for this is 0.073, as against 0.070 for the Hartree field. We have also found $F(q')$ for nitrogen with analytic wave functions. These functions were fitted to the numerical values of Brown, Bartlett and Dunn. The results are

$$f_1=34.2re^{-6.64r},$$

$$f_2=7.81re^{-3.44r}-r^2(8.64e^{-2.531r}+0.805e^{-1.239r}),$$

$$f_3=r^2(6.89e^{-2.802r}+0.935e^{-1.081r}).$$

These are normalized so that

$$\int_0^\infty f^2dr=1.$$

In Table I are listed the values of $F(q')$ for the Thomas-Fermi atom. These are partly from the table of Bragg and West, and partly from our computations. Table II gives the corresponding form factors found with Hartree functions for mercury, and Table III the values of $F(q')$ calculated by us with analytic wave functions.

[8] W. L. Bragg and J. West, Zeits f. Krist. **69**, 137 (1929).
[9] H. A. Bethe, Ann. d. Physik **5**, 385 (1930).

Cross section for mercury

For mercury, $F(q'=28)=0.07$, so that we have set $F(q')=0$ for $q'>28$ and estimated the error involved. For $q'\leq 28$, ζ may be neglected.

Let $\chi=(k\varphi_k/E_0\bar{\varphi})$, where φ_k is the cross section for emission of a quantum k in the range $dk/(E_0-\mu)$; $\chi(28)$ = contribution to this from $q'<28$; $\chi_F=(k\varphi_k/E_0\bar{\varphi})$ with screening; and $\chi_F(28)$ = contribution from $q'<28$. Also set $s=(q'/\delta')$.

$$\chi_F=\chi+\chi_F(28)-\chi(28)-\text{error}$$

$$\chi_F(28)=(32\mu^2 p/2\pi p_0 E_0 E)\int_\delta^{28\hbar c}(dq/q^3)[1-F(q')]^2$$
$$\times\left\{(E_0^2+E^2)(\pi/4\mu^2)(q-\delta)^2\right.$$
$$\left.-(\pi/6\mu^2)E_0E(q^2-\delta^2)\left(2\frac{\delta^3}{q^3}-3\frac{\delta^2}{q^2}+1\right)\right\}$$
$$\leqq(4/E_0^2)\int_1^{28/\delta'}\frac{ds}{s}[1-F(q')]^2$$
$$\times\{(E_0^2+E^2)(1-s^{-1})^2$$
$$-\tfrac{2}{3}E_0E(1-s^{-2})(2s^{-3}-3s^{-2}+1)\}$$
$$=4\left\{\left[1+\left(\frac{E}{E_0}\right)^2\right]I_F(28)-\frac{2}{3}\frac{E}{E_0}J_F(28)\right\},\quad(5)$$

where

$$I_F(28)=\int_1^{28/\delta'}(ds/s)[1-F(q')]^2(1-s^{-1})^2$$

and

$$J_F(28)=\int_1^{28/\delta'}(ds/s)[1-F(q')]^2$$
$$\times(1-s^{-2})(2s^{-3}-3s^{-2}+1).$$

TABLE IV. *Values of $I_F(28)$ and $J_F(28)$.*

	k/E_0	δ'	$I_F(28)$	$J_F(28)$
$E_0=1000\mu$	0.1	0.00761	1.29	1.29
	0.5	0.0685	1.27	1.29
	0.7	0.1598	1.23	1.27
	0.8	0.274	1.17	1.26
	0.9	0.6165	1.08	1.23
$E_0=100\mu$	0.1	0.0761	1.24	1.28
	0.5	0.685	1.09	1.22
	0.7	1.598	0.87	1.08
	0.8	2.740	0.66	0.88
	0.9	6.165	0.32	0.52

The unshielded integrals $I(28)$ and $J(28)$ are readily calculated.

$$I(28)=\left(\ln s+\frac{2}{s}-\frac{1}{2s^2}\right)\Bigg|_1^{28/\delta'}\leqq\ln(28/\delta')-\tfrac{3}{2}$$
$$\text{(if } \delta'\ll 28),\quad(6)$$
$$J(28)=\left(\ln s+\frac{2}{s}-\frac{2}{3s^3}-\frac{3}{4s^4}+\frac{2}{5s^5}\right)\Bigg|_1^{28/\delta'}$$
$$\leqq\ln(28/\delta')-\frac{59}{60}.$$

To obtain $I_F(28)$ and $J_F(28)$, the integrands were plotted and the areas planimetered. As $\delta\to 0$, these integrals approach the common value

$$\int_1^{28}(dq'/q')[1-F(q')]^2=1.29.$$

From Eq. (2),

$$\delta'=(\delta/\hbar c)\leqq(k/E_0)(\mu/E)(\mu/2\hbar c)$$
$$=(k/E_0)(\mu/E)\times 68.5\ \text{(atomic units)}.$$

Thus, if $E_0=1000\mu$ and $k=0.1E$,

$$\delta'=(68.5/9000)=0.00761.$$

In Table IV, we give the values of $I_F(28)$ and $J_F(28)$. For high energies,

$$\chi=2[2\ln(2E_0E/\mu k)-1]$$
$$\times[-(2E/3E_0)+1+(E/E_0)^2]$$
$$=2[2\ln(\mu/\delta)-1]\quad(7)$$
$$\times[-(2E/3E_0)+1+(E/E_0)^2].$$

If (4), (5), (6) and (7), are combined,

$$\chi_F=[1+(E/E_0)^2][4\{I_F(28)-I(28)-\epsilon_{28}\}$$
$$+4\ln(\mu/\delta)-2]-(2E/3E_0)[4\{J_F(28)$$
$$-J(28)-\epsilon_{28}\}+4\ln(\mu/\delta)-2]$$
$$=[1+(E/E_0)^2-(2E/3E_0)][4I_F(28)$$
$$+4\ln(137/28)-4\epsilon_{28}-2]\quad(8)$$
$$+6[1+(E/E_0)^2]$$
$$-(2E/3E_0)(59/15)$$
$$=4\{[1+(E/E_0)^2-(2E/3E_0)]3.81$$
$$+(31/90)(E/E_0)\}.$$

(The value of ϵ_{28} has been taken to be 0.07, which is that found for nitrogen (see below) with analytic functions.)

The values of the χ's are listed in Table V.

TABLE V. *Values of the χ functions.*

	k/E_0=0.1	0.5	0.7	0.8	0.9
E_0= 1000μ	$\chi_F(28)$= 6.22	4.63	4.33	4.22	4.08
	$\chi(28)$ =31.24	15.86	12.64	11.06	8.60
	χ=45.0	26.64	22.26	20.74	18.50
	χ_F=19.6	14.6	13.7	13.6	13.7
E_0= 100μ	$\chi_F(28)$= 5.92	3.82	2.93	2.29	1.24
	$\chi(28)$=20.1	7.60	4.92	3.50	1.65
	χ=33.86	17.59	14.07	12.36	9.82
	χ_F=19.3	13.6	11.8	10.9	9.1

Cross section for nitrogen

We shall limit ourselves to finding the cross section for high energies. Observing that $F(q')$ is small for $q_N'>12.43$, we may write (neglecting F^2)

$$\chi_F=\chi+\chi_F(\infty)-\chi(\infty)$$
$$=[1+(E/E_0)^2-(2E/3E_0)]$$
$$\times[4I_F(12.43)+4\ln(137/12.43)-2$$
$$-4\int_{12.43}^{\infty}2F(dq'/q')]$$
$$+6[1+(E/E_0)^2]-(118E/45E_0).$$

By numerical integration, $I_F(12.43)=1.24$, and by analytical integration,

$$\int_{12.43}^{\infty}2F(dq'/q')=0.070.$$

Substituting,

$$\chi_F=4[1+(E/E_0)^2-(2E/3E_0)]$$
$$\times[I_F+4\ln(137/12.43)+1-0.07]$$
$$-(2E/3E_0)(-31/15)$$
$$=4\{[1+(E/E_0)^2-(2E/3E_0)]4.57$$
$$+(31/90)(E/E_0)\}.$$

This may be compared with formula (54),[1] by setting $I_F(12.43)+0.93+\ln(137/12.43)=\ln aZ^{-\frac{1}{3}}$. With $Z=7$, we obtain $a=185$. If we use the Thomas-Fermi atom, where $I_F(12.43)=1.29$, we obtain $a=194$, as against Bethe's value of 183 for the same field.

CONCLUSION

The stopping power for cosmic-ray electrons is not very sensitive to the approximate wave functions employed. The largest effect is found for nitrogen, where we find $a=185$ with analytic wave functions, and $a=194$ with a Thomas-Fermi field.

Our formula (8) for the quantity χ is also different from the corresponding one due to Bethe in that we have a coefficient (31/90) in place of his (1/9). This makes a ten percent increase for small values of (k/E_0).

Finally, we wish to acknowledge the aid given us in the form of a grant from the Graduate School of the University of Illinois. We also appreciate the assistance given us with the calculations by Mr. R. P. Jones and Mr. R. N. Griesheimer.

Nuclear Isomerism in Element 43

G. T. SEABORG, *Chemistry Department, University of California, Berkeley, California*

AND

E. SEGRÈ, *Radiation Laboratory, Physics Department, University of California, Berkeley, California*

A case of nuclear isomerism in element 43 has been thoroughly studied and is described. An activity of 6.6 hours half-life, which grows from a 67-hour molybdenum activity and has been chemically identified as element 43, decays with the emission of a line spectrum of electrons and no observable nuclear beta-particles. Absorption measurements in aluminum and measurements with a magnetic spectrograph give an energy for the electrons of 116 kev. This line spectrum must be due to the conversion electrons of a highly converted gamma-ray of energy 136 kev and arises as the result of a transition from an excited state of this isotope of element 43. The ground state is either stable or very long-lived. X-rays are also observed, and critical absorption measurements, as well as observations with a bent crystal spectrograph, show that they are to be ascribed to the $K\alpha$ line of element 43, as is to be expected from this interpretation. The 6.6-hour activity also emits gamma-rays of about 180 kev energy; the measurements show that these are to be interpreted as following the transition which gives rise to the conversion electrons. A description of the chemical identification of the 6.6-hour activity is given. Other activities of element 43 are mentioned.

1. INTRODUCTION

IN an investigation of the artificial radioactivities of element 43 we have found some features interesting with respect to the general problem of nuclear isomerism. In a letter[1] to the *Physical Review* we have summarized our main results. In this paper we shall give a detailed account of the investigation.

2. APPARATUS

The samples were activated with deuterons or neutrons from the Berkeley cyclotron. For several of the deuteron bombardments inner targets of the type described by Wilson and Kamen[2] were used. The activities were usually measured with ionization chambers connected to a vacuum tube electrometer system of the type described by Hafstad.[3] Two chambers were used, of the type described by Segrè[4] and Amaldi and Fermi.[5] One was made entirely of aluminum and the inner cylinder had a diameter of 10 cm and a height of 10 cm. This chamber was filled with air at atmospheric pressure and the window through which the electrons were admitted had a diameter of six cm and a thickness of 0.16 mg/cm². The outer cylinder of the other chamber was made of brass, lined on the inside with cardboard, and the inner cylinder was a copper net of nine cm diameter and height. It was filled with methyl bromide slightly above atmospheric pressure. The window was aluminum of 20 mg/cm² thickness.

The chemical identifications and separations are described in detail at the end of the paper in Section 8.

3. ISOMERISM IN ELEMENT 43

Molybdenum was irradiated with deuterons and neutrons. A strong activity of 67 ± 2 hours half-life was observed and a decay curve of this activity is shown in Fig. 1. This curve starts some days after the end of the bombardment and chemical separation. The most probable identification of this activity is with Mo^{99} or Mo^{101}. The particles emitted are negative electrons (as determined by magnetic deflection) so that the decay product must be an isotope of element 43. Since, according to current ideas about nuclear stability,[6] this element is unlikely to have any stable isotopes, it is natural to look for a daughter activity. Therefore we looked for the growth of a radioactive isotope of element 43 by successive chemical separations from the active molybdenum. In all of these successive separations we found an electron-emitting activity of 6.6 ± 0.4 hours half-life and this was identified

[1] E. Segrè and G. T. Seaborg, Phys. Rev. **54**, 772 (1938).
[2] R. R. Wilson and M. D. Kamen, Phys. Rev. **54**, 1031 (1938).
[3] L. R. Hafstad, Phys. Rev. **44**, 201 (1933).
[4] E. Segrè, Nuovo Cimento **12**, 232 (1935).
[5] E. Amaldi and E. Fermi, Phys. Rev. **50**, 899 (1936).
[6] See e.g. H. Jensen, Naturwiss. **26**, 381 (1938).

chemically as element 43. A sample decay curve of such an extraction is shown in Fig. 2 and an absorption curve in aluminum of the electrons is shown in Fig. 3, curve (a). This curve was taken on the air chamber with a distance of 1.5 cm between the source and the window and with the aluminum absorbers close to the window. The curve is strikingly different from an ordinary absorption curve of beta-particles having the same half-value thickness, as is shown by comparison with curve (b) of the same figure in which the absorption of the beta-particles of the radioactive isotope of cobalt of 6–8 years period[7] is shown. Moreover, from the end-point of this absorption curve, an energy for the electrons of about 120 kev is obtained and this energy, according to the Sargent relation, could not correspond to a beta-radioactivity of six hours half-life. The form of the curve compared with the results of Varder[8] and Eddy,[9] even taking into account the different geometry, points to monokinetic electrons. That this is the case was confirmed by Mr. D. C. Kalbfell[10] who put a chemically separated sample of the 6.6-hour activity in his magnetic spectrograph and found

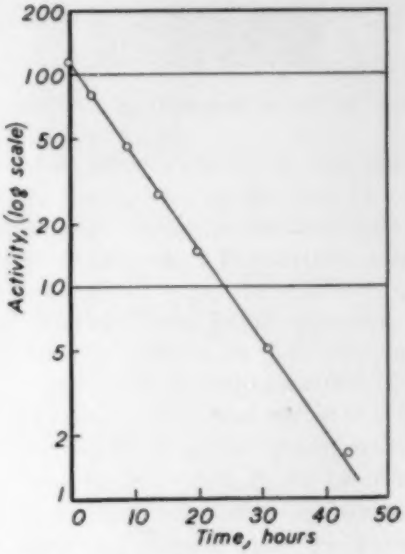

FIG. 2. Decay of radioactive 43. Half-life 6.6±0.4 hours.

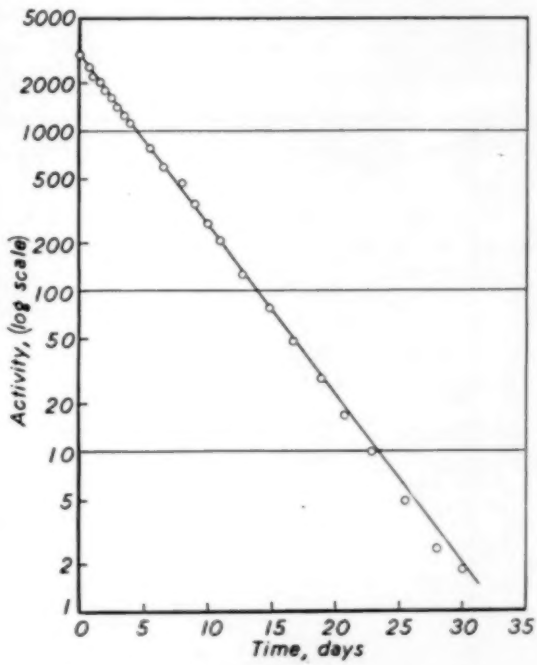

FIG. 1. Decay of radioactive molybdenum. Half-life 67±2 hours.

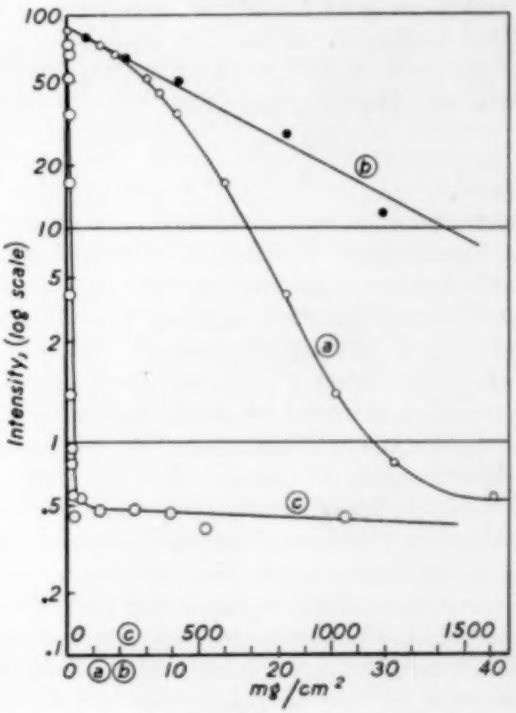

FIG. 3. (a) and (c) Absorption in aluminum of the electrons of 43. (b) Absorption in aluminum of the β-rays of cobalt (6–8-year period).

[7] J. J. Livingood and G. T. Seaborg, Phys. Rev. **53**, 847 (1938). Continued measurements by these authors and G. Barresi have shown that this period is 6–8 years.

[8] R. W. Varder, Phil. Mag. **29**, 726 (1915).

[9] C. E. Eddy, Proc. Camb. Phil. Soc. **25**, 50 (1929).

[10] D. C. Kalbfell, Phys. Rev. **54**, 543 (1938).

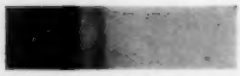

FIG. 4. Electron lines of element 43 (K and L conversion).

an electron line of 116 kev energy and a weaker one of 133 kev energy, as shown in Fig. 4. These electrons are obviously the K and L conversion electrons of a gamma-ray of 136 kev energy.

This unusually strong line of electrons immediately suggests that we are dealing with either a case of K-electron capture, followed by a gamma-ray which is highly internally converted, or with a transition between isomeric levels of an isotope of element 43 which, according to current ideas about isomerism, should also manifest itself by a gamma-ray of high internal conversion. The process contemplated in the first hypothesis would be of the following type:

$$_{42}\mathrm{Mo}^{**} \rightarrow 43 + {}_{-1}e$$
$$43 + {}_{-1}e \rightarrow {}_{42}\mathrm{Mo}^{*}$$
$$_{42}\mathrm{Mo}^{*} \rightarrow {}_{42}\mathrm{Mo} + h\nu$$

in which the nuclei with the asterisks are in excited states. It is seen at once that this explanation is highly artificial. The second alternative would be described thus:

$$_{42}\mathrm{Mo} \rightarrow 43^{*} + {}_{-1}e$$
$$43^{*} \rightarrow 43 + h\nu.$$

However, to decide experimentally between the two hypotheses it is sufficient to determine the atomic number of the nucleus emitting the converted gamma-ray. One could do this either by measuring the difference in energy of the K and L conversion electrons or by identifying the characteristic x-radiation which is generated in the rearrangement of the atom after the ejection of the conversion electrons.

We have adopted the latter method, identifying the x-rays by their characteristic absorption. The methyl bromide chamber was used, which enhances the ionization due to the x-rays to a great extent. The aluminum window was of such a thickness (20 mg/cm²) as to stop all of the conversion electrons. Fig. 5(a) shows an absorption curve in aluminum. The radiation is obviously composed of at least two parts, a soft and a hard component. The hard component is a gamma-ray and when this is substracted the soft component has an absorption coefficient corresponding to the K x-radiation of an element in the neighborhood of molybdenum. The exact assignment of the element was obtained by comparison of the absorption of the x-rays in zirconium, columbium and molybdenum. Since sheets of these elements of the proper thickness were not available to us the absorbers were made by filtering fine suspensions of the oxides (ZrO_2, Cb_2O_5 and MoO_3) through identical filter papers. The layers were fairly homogeneous and for each substance had thicknesses of 5, 10, 20 and 30 mg/cm² of the element. The absorption by the oxygen in these substances and by the filter paper was negligible.

The absorption curves for the x-rays (corrected for the gamma-rays) are shown in Fig. 5(b, c, d). It is seen at once that the discontinuity in the absorption coefficient occurs between zirconium and columbium as one would expect for the K radiation of element 43, whereas for the K radiation of molybdenum the discontinuity would have occurred between zirconium and yttrium. This experiment also rules out the possibility that the x-rays are emitted by ruthenium (discontinuity between columbium

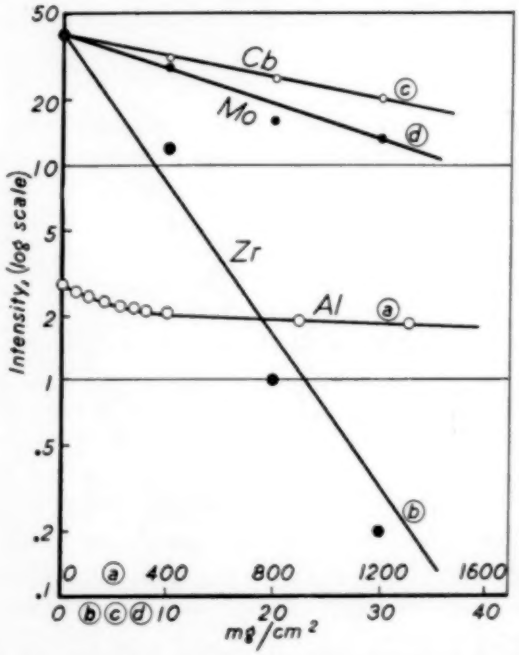

FIG. 5. Absorption curves of x- and γ-rays of element 43. (a) Absorption in aluminum of x- and γ-rays. (b) Absorption of x-rays in Zr. (c) Absorption of x-rays in Cb. (d) Absorption of x-rays in Mo.

and molybdenum) as would be the case if the radioactive element 43 were decaying by the usual type of beta-emission. It is remarkable that in spite of the bad geometry (diameter of source 3 cm; distance between source and absorber 2.5 cm; distance between source and chamber 5 cm) the absolute values of the absorption coefficients are not far from the theoretical ones. The measured values of the high and low mass absorption coefficients are 170 and 35 cm^2/g, which are to be compared, in the absence of any experimental values for element 43, with the absorption coefficients of 114 and 19 cm^2/g for the absorption coefficients of the K x-rays of molybdenum in yttrium and zirconium.

This result has been confirmed by a direct photograph of the x-ray line with a bent crystal spectrograph taken by Mr. P. Abelson.

4. Gamma-Rays and Intensity Relations

In order to get a further insight into the processes involved, an attempt was made to establish the ratio between the number of disintegration electrons of molybdenum and the conversion electrons of the daughter element 43 and to study the gamma-rays emitted by the 6.6-hour activity of element 43. Because of the well-known difficulties in work of this type this part of the investigation is still incomplete, especially with respect to the important point of establishing the conversion coefficient of the gamma-rays corresponding to the conversion electrons of element 43.

a. Intensity ratio between molybdenum beta-rays and electrons of element 43

An extremely thin layer of carefully purified radioactive molybdenum was placed above the thin window of the air ionization chamber and the decay curve is shown in Fig. 6. This curve shows the growth of the activity of element 43 from the molybdenum and one can find the ratio of the ionization produced by element 43 to the ionization produced by molybdenum when they are at transient equilibrium. This ratio, correcting for the window thickness, is 0.30. Approximately the same value is obtained when the two activities in equilibrium are separated chemically and measured. In order to pass from the ratio of the ionization of the two activities to the ratio of the number of particles from the activities one must estimate from their ionizing powers the relative number of ions produced by the particles, taking into account the fact that the geometry was such that the range of the particles was long compared with their paths in the chamber. In order to measure the average energy of the electrons, which is necessary for estimating their ionizing power, an absorption curve of the molybdenum electrons was taken. The absorption curve of the electrons in aluminum (with the air chamber) is given in Fig. 7 together with the absorption curves of P^{32} and

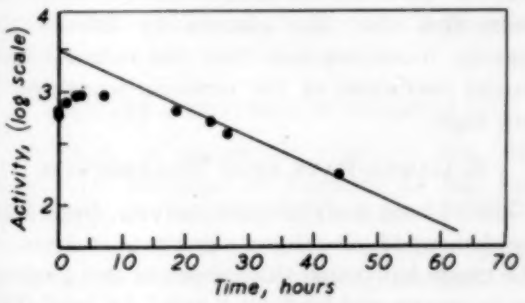

Fig. 6. Curve showing growth of radioactive element 43 in radioactive molybdenum.

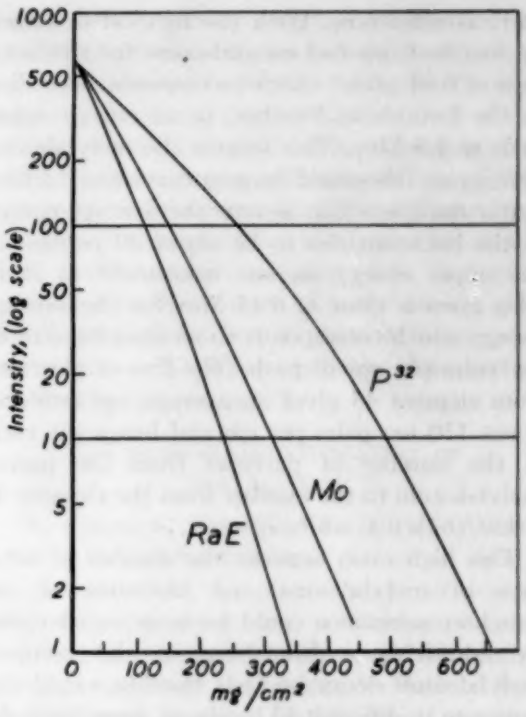

Fig. 7. Absorption curves of electrons of Mo in aluminum. RaE and P^{32} as references.

RaE as references. With the method described by Feather[11] we find an end-point for the beta-rays of 0.64 g/cm² which corresponds, according to the formula of Feather, to an energy upper limit of 1.5 Mev. This locates the molybdenum activity on the second Sargent curve and, lacking better data, one can assume the average energy of the beta-particles to be about 30 percent of the upper energy as was measured[12] in RaE. This gives a value of 0.45 Mev for the average energy which corresponds to an ionization of 62 ion pairs per cm of path. The line of electrons from element 43 gives an average ionization of about 150 ion pairs per cm and hence the ratio of the number of particles from the parent molybdenum to the number from the element 43 is $150/(62\times0.3)=8$.*

This high ratio between the number of beta-rays of molybdenum and electrons of the daughter substance could be interpreted either by admitting a branching in the primary molybdenum decay, so that the Mo would disintegrate to different 43 levels, or, more unlikely, that the molybdenum decays to a single excited state of the element 43 which reverts to the ground state by the emission of a gamma-ray which has a low internal conversion coefficient. Evidence against the latter of these two alternatives was supplied by a study of the intensity ratio between the gamma-rays and the electrons of the 6.6-hour activity. In fact, in this case one would expect approximately one gamma-quantum for every molybdenum disintegration electron.

b. Intensity ratio between gamma-rays and electrons and energy of gamma-rays in element 43

In order to decide the alternative proposed at the end of Part (a) of this section and, more important, to obtain some more experimental data relevant to the general theory of isomerism, an endeavor was made to measure the energy of the gamma-rays and the number of gamma-quanta per electron in this transition. The mass absorption coefficients of the gamma-rays in lead and copper, with the methyl bromide chamber, were measured. The value of μ/ρ for lead is 2.0 g/cm² and that for copper is 0.18 g/cm² which corresponds in each case to an energy of about 180 kev. The same value is obtained by measuring the absorption coefficient in Cellophane of the electrons ejected from lead and from copper by the gamma-rays and using the data of Vette.[13] This value can be assumed only as a rough indication of the energy of the gamma-rays because of the fundamental uncertainty about the homogeneity of the gamma-rays and because intensity considerations made it necessary to use bad geometry. However, with the same geometry we obtained the correct value for the absorption coefficient for the annihilation radiation of positrons.

The intensity ratio between the electrons and the gamma-rays was determined by using the ionization ratio between the electrons and gamma-rays in the air chamber, where the value 170 was found (as can be seen from Fig. 3(c)). For comparison, the ionization ratio between the positrons and the annihilation radiation of Cu^{61} (3.4 hours half-life) was determined under the same conditions and the value 55 was found. For the geometry adopted there are two annihilation gamma-rays per positron which enter the chamber and a special investigation (see appendix) has shown that there are no other gamma-rays of appreciable intensity. Assuming that the gamma-rays from element 43 ionize about the same as the annihilation gamma-rays and taking into account the fact that the electrons from element 43 ionize about 2.5 times as much as the beta-particles of Cu^{61} we find that the gamma-rays and electrons from element 43 are, very roughly, equal in number.

These observations are consistent with the assumption that the gamma-ray follows the isomeric transition and that the internal conversion coefficient of the isomeric transition is very high.

5. Gamma-Rays from Molybdenum

The 67-hour molybdenum activity, freed from the element 43, also shows a gamma-ray activity. The crude half-value thicknesses of this gamma-ray in copper and lead are 5 and 2.5 g/cm². This

[11] N. Feather, Proc. Camb. Phil. Soc. **34**, 599 (1938).
[12] C. D. Ellis and W. A. Wooster, Proc. Roy. Soc. **A117**, 109 (1927).
* Because of the uncertainty of the method, we think that this estimate may be wrong by a factor 2.
[13] E. Vette, Ann. d. Physik **5**, 929 (1930).

corresponds to an energy definitely larger than the energy of the gamma-ray of element 43 and can be set at about 400 kev. The ratio of the ionization of the beta-particles to that of the gamma-rays in the air chamber is about 500. This indicates that the intensity of the gamma-ray is relatively weak (0.2 quanta per disintegration).

6. The Lower Isomeric State of Element 43

It has been pointed out that no stable isotopes of element 43 are expected so that it was of interest to determine whether, after the isomeric transition, there is a further beta-decay to ruthenium. If such a decay of life shorter or comparable to six hours should be present one would have had as many beta-rays as conversion electrons and in case these beta-rays had a normal spectral distribution we would have observed them in the absorption curve in Fig. 3(a). Therefore it seems that the ground state does not decay to ruthenium with a short life. On the other hand, we have prepared samples of element 43 strong enough to follow the decay over a factor of 1000 on the air chamber and no tailing has been observed. This gives a lower limit for the period of the daughter substance of about 6000 hours. Element 43 was also separated and found to be inactive from an old sample of molybdenum which initially contained only the 67-hour activity. The fact that this sample had decayed exponentially by a factor of 60,000 sets a still longer lower limit of 40 years for the period of the element 43 daughter substance (after taking into account the branching ratio of the 67-hour activity). This rules out the possibility that the 6.6-hour activity is isomeric with any of the known radioactive isotopes[14] of element 43. It is still open to question whether the lower state is stable or is radioactive with a very long life or with extremely soft electrons.

7. Other Activities of Element 43

Although no systematic study of the other short-lived activities of element 43 has been made, still in the initial separations of element 43, made in order to separate from molybdenum all of the products formed during the bombardment, we have observed some new activities. These are reasonably assigned to element 43, though no chemical separations from ruthenium were performed. Provisional values for the half-lives are two hours and two days.

The two-day activity emits strong x-rays, which we have shown by characteristic absorption to be molybdenum $K\alpha$. This indicates that this period belongs to an isotope which decays into molybdenum, probably by K-electron capture. The $K\alpha$ x-rays of molybdenum were also found to be present in old samples of radioactive element 43, which contained the activities reported by Cacciapuoti.[14]

8. Chemical Identification of the Activity

The chemical identification of the 67-hour activity as molybdenum was performed upon a neutron-activated sample of pure ammonium molybdate by separating columbium by hydrolysis of potassium columbate and by precipitating zirconium as the hydroxide. Both of these fractions were inactive. Molybdenum was then precipitated by the addition of 8-hydroxyquinoline, which does not precipitate element 43 and ruthenium. Rhenium in the form of perrhenic acid was added as carrier for element 43. The molybdenum contained the 67-hour activity. In order to have this activity radioactively pure in the case of the deuteron bombardment of molybdenum, where other transmutation products are formed, it is necessary to purify further this 8-hydroxyquinoline precipitate. This is done by dissolving the precipitate with concentrated nitric acid, evaporating to dryness, redissolving the residue with water (slightly alkaline with ammonium hydroxide if necessary) and reprecipitating. The fraction of the total activity of element 43 carried down by the 8-hydroxyquinoline molybdenum precipitate is about three percent, so that one reprecipitation reduces this impurity to 0.1 percent.

The 6.6-hour activity is separated from a purified molybdenum fraction, some hours after the purification, by dissolving the 8-hydroxyquinoline precipitate as described above. Rhenium is added as a carrier, the molybdenum is reprecipitated with 8-hydroxyquinoline and filtered off, the filtrate is made strongly acid with hydrochloric acid and the element 43 is precipi-

[14] B. N. Cacciapuoti, Phys. Rev. **55**, 110 (1939).

tated with the rhenium as a sulfide by passing in hydrogen sulfide. Since ruthenium, the element above element 43, would also be precipitated with rhenium in this procedure it was decided to make a further separation of element 43 and ruthenium as a check. The rhenium sulfide, containing element 43, was dissolved with a hydrogen peroxide solution. After the addition of ruthenium, as ammonium chlororuthenate, the rhenium and element 43 were precipitated with nitron (diphenyl-endo-anilo-hydro-triazole). The ruthenium was precipitated from the filtrate with hydrogen sulfide. More than 99 percent of the activity was found in the nitron precipitate.

A complete description of the known chemistry of element 43 and its separation from the neighboring elements is given by Perrier and Segrè.[15]

In conclusion we thank Professor E. O. Lawrence for his interest in this work and the Research Corporation for continued support.

Appendix on the Calibration of the Ionization Chamber

W. GENTNER AND E. SEGRÈ
Radiation Laboratory, Physics Department, University of California, Berkeley, California
(Received March 15, 1939)

We report here some details about the calibration of the ionization chamber which we think might also be of interest to other investigators.

We determined the absorption coefficient of a known radiation (annihilation radiation) and also the ratio between the ionization produced by beta-particles and γ-rays in a simple case, where equal numbers of β- and γ-rays were present, using our standard geometry in order to have a reference for other work.

As a source we used the positron emitter Cu^{61} of 3.5 hours half-life, obtained by the deuteron bombardment of nickel. The copper fraction was deposited by reduction on a thin circular Fe sheet (10 mg/cm^2 thickness) of 3.5 cm diameter.

The distance between source and window was 2.5 cm and the absorbers were about 0.6 cm above the window.

The first step was to ascertain that Cu^{61} does not emit nuclear γ-rays. This was done by absorbing completely the β-rays, whose absorption curve is practically identical with the absorption curve of Mo (Fig. 7, endpoint at 1.5 Mev), and then placing 1.5 cm of paraffin directly above the source. The residual activity, due to annihilation radiation, was thus multiplied by a factor 1.9. The paraffin absorbs the positrons emitted in the upper solid angle and transforms them into isotropic annihilation radiation. Since the positron absorption occurs in a small region, very close to the source, the whole process is equivalent to doubling the intensity of the annihilation radiation, because without paraffin the greatest part of the positrons emitted in the upper hemisphere are annihilated in air so far from the chamber as to be ineffective.

In an ideal case the ratio between the ionization produced by annihilation radiation with and without upper paraffin should hence be 2. Any nuclear γ-ray would lower this ratio, bringing it to 1.5 if its ionization were comparable to the annihilation radiation. In our case, as was stated above, we found a ratio of 1.9 which, taking into account the thickness of the source itself and the annihilation in the air, seems to be close enough to 2 to rule out a nuclear γ-ray of intensity comparable with the annihilation radiation.[15a]

Another argument for the absence of nuclear gamma-rays is that the half-value thickness for the radiation emitted, in lead, with or without paraffin on top of the source, is constant and equal to 4.0 g/cm^2 for thickness between 2 and 14 g/cm^2. This absolute value is close to the correct one (4.1 g/cm^2).[16]

The ratio between the ionization produced by the β-rays and the annihilation radiation, with paraffin above, is 55 and since there are two quanta per positron annihilated, one has 110 in the case of one quantum per electron.

The correct value for the absorption coefficient of the annihilation radiation was also obtained when absorption measurements were made with the methyl bromide chamber.

[15] C. Perrier and E. Segrè, J. Chem. Phys. **5**, 715 (1937); **6**, 155 (1939).
[15a] This method has been used by H. R. Crane and C. C. Lauritsen, Phys. Rev. **45**, 430 (1934).
[16] W. Gentner, Physik. Zeits. **38**, 836 (1937).

The Townsend Coefficients for Ionization by Collision in Pure and Contaminated Hydrogen as a Function of the Cathode Material

DONALD H. HALE
Department of Physics, University of California, Berkeley, California
(Received March 13, 1939)

The Townsend coefficients for ionization by collision were measured for pure mercury-free hydrogen and for hydrogen contaminated with sodium and NaH vapor. Cathodes of platinum and sodium and NaH-coated platinum were used. The values of α/p at values of X/p below 300 are found to be smaller for pure hydrogen than for hydrogen contaminated with mercury vapor. The values of α/p for hydrogen contaminated with sodium and NaH are as much as twice as great as those for pure hydrogen at the lower values of X/p. The curve of α/p plotted as a function of X/p, for this case, shows a sharp peak at an X/p of 350. This peak indicated the presence of some substance which is ionized by the excitation of hydrogen. The curves of β/α and γ for the platinum cathode plotted as functions of X/p show peaks at the lower values of X/p which are analogous to those shown by Bowls. The curves for the NaH cathode show a narrow but remarkably high peak at an X/p of 10. There are also several lower peaks but no general rise for the NaH cathode. These peaks indicate relatively large photoemission effects ($\Theta\eta g/\alpha$) at the cathodes at the lower values of X/p. In the case of the platinum cathode at the higher values of X/p the curves show a general rise caused by electron emission due to the bombardment of the cathode by positive ions. The values of β/α and γ for the sodium surfaces are much smaller than in the case of platinum for the higher values of X/p indicating that these surfaces are relatively poor emitters under positive ion bombardment. In the course of the work it was possible, in most cases, to measure a sparking potential at the conclusion of the experimental work at each value of X/p. These data for the sparking potentials give curves which agree fairly well with the experimental curves as derived by Ehrenkranz. From the values found for the γ-coefficient, the sparking potentials were calculated and these potentials gave sparking potential curves which are in rough agreement with the experimentally derived curves of Ehrenkranz.

INTRODUCTION

CONSIDERABLE work has been done in the past to determine the values of the Townsend α- and β-coefficients for ionization by collision in pure hydrogen. However, a study of the experimental procedures used in these researches shows that certainly mercury vapor was present as a contamination in the ionization chambers. Penning[1] has shown that a trace of mercury vapor will greatly alter the value of the α-coefficient in the inert gases. Bowls[2] has shown that a small amount of mercury vapor, present as a contamination in otherwise pure nitrogen, will change the value of α by as much as seventeen percent. It was found early in this work that traces of mercury would alter the value of α for otherwise pure hydrogen by as much as fifty percent at certain values of X/p.

Recent work has also shown that the second Townsend coefficient represents a cathode mechanism[3] and therefore in the presence of mercury vapor the value found for this coefficient would not be that for an uncontaminated surface.

It was the purpose of this investigation to determine the first and second ionization coefficients for hydrogen gas with the modern techniques to secure pure gas and to exclude mercury vapor from the ionization chamber. The second coefficient β has been determined for both platinum and NaH surfaces. Two NaH surfaces were used. The apparatus and experimental procedure used in this work were essentially that described by Bowls.[2] In all cases the illumination of the cathode was reduced to the lowest intensity which would give a measurable photoelectric current i_0 in order that space charge effects[4] might be reduced to a minimum. In most cases the photoelectric current was less than 5×10^{-15} ampere per cm^2 of illuminated surface on the cathode.

Tank hydrogen was used. It was purified by passing through a purifying train and two liquid-air traps. It was found early in the work that at the higher pressures of the gas in the ionization chamber mercury was at times admitted. This mercury contamination was evident as in these cases the value found for α/p lay upon the curve

[1] F. M. Penning, Phil. Mag. **11**, 979 (1931).
[2] W. E. Bowls, Phys. Rev. **53**, 293 (1938).
[3] L. B. Loeb, Rev. Mod. Phys. **8**, 267 (1936).
[4] Varney, White, Loeb and Posin, Phys. Rev. **48**, 818 (1935).

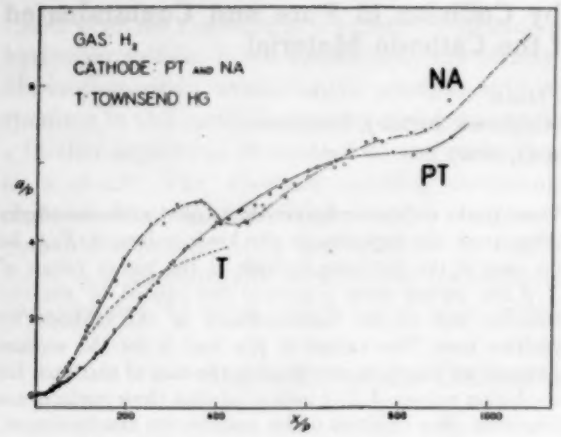

FIG. 1. Values of α/p as a function of X/p. Two sodium surfaces were used and are shown as circles and crosses.

given by Townsend. The contamination was avoided by adding a fine leak and a spiral-type liquid-air trap. The chamber was pumped out at the close of each day's work. In no case was the gas used after it had stood overnight in the ionization chamber.

The tube was baked out at 375°C for periods of 16 to 20 hours each time air was admitted. Every time mercury contamination was suspected the chamber was given a thorough cleaning before more data were taken. The plate surfaces were subject to heavy discharges, in an atmosphere of hydrogen, except in the case of the second NaH surface.

All pressures given in this paper were reduced to 22°C.

EXPERIMENTAL RESULTS

The data for hydrogen gave the characteristic curves when $(1/p)\log i/i_0$ was plotted as a function of d, the plate separation.[5] The values of α/p plotted as a function of X/p are shown in Fig. 1. Two sodium cathodes were used in this work. In the first case a thin layer of sodium was distilled on the platinum cathode after which a discharge was run for thirty minutes in an atmosphere of hydrogen. This gave a surface of NaH. The second sodium surface was heavier and no discharge was set up at any time during the measurements with this surface. It was hoped that with the second cathode it would be possible to get data for a sodium surface but the first few runs showed a constant change of the photosensitivity of the surface with time and this was taken to indicate that a NaH surface was being formed. After the potential had been applied to the chamber for some twelve hours the photoemission became steady. In all the curves shown the data derived with the first sodium surface are shown as circles and those taken with the second surface are indicated by crosses.

The data for the second coefficient was computed in two ways. (1) The Townsend[6] equation

$$i=i_0\frac{(\alpha-\beta)e^{(\alpha-\beta)d}}{\alpha-\beta e^{(\alpha-\beta)d}} \qquad (1)$$

was assumed. This equation gave the quantity β. (2) The modified Townsend equation, which was independently derived by Thomson,[7]

$$i=i_0\frac{e^{\alpha d}}{1-\gamma(e^{\alpha d}-1)} \qquad (2)$$

was used to compute the quantity γ. This latter equation involves a cathode secondary emission process. Loeb[3] has shown that the mechanism assumed by Townsend, leading to Eq. (1), does not occur under the conditions met with in this work. He also has shown that if β is small compared with α, then β can be interpreted either in

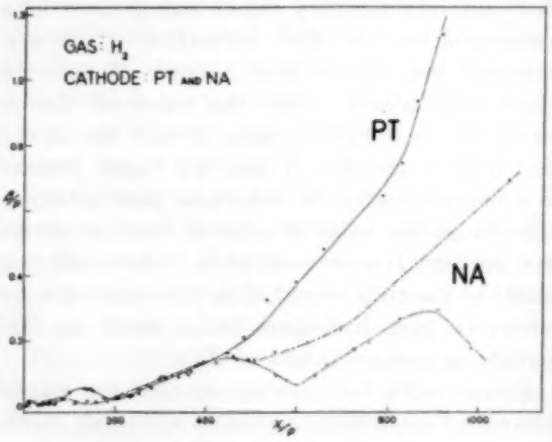

FIG. 2. Values of β/p as a function of X/p.

[5] For the terminology and the method of reduction of data the reader is referred to Bowl's paper (reference 2) and Loeb's treatment of this field (reference 3).

[6] J. S. Townsend, *Electricity in Gases* (Oxford University Press, 1914), p. 314.

[7] J. J. Thomson and G. P. Thompson, *Conduction of Electricity through Gases* (Cambridge University Press, second edition), Vol. II, p. 518.

terms of γ or in terms of a photoelectric mechanism. Thus to an approximation one sets $\beta/\alpha=\gamma=\Theta\eta g/\alpha$ where Θ, η and g are constants which determine the photoemission from the cathode surface. The derivations of β and γ (Eqs. (1) and (2)) are rigorous while that for $\eta\Theta g$ is only approximate. In this case α is not much greater than β and the β value found cannot accurately be substituted for either $\Theta\eta g$ or for γ. However for purposes of comparison β and γ were computed, from Eqs. (1) and (2).

The values of β/p, β/α and γ are plotted as functions of X/p in Figs. 2, 3 and 4. A comparison of Figs. 3 and 4 shows that β/α and γ are not essentially different except in the absolute values at the peaks. The β/p curve of Fig. 2 shows the same general characteristics as Bowls' curve for mercury-free surfaces of platinum and NaH in nitrogen. In this work, with somewhat better resolving power, the curves show a more complex structure. The γ curve, for the platinum surface, shows a prominent peak at an X/p of 125. This curve eventually starts a rapid rise at values of X/p greater than about 600. When the NaH cathode was used the values of γ showed an exceptionally high peak at an X/p of 10, followed by lower peaks at values of X/p of 50, 450 and 825. The general rise which is found for the platinum cathode does not appear in this case. The highest value of γ occurs at an X/p of 10. In the case of the second sodium surface, which was a heavy layer of sodium with some NaH present, the γ curve shows a gradual rise at the higher values of X/p.

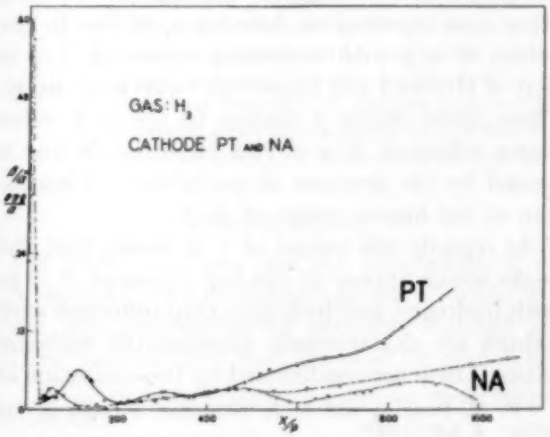

FIG. 3. The values of β/α as a function of X/p.

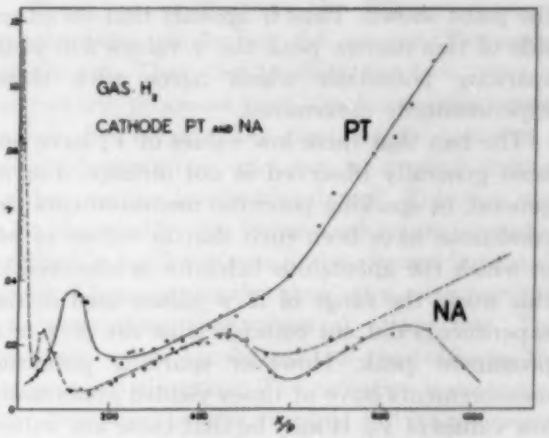

FIG. 4. Values of γ as a function of X/p.

Florence Ehrenkranz[8] has experimentally determined the sparking potentials for platinum and NaH cathodes in mercury-free hydrogen. Fig. 5 shows the Ehrenkranz curve for the NaH cathode and also a curve calculated from the α and γ values as given in this paper and the method of calculation outlined in Loeb's article.[3] The agreement is quite good, within 5 to 7 percent, over the short range of values of $p\delta$ for which it was possible to calculate V_s from the experimentally determined γ values of this work. All of the γ values used in the calculations lay below an X/p of 500. The sparking potential curve was also calculated for the platinum cathode and gave about the same sort of agreement. The deviation near the minimum of Fig. 5 could be caused by a difference in the conditioning of the two NaH surfaces. In the Ehrenkranz experiments the cathode was subject to larger currents and repeated heavy discharges. The sparking potentials were also experimentally observed in this work and for both cathodes gave curves of V_s plotted against $p\delta$ which lie from 5 to 8 percent above the curves of Ehrenkranz.

If in the calculations of the sparking potential curve one uses those values of γ which lie in the region of the narrow peak at the lower values of X/p the resulting values for V_s do not lie on the Ehrenkranz curve. As an example the calculated V_s for the γ value at X/p equals 20.4 is shown in Fig. 5. The value of γ at X/p equals 8.65 gives even worse agreement while the γ value at X/p equals 5.85 gives about the same agreement as

[8] Florence Ehrenkranz, Phys. Rev. **55**, 219 (1939).

the point shown. Thus it appears that on either side of this narrow peak the γ values will yield sparking potentials which agree with those experimentally determined.

The fact that these low values of V_s have not been generally observed is not strange. For in general, in sparking potential measurements the conditions have been such that at values of $p\delta$, in which the anomalous behavior is observed in this work, the range of X/p values used in the experiments did not coincide with the X/p of a prominent peak. However sparking potential measurements have at times yielded abnormally low values of V_s. It may be that these low values were, in some cases, caused by use of a $p\delta$ value which had an X/p value in the region of a peak. In general such values of X/p would require large values of $p\delta$.

Discussion of the Experimental Results

The values found for α/p as a function of X/p in pure hydrogen at the higher pressures are not seriously different from those of Ayres.[9] At the lower pressures and higher values of X/p, where the percentage of mercury contamination becomes appreciable, the Ayres and Townsend curves rise to nearly twice the values of α/p observed here. However values of α/p which lie upon the Townsend curve were found in this work when the gas was admitted too rapidly and thus carried mercury from the gauges to the ionization chamber. The low values of α/p in the absence of mercury are in agreement with Bowls'[2] work and thus are not surprising.

The α/p curve obtained when sodium was distilled into the chamber is interesting. In agreement with the observations of Ehrenkranz and Bowls sodium in the presence of hydrogen and nitrogen yields some volatile compound of low ionizing potential which is present at a pressure of at least 10^{-3} mm. In nitrogen this raised α/p some 25 percent at the highest values of X/p studied. In this work it increased α/p by as much as 100 percent at the lower values of X/p. Above an X/p of 350 the values of α/p show a decrease until they are approximately the same as those for the normal curve. There appears to be no doubt as to the interpretation. There is some substance in the presence of sodium which is very effectively ionized at low values of X/p in hydrogen and which shows a decreasing efficiency of ionization at the higher X/p and thus electron energies. This can only be caused by an ionization by excited states in hydrogen of some easily ionized sodium compound present in traces only. That such actions occur is indicated by the peaks in the values of γ at low values of X/p.

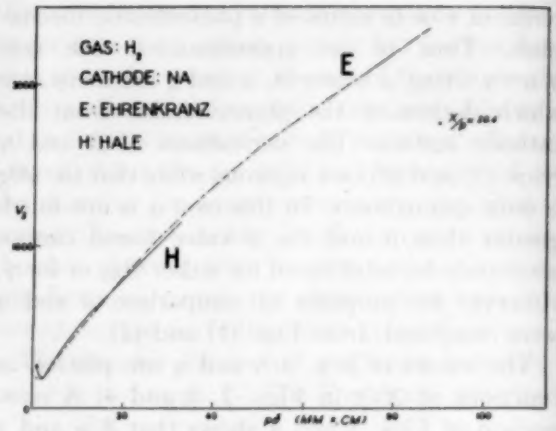

Fig. 5. The sparking potentials V_s in volts as a function of $p\delta$.

This appears to be the first evidence for a pronounced action of this kind. The results of Penning and Kruithoff[10] in the proper admixture of argon and neon have yielded similar but not as pronounced peaks for α/p. It will be observed that there is an indication in Fig. 1 of a second such rise in the α/p curve above values of X/p of 1000. However these points are near the limit of the present ionization chamber and the precision of the measurements is not good. The only other case reported to date for a decline in the values of α/p with increasing values of X/p is that of Huxford and Engstrom[11] who used argon. Their curve shows a decline in the α/p value above values of X/p of 700. Here the decline is caused by the decrease in probability of ionization at the higher values of X/p.

As regards the values of γ it seems that the peaks which appear at the low values of X/p in both hydrogen and hydrogen contaminated with sodium are characteristic photoelectric emission peaks. These are conditioned by the excitation of

[9] T. L. R. Ayres, Phil. Mag. **45**, 353 (1923).

[10] F. M. Penning and A. A. Kruithoff, Physica **3**, 515 (1936); **4**, 430 (1937).

[11] W. S. Huxford and R. W. Engstrom report these results in a letter to Professor Loeb.

certain lines in hydrogen as the average electron energy passes through peaks in the excitation curves. These excitation or photon yields have their effect on γ modified by absorption in the gas and by photoelectric peculiarities of the cathode surface. Note for example the difference in the locations of the peaks for the platinum and the NaH surfaces. In agreement with this it should be noted that the peaks in the γ curve for the NaH cathode disappear at those values of X/p where α/p has its maximum point. Here hydrogen is being excited but the sodium compound removes some photons by ionization. At the higher values of X/p the platinum surface in hydrogen, as is known from the results of Curtis,[12] is a good secondary electron emitter under proton bombardment. NaH on the other hand is a sensitive photoelectric emitter but appears to be relatively insensitive to secondary electron emission on bombardment by ions of sodium and protons.

[12] L. F. Curtis, Phys. Rev. **31**, 1010, 1127 (1928).

These results illustrate the different types of mechanisms producing the second Townsend coefficient. They clearly show the two types of secondary processes and the conditions under which they occur. They illustrate the fact that a good photoemitter may not be a good emitter under positive ion bombardment. This fact was also observed by the Farnsworth group in studies of the Cs-Ag-O surfaces under *electron* bombardment. These results also show why, with mercury contamination, the values of γ are low. The mercury vapor causes most of the peaks in the γ-curves to disappear. The radiation is destroyed by absorption by the mercury and its ionization while the mercury ions are known to be inefficient in producing secondary emission by ion bombardment of the cathodes.

In conclusion the writer wishes to express his thanks to Professor L. B. Loeb who suggested this problem and who has given generously of his time in discussions of the experimental results.

MAY 1, 1939 PHYSICAL REVIEW VOLUME 55

The Resonance Scattering of Protons by Lithium

E. C. Creutz
University of Wisconsin, Madison, Wisconsin

(Received April 1, 1939)

The scattering of protons by a thick target of lithium has been studied in the energy region 272–586 kev at an angle of 156°, with a ball counter. The number of counts per microcoulomb at 458 kev is 2.08 times its value at 408 kev, and at 487 kev it has dropped to 1.48 times the value at 408 kev. The energy at which the maximum slope of the thick target curve occurs is within five kev of the energy for the lithium gamma-ray resonance maximum. The fact that the scattering from a beryllium crystal increased smoothly with proton energy throughout the region, showed that the resonance effect is not a peculiarity of the counter. This scattering anomaly indicates: (1) that the gamma-radiation obtained when Li^7 is bombarded with 440-kev protons arises from a virtual level of Be^8; (2) that the Be^8 state is odd; and (3) that there are no odd excited states of the alpha-particle below approximately 13 Mev.

Introduction

IN 1934 Lauritsen and his collaborators[1] observed gamma-radiation produced when lithium was bombarded by protons. Hafstad and Tuve[2] showed later that the reaction occurs as a sharp resonance at 440-kev proton energy, and later work by them, with Heydenburg[3] showed the resonance half-width to be about 11 kev.

The process of this gamma-ray emission was not known.[4] Crane and Lauritsen assumed that

[1] Crane, Delsasso, Fowler and Lauritsen, Phys. Rev. **46**, 531 (1934).

[2] L. R. Hafstad and M. A. Tuve, Phys. Rev. **47**, 506 (1935).

[3] Hafstad, Heydenburg and Tuve, Phys. Rev. **50**, 504 (1936).

[4] This problem is discussed by Breit in the paper by Hafstad, Heydenburg and Tuve, reference 3, pp. 510–514.

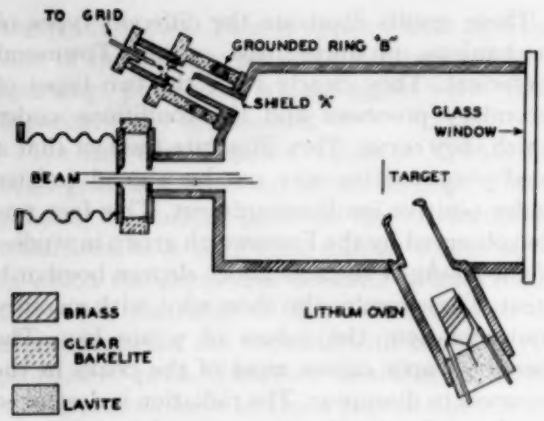

FIG. 1. Scattering chamber and proton counter.

semi-stable Be^8 was first formed, which disintegrated into two alpha-particles, one of which was excited and later emitted the gamma-radiation. Another possibility was that the emission was caused by Be^8 dropping from the excited to the normal state. In this case there should be a rather large probability for the Be^8 to disintegrate again into Li^7 and a proton, and thus give anomalous scattering of protons by lithium in the resonance region. Professor Breit suggested that experiments on the scattering of protons by lithium should help in differentiating between the two processes.

APPARATUS AND PROCEDURE

The small Van de Graaff type electrostatic generator constructed by R. G. Herb and collaborators,[5] modified so as to give steady voltages up to 600 kev, was used to produce the high energy protons for these experiments. Essential modifications were: the construction of a new porcelain section accelerating tube, by Herb, of the type now used by him in the 2.4-Mv generator at this laboratory,[6] a new high voltage electrode with spun copper ends, by G. J. Plain; and remodeling of the proton source after the design now used by Herb,[6] which, because of its larger power consumption, necessitated the installation of a larger driving motor for the charging belt. With the generator at the higher voltages it was necessary to place tinfoil bands at three-inch intervals on the Pyrex capillary hydrogen lead (Fig. 2, reference 5) from ground to the high voltage electrode to prevent sparking down it and final explosion. Air at 45 lb./in.^{2} pressure in the generator was dried by KOH and kept saturated with CCl_4 as suggested by Herb.[7]

The scattering chamber and proton counter are shown in Fig. 1. Since preliminary experiments with a proportional counter carried out by G. J. Plain and the author indicated that the results of using it to count protons in this energy region would be difficult to interpret, several ball counters of the type shown in Fig. 1 were tried. Although not completely reliable these often gave consistent results from day to day. It was found necessary to shield all dielectrics in the counter in the region of the discharge and to keep the voltage on it constant to within one percent by means of a regulator, which was built with an Eimac 35T triode, manufactured by Eitel McCullough Incorporated, San Bruno, California.

Air at atmospheric pressure was used in the counter, the wall of which was kept at plus 1300 volts. The ball was connected to the grid of an amplifier whose output went to a scale-of-eight thyratron set, which activated a Cenco mechanical counter. The counter window was aluminum foil 0.00004 inch in thickness, fastened with clear Glyptal. The Glyptal was shielded from the ball by a platinum sheet. The ball was of platinum about one-tenth millimeter diameter made on platinum wire by holding it in a torch-flame.

Shields (not shown) were placed above and below the target so that protons scattered from other parts of the chamber, e.g., the glass

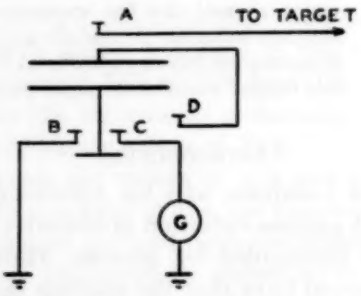

FIG. 2. Switching arrangement for measuring number of protons incident on target.

[5] Herb, Parkinson and Kerst, Rev. Sci. Inst. **6**, 261 (1935).
[6] Parkinson, Herb, Bernet and Mckibben, Phys. Rev. **53**, 642 (1938).
[7] M. T. Rodine and R. G. Herb, Phys. Rev. **51**, 508 (1937).

window, would be less likely to enter the counter. The number of protons entering the chamber was measured by leading them to the condenser, which was later discharged through a ballistic galvanometer. Protons striking the edge of the exit hole of the chamber knocked out secondary electrons which were pulled over to the counter wall by a rather strong field. This gave a false reading of the incident charge until the use of shield "*A*," eliminated this difficulty. Leakage across the insulating support of the counter was prevented by the grounded brass ring *B*.

Thick lithium films were evaporated by means of the oven onto a nickel sheet, freshly for each run, for about one hour at eight amp. oven current. The check runs on beryllium were made by scattering from a beryllium crystal, ground flat, polished and cleaned.

The switching arrangement used for charging and discharging the condenser, shown in Fig. 2 allows the same galvanometer to be used to measure the charging current and later the total collected charge. When charging, switches *A* and *C* are closed, and *B* and *D* are open. To interrupt charging, *A* is opened. To measure the charge, *A* is left open, *C* is opened, and *B* and *D* are closed. A Leeds & Northrup ballistic galvanometer was used, the current readings of which were of interest as to order of magnitude only. Proton currents of 0.01 to 0.2 microampere were used. After making a run on lithium, two or three check points were always made on beryllium, and several times complete runs were made on beryllium to certify that the efficiency of the counter was a smooth function of proton energy. Checks were also made by scattering first from lithium, then from beryllium, then from lithium again, finally changing the voltage and repeating the series lithium-beryllium-lithium. Good agreement was found in each case. This indicates that the observed resonance is not caused by a fluctuation in the counter sensitivity. The generating voltmeter was calibrated from the lithium gamma-ray resonance, which was observed with a Lauritsen electroscope.

Results and Discussion

Curve *A* of Fig. 3 shows on an arbitrary scale the number of counts per incident proton obtained from a thick lithium film at a scattering angle of 156°. Curve *C* shows similarly the number of counts from the Be crystal at the same scattering angle. Each experimental point in these curves represents 1440 counts. Curve *A* has a peak at about 460 kev where the apparent yield is 2.1 times greater than at 408 kev. On the right of the peak (487 kev) the yield is 1.5 times greater than on the left (408 kev). Curve *C* can be used as a rough indicator of counter efficiency and a check on the reality of the scattering anomaly indicated by curve *A*. In comparing the two yield curves account must be taken of the variation of counter efficiency with proton energy and of the difference in recoil energy for the two targets. The fractions of the original energy retained on single scattering from Li^7 and Be^9 are, respectively, 0.577 and 0.65. Multiplying the abscissae of curve *C* by $0.65/0.577=1.125$ one obtains, therefore, a corrected Be scattering curve the abscissae of which correspond approximately to the same energy of protons at the counter as for the lithium curve *A*. Curve *D* of Fig. 3 has been obtained in this way. It is smooth in the energy region in which the Li curve shows a peak and indicates the reality of the scattering

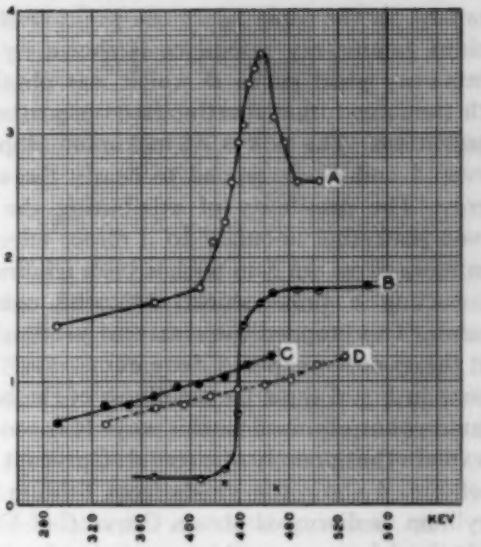

FIG. 3. Curve *A*: Yield of protons scattered from lithium thick target. Ordinate scale arbitrary. Curve *B*: Gamma-ray intensity from lithium thick target bombarded with protons. Ordinate scale: electroscope divisions per microampere per minute. Curve *C*: Yield of protons scattered from beryllium crystal. Ordinate scale arbitrary. Curve *D*: same as *C*, with abscissae multiplied by 1.125 (See Discussion). Crosses show background counts with brass shield covering counter window.

anomaly. In the same figure the position of the lithium gamma-ray resonance is shown by the gamma-ray yield curve *B* which was obtained with the same target shortly after the scattering observations. The points of maximum slope of curves *A* and *B* correspond to nearly the same energy. The possibility of attributing the observed scattering anomaly to a direct effect of gamma-rays on the counter has been eliminated by putting a brass shield over the counter window. This stopped the scattered protons but left the counter exposed to gamma-rays. The crosses in Fig. 3 show the smallness of the background count obtained in this way. It is too low to explain the anomaly of curve *A*. Curves *A* and *B* of Fig. 4 show the yields from lithium and beryllium as discussed above. Curve *C* of Fig. 4 is obtained from curve *B* by correcting for recoil as has been explained for curve *D* of Fig. 3. Since different currents were required to give about the same number of counts per minute from the two targets many more adjustments of the apparatus were required during this run which probably accounts for the scattering of the lithium points which is worse than in Fig. 3. All lithium runs taken since November 8, 1937 have been plotted for curve *D* of Fig. 4. Since the counter sensitivity varied from day to day, the ordinates have been adjusted to coincide at 508 kev. Such an adjustment does not take into account the variation of the "experimental width" with existing conditions, and tends to make the peak less pronounced, especially for those runs in which no points happened to be taken at the most effective energy, 460 kev.

Although a thick film of lithium was used, the yield of scattered protons drops down again after the resonance voltage is passed, because then protons which are to be resonantly scattered must have penetrated the film, and decrease in energy until they reach a value in the resonance region. If the incident energy is appreciably greater than 440 kev, the protons will have had to penetrate the film so deeply to reach the resonance region that they will be absorbed on their way out of the film, or at least slowed up so much that they cannot penetrate the counter window with enough energy to trip the counter. The countable yield expected for Coulomb scattering will now be estimated.

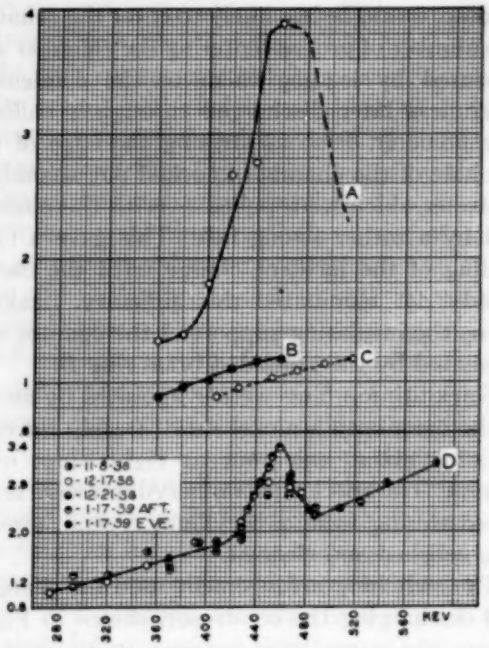

FIG. 4. Curve *A*: Yield of protons scattered from lithium thick film. Points taken alternately with those of curve *B*. Curve *B*: Yield of protons scattered from beryllium crystal. Curve *C*: same as *B* with abscissae multiplied by 1.125. Curve *D*: Yield of protons scattered from lithium thick film. Ordinate at 508 kev adjusted to coincide for all runs.

According to the Rutherford formula n, the number of protons scattered per incident proton, per unit thickness of film, per unit solid angle, at a given scattering angle, is inversely proportional to the square of their energy. Thus from film thickness dx, the number scattered is

$$ndx = KE^{-2}dx,$$

where K is a constant. The total number scattered from a film of thickness λ is then

$$N = \int_0^{\lambda} KE^{-2}dx.$$

For a small spread of energies, the range of the protons is approximately proportional to their energy, and that lost per centimeter of range (the "stopping power" of the film) is approximately independent of their energy, equal to a constant a. Thus if the energy when incident is E_0, that retained at a depth x in the film is

$$E = E_0 - ax.$$

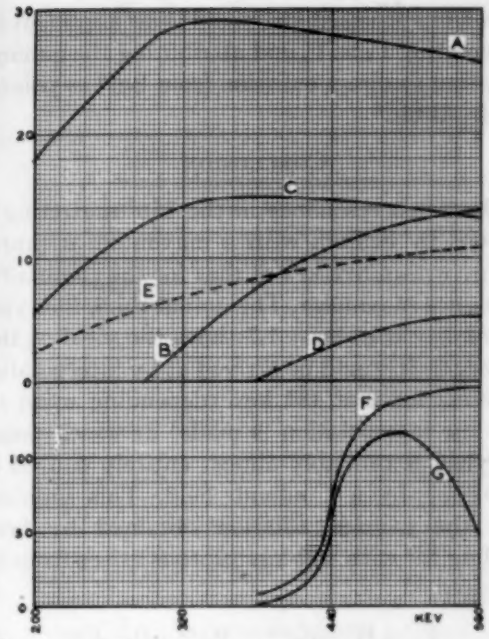

FIG. 5. Calculated curves, showing expected countable yield of scattered protons. Curve A: Yield from beryllium, counter cut-off 100 kev. Curve B: Yield from beryllium, counter cut-off 200 kev. Curve C: Yield from lithium, neglecting anomaly, counter cut-off 100 kev. Curve D: Yield from lithium, neglecting anomaly, counter cut-off 200 kev. Curve E: Yield from lithium, assuming all protons returned to counter with energy greater than 200 kev. are counted, as well as 50 percent of those with energy greater than 100 kev but less than 200 kev. Curve F: Yield of protons anomalously scattered from Li, cut-off 50 kev. Curve G: Same as F, counter cut-off 200 kev.

Thus the number scattered, of incident energy E_0, is

$$N=\int_0^{\lambda} K(E_0-ax)^{-2}dx.$$

Upon being scattered, the proton loses the fraction $(1-B)$ of its energy as recoil of the scattering particle, and retains the fraction B. Thus immediately after being scattered at a depth x the proton has a total energy $B(E_0-ax)$ of which it loses $ax/\cos\theta$ in getting back out, where θ is the supplement of the scattering angle. Thus upon reaching the counter, the total energy retained is

$$B(E_0-ax)-ax/\cos\theta$$

which must be greater than some value C, in order for it to trip the counter. Thus λ, the upper limit of the integral is evaluated, as the maximum depth in the film which will still yield countable scattered protons:

$$B(E_0-a\lambda)-a\lambda/\cos\theta=C.$$

The approximation $\cos\theta=1$ was used. The integral then gives for the countable yield of protons

$$N=K(BE_0-C)a^{-1}E_0^{-1}(E_0+C)^{-1}.$$

Curves of this function of E for various values of C, for $B=0.577$ corresponding to Li^7 and to Be^9 $(B=0.65)$ are shown in Fig. 5, curves A, B, C, D. The value of a was computed from Bragg's law (atomic stopping power proportional to the square root of atomic wt.) and Herb's data for the stopping power of aluminum.[8]

As a first approximation to the expected yield of anomalously scattered protons, the cross section for such scattering was assumed to follow the law

$$\sigma=\sigma_m\frac{\Gamma^2}{(E-E_m)^2+\Gamma^2},$$

where σ_m, the maximum value of σ, was taken to be roughly five times the Rutherford scattering cross section at 440 kev, E_m was taken as 440 kev, a half-width of 40 kev was used, and Γ was found accordingly. Curves of the countable anomalous yield for $C=50$ kev and $C=200$ kev are shown in Fig. 5, curves F and G, respectively. The half-width used (40 kev) is higher than the observed 12 kev. The conclusions will not be affected since this only tends to widen the peak of curve G and the step of curve F as well as to increase the expected relative importance of the anomaly.

A counter of the type used does not have a definite cut-off voltage (value of C), but if one assumes, for instance, that all protons incident on the counter window with energy greater than 200 kev are counted, as well as 50 percent of those with energy less than 200, but greater than 100 kev, the curve obtained is much the same as one for a value of C between 100 and 150, except for small values of E, as shown by the dotted curve of Fig. 5E, which was calculated in this way. Both curves F and G in Fig. 5, although calculated for widely different values of C, show a maximum positive slope very close to 440 kev, the value used for the resonance maximum in

[8] Parkinson, Herb, Bellamy and Hudson, Phys. Rev. 52, 75 (1937).

these calculations, which indicates that the actual resonance maximum may be given closely by the energy corresponding to the greatest slope of the experimental curve, independently of the counter cut-off. Curves *A*, *B* of Fig. 3 show that the points of greatest slope for scattering and gamma-rays correspond to the same energy within five kev.

According to the Breit-Wigner formula, the cross section for a resonance process of this sort is given by

$$\sigma=\frac{\lambda^2}{\pi}S\frac{\Gamma_s\Gamma_r}{(E-E_m)^2+(\Gamma_s+\Gamma_r)^2},$$

where λ is the wave-length of the incident particle, E its energy, and E_m its energy at the resonance maximum; the statistical factor S is of the order of magnitude of unity and matters little in the estimates made below.

The contributions to the half-width of the resonance due to the probability of the compound nucleus scattering the incident particle, and emitting radiation are $2\Gamma_s$ and $2\Gamma_r$, respectively. The γ-yield at resonance as estimated by Gentner[9] is about eight percent of the number of disintegrations per proton in the reaction

$$Li^7+H^1\rightarrow He^4+He^4,$$

the cross section for which is about 2×10^{-27} cm^2 at 440 kev. Using these values and the wave-length of a 440-kev proton (4.3×10^{-12} cm) one obtains for one of the Γ's

$$\Gamma_1\leqq 2 \text{ ev},$$

while the rest of the width (about 5500 kev for Γ to give the total measured by Hafstad, Heydenburg and Tuve[2]) must be due to Γ_2. If the radiation takes place from an excited alpha-particle and Γ_1 be interpreted as Γ_r, the width is due to the disintegration

$$Be^{8*}\rightarrow He^4+He^{4*},$$

which would be expected to have a greater probability than indicated by such a small value of Γ, although the nuclear penetration factor for the alpha-particles depends on their energy which is not definitely known, because of the uncertainty in the gamma-ray energy. The fact that anomalous scattering is found is an argument for interpreting Γ_2 as Γ_s and attributing the gamma-radiation to direct emission from Be^{8*} as pointed out by Breit.[3]

[9] W. Gentner, Zeits. f. Physik **107**, 354 (1937), see page 357.

Conclusion

There is a resonance in the 156° scattering of protons by lithium with a maximum at proton energy within five kev of that for the gamma-ray resonance maximum. The actual thick film yield at 458 kev is at least 1.7 times the yield at that voltage as it would be arrived at by interpolating between 408 and 487 kev (depending upon the way the interpolation is made) at which points the yield is probably almost entirely caused by scattering by a Coulomb field. This indicates that the gamma-radiation obtained by bombarding Li^7 with 440-kev protons arises from the reaction

$$Li^7+H^1\rightarrow Be^{8*};\quad Be^{8*}\rightarrow Be^8+\gamma \qquad (1)$$

and not from the reaction

$$Li^7+H^1\rightarrow He^4+He^{4*};\quad He^{4*}\rightarrow He^4+\gamma \qquad (2)$$

unless an explanation is found for the small nuclear penetration factor required to give process (2) a probability about 1/2700 of that for proton scattering. The experiment also shows, almost with certainty, that the excited state of Be^8 is odd, because if it were even there could be disintegration into two alpha-particles, which would exclude the anomalous scattering. Similarly the possibility of odd excited states of the alpha-particle below approximately 13 Mev is improbable because the disintegration into a normal and an excited alpha-particle would be then likely to suppress the chance of re-emission of the proton.

The author wishes to express his appreciation to Professor Breit, who suggested the problem and who furnished invaluable advice and assistance throughout the work; to Professor Herb for generous advice; to G. J. Plain who constructed some of the apparatus and with whom preliminary tests were made; and to Mrs. E. C. Creutz who read the electroscope during the gamma-ray runs. The author is also grateful for having received the Charles E. Mendenhall fellowship which helped support the work during the summer of 1938.

Nuclear Spins and Magnetic Moments by the α-Particle Model

R. G. SACHS
Johns Hopkins University, Baltimore, Maryland
(Received April 3, 1939)

Some properties of the light nuclei of the type $n\alpha\pm1$ have been calculated on the basis of the α-particle model. By means of this description, spins and magnetic moments of the same nuclei are calculated here. The results for the magnetic moments of many of the nuclei are undetermined within a certain range of possible values since the relative order of magnitude of the spin-orbit coupling and the separation of rotational levels is unknown. This ambiguity does not appear in the Hartree model, so that the magnetic moments as calculated by the two models are somewhat different. The most notable difference occurs for the spins of C^{13}, N^{13}, which have not yet been measured; the Hartree model predicts a spin of $\frac{1}{2}$ for them whereas the α-model yields a spin of $1\frac{1}{2}$. The α-model appears to give slightly better agreement for those magnetic moments that have been measured.

INTRODUCTION

THE α-particle model[1] has been successful in explaining many qualitative features of light nuclei. It has recently[2] been applied with some success to nuclei that contain α-particles plus or minus a neutron or proton. However, there is no reason to claim that the α-particle model gives an exact, or even an accurate, description of the structure of light nuclei. The description given by the Hartree model, which is more difficult to apply, is certainly more fundamental since it takes the (unknown) forces between individual particles into account explicitly.

In order to determine which model is closer to the truth, it is necessary to calculate with both and to compare the results with experiment. Total angular momenta (spins) and magnetic moments of light nuclei in their ground states have been calculated[3] on the basis of the Hartree model. It is the purpose of this paper to find what differences, if any, arise when the same properties are calculated by means of the α-particle model. This calculation has already been made[4] for Li^7, but will be repeated here for completeness.

It has already been pointed out that the saturated systems which contain an integral number of α-particles have zero angular momentum and magnetic moment in the ground state. The interest here will be in the systems which contain an added or subtracted particle. Since this model is essentially molecular, the notation used will follow that of molecular spectroscopy as closely as possible.

1. GENERAL METHOD

The proper functions, $\psi_{K,m,\Lambda}$ of the orbital-rotational levels of the nuclei considered here have been determined by Hafstad and Teller. Since the systems are spherical or symmetrical tops, they are characterized by at most three quantum numbers:[5] K, the rotational angular momentum; m, its projection on the space-fixed z axis; and Λ, its projection on the symmetry axis of the body, called the ζ axis of the body-fixed coordinate system.

Were there no spin, the characterization of the levels would be complete. However, an added or subtracted particle introduces a spin of $\frac{1}{2}$, which means that K and m are no longer true quantum numbers but that the levels must be described by a linear combination of products of spin and rotational wave functions. These states will always be characterized by a total angular momentum $J=K\pm\frac{1}{2}$, and by M, the projection of J on the space-fixed z axis.

A state corresponding to a given value of M includes those rotational states for which $m=M\pm\frac{1}{2}$; the mixing of these m values is determined by the symmetry of the system and is

[1] J. H. Bartlett, Jr., Nature **130**, 165 (1932); W. Wefelmeier, Zeits. f. Physik **107**, 332 (1937); J. A. Wheeler, Phys. Rev. **52**, 1083 (1937); C. F. von Weizsäcker, Naturwiss. **26**, 209, 225 (1938).
[2] L. R. Hafstad and E. Teller, Phys. Rev. **54**, 681 (1938).
[3] M. E. Rose and H. A. Bethe, Phys. Rev. **51**, 205 (1937).
[4] H. Bethe, Phys. Rev. **53**, 842 (1938).
[5] The notation used here differs from that used in reference 2 in that the J, K there become K, Λ here, respectively.

therefore completely independent of the spin-orbit interaction.

A fixed value of J may arise from two K values, $K=J+\frac{1}{2}$ and $K=J-\frac{1}{2}$. The way in which these two states mix is determined by the spin-orbit interaction. This interaction also determines which of the two $(2J+1)$-fold degenerate levels, $J=K+\frac{1}{2}$, $J=K-\frac{1}{2}$, has the lower energy. The J value, J_0, for the lowest energy is the "spin" of the nucleus.

If φ_σ, $\sigma=\pm\frac{1}{2}$, is the spin proper-function for which σ is the projection of the spin on the space-fixed z axis, the above linear combination may be written as

$$\Psi_{M,\,J-K+\frac{1}{2}}=\sum_{m+\sigma=M}\{C_{K,\,m,\,\sigma}\psi_{K,\,m,\,\Lambda}\varphi_\sigma + C_{K+1,\,m,\,\sigma}\psi_{K+1,\,m,\,\Lambda}\varphi_\sigma\}.$$

According to the above, for a given value of K, the ratios of the $C_{K,\,m,\,\sigma}$ to each other are determined by the symmetry, but the ratios of the $C_{K,\,m,\,\sigma}$ to the $C_{K+1,\,m,\,\sigma}$ depend on the spin-orbit coupling. It happens that, in the cases considered, Λ values are not mixed, as is indicated by the summation indices.

The following particular cases will occur:

$$\Psi_{\frac{1}{2},\,\frac{1}{2}}=a_0\psi_{0,\,0,\,\Lambda}\varphi_{\frac{1}{2}}+a_1[\sqrt{\tfrac{1}{3}}\psi_{1,\,0,\,\Lambda}\varphi_{\frac{1}{2}} \cdot -\sqrt{\tfrac{2}{3}}\psi_{1,\,1,\,\Lambda}\varphi_{-\frac{1}{2}}], \quad (1a)$$

$$\Psi_{1\frac{1}{2},\,1\frac{1}{2}}=b_1\psi_{1,\,1,\,\Lambda}\varphi_{\frac{1}{2}}+b_2[1/\sqrt{5}\,\psi_{2,\,1,\,\Lambda}\varphi_{\frac{1}{2}} -2/\sqrt{5}\,\psi_{2,\,2,\,\Lambda}\varphi_{-\frac{1}{2}}]. \quad (1b)$$

Normalization of the wave functions requires that

$$a_0^2+a_1^2=1; \quad b_1^2+b_2^2=1. \quad (2)$$

Knowledge of the eigenfunctions makes it possible to calculate the average value of the z component of the magnetic moment in that ground state of the system for which $M=J_0$ (J_0 is the angular momentum in the ground state):

$$\bar{\mu}_z=(\Psi_{J_0,\,J_0};\,\mu_z\Psi_{J_0,\,J_0}).$$

μ_z is additively composed of the moment due to the spin of the added or subtracted particle and of that due to the rotation of the system as a whole. Of these contributions, the first is connected to the spin with a fixed proportionality factor g_s, depending on whether the particle is a neutron or proton, and may be calculated immediately as

$$g_s\sum_{K=J_0-\frac{1}{2}}^{J_0+\frac{1}{2}}\sum_{m+\sigma=M}(C_{K,\,m,\,\sigma})^2\sigma. \quad (3a)$$

In order to calculate the contribution due to rotation, the gyromagnetic ratio of magnetic to angular momentum for rotation of the system must be determined in the body-fixed ξ, η, ζ axes. If the extra particle or hole is assumed, in the average, to be distributed uniformly over the system (see Section 4), the values of g_ξ and g_η are completely determined and $g_\xi=g_\eta=$ ratio of total charge to total mass. However, the angular momentum about the ζ axis is sometimes composed additively of motion of the system as a whole and of orbital motion of the extra particle with respect to the system. Since the g factor is different for the two motions, g_ζ will depend on this distribution of angular momentum and will in general be different from g_ξ.

If we choose to write the Landé factor, g_ζ, as $(g_\zeta-g_\xi)+g_\xi$ the last term and the ξ, η components of the magnetic moment give the simple contribution

$$g_\xi\sum_{K=J_0-\frac{1}{2}}^{J_0+\frac{1}{2}}\sum_{m+\sigma=M}(C_{K,\,m,\,\sigma})^2m, \quad (3b)$$

since the three together transform from one coordinate system to the other simply as a constant (g_ξ) times the angular momentum.

For the calculation of the contribution due to $g_\zeta-g_\xi$, the direction cosine between the body-fixed ζ axis and space-fixed z axis must be used. These matrices have been calculated[6] for the asymmetrical top; they have elements referring to the transition K to $K\pm1$ as well as elements diagonal in K, but they are completely diagonal in m, Λ. If $(K, m, \Lambda|D_{z\zeta}|\Lambda, m, K')$ be an element of these matrix direction cosines, the contribution due to $(g_\zeta-g_\xi)$ is:

$$\sum_{K,\,K',\,m+\sigma=M}(C_{K,\,m,\,\sigma})(C_{K',\,m,\,\sigma})\,\Lambda(K, m, \Lambda|D_{z\zeta}|\Lambda, m, K')(g_\zeta-g_\xi). \quad (3c)$$

[6] H. B. G. Casimir, Zeits. f. Physik **59**, 623 (1930). For the table of direction cosines in the notation used here, see G. Placzek and E. Teller, Zeits. f. Physik **81**, 209 (1933).

In particular, the following elements of the direction cosine matrix will be used:[6]

$$\begin{aligned}&(1,1,1|D_{z\zeta}|1,1,1)=\tfrac{1}{2},\\&(2,1,1|D_{z\zeta}|1,1,2)=\tfrac{1}{6},\\&(2,2,1|D_{z\zeta}|1,2,2)=\tfrac{1}{3},\\&(1,1,1|D_{z\zeta}|1,1,2)=(2,1,1|D_{z\zeta}|1,1,1)\\&\qquad=\tfrac{1}{2}(\tfrac{2}{3})^{\frac{1}{2}}.\end{aligned}\tag{4}$$

Equations (1 a and b), (3 a, b, c) and (4) give for $M=J_0=\frac{1}{2}$, $\Lambda=1$:

$$\mu=\bar{\mu}_s=\tfrac{1}{2}g_s\{a_0^2-\tfrac{1}{3}a_1^2\}+\tfrac{1}{3}a_1^2(g_\xi+g_\zeta)\tag{5a}$$

and for $M=J_0=\frac{3}{2}$, $\Lambda=1$:

$$\begin{aligned}\mu=&\tfrac{1}{2}g_s\{b_1^2-\tfrac{3}{5}b_2^2\}\\&+g_\xi\{\tfrac{1}{2}b_1^2+\tfrac{3}{2}b_2^2-\tfrac{1}{5}(3)^{\frac{1}{2}}b_1b_2\}\\&+g_\zeta\{\tfrac{1}{2}b_1^2+3/10b_2^2+\tfrac{1}{5}(3)^{\frac{1}{2}}b_1b_2\}.\end{aligned}\tag{5b}$$

2. Spin-Orbit Interaction

Although the spin-orbit coupling energy arises from both Larmor and Thomas precession, it has been pointed out[7] that, in nuclei, the Larmor term may be neglected as compared to the Thomas term since the Coulomb forces are much smaller than the nuclear forces. The interaction energy is therefore[8] $V=(\mathbf{a}\times\mathbf{v}/2c^2\cdot\mathbf{S}\hbar)$, where $\mathbf{a}$ is the acceleration of a particle with spin $\mathbf{S}$ and velocity $\mathbf{v}$ relative to the α-particles that give rise to $\mathbf{a}$. The acceleration $\mathbf{a}$ is the resultant of the acceleration due to the field of the α-particles plus the Coriolis acceleration,[9] and $\mathbf{v}$ is the sum of the body-fixed velocity of the neutron (proton) and the velocity of the neutron with respect to the α-particles due to rotation of the entire system. If the spin-orbit coupling is expressed in terms of these quantities, it takes the form $V=-\alpha(\mathbf{L}_0\cdot\mathbf{S})-\beta(\mathbf{L}_R\cdot\mathbf{S})$, $\alpha,\beta>0$, where $\mathbf{L}_0$ is the orbital angular momentum of the neutron (proton) relative to the α-particles, and $\mathbf{L}_R$ is the rotational angular momentum of the complete system.

The angular momenta for the rotational states of the nuclei can be taken directly from the results of Hafstad and Teller;[3] however, since they are different for different systems, the form of the spin-orbit interactions will be different. Therefore, for the calculation of the ground states of the nuclei, each system will be considered separately; the order in which they are considered will simply be that of complication.

3. Ground States

O^{17}, F^{17}

The system consists of four α-particles at the vertices of a tetrahedron plus a particle with a spherical node through the α-particles. The ground state therefore arises from $K=0$ and has an angular momentum equal to the spin of the added particle; thus $J_0=\frac{1}{2}$. The magnetic moment is given by the magnetic moment of the added particle.

C^{13}, N^{13}; $\Lambda=0$, $K=1$[10]

The three α-particles form an equilateral triangle, and the added particle has a node in the plane of this triangle so it can have no orbital angular momentum in the body-fixed system. The angular momentum is then due only to rotation of the system as a whole. This yields the interaction $V=-\beta(K\cdot S)$, $\beta>0$.

The usual angular momentum matrices give the energy matrix:

$$\begin{aligned}&-(K,m,\sigma|V|\sigma',m',K')\\&=\beta(K,m,\sigma|\sum_{j=x,y,z}K_jS_j|\sigma',m',K')\\&=\beta\delta_{K}{}^{K'}\sum_j(K,m|K_j|m',K)(\sigma|S_j|\sigma')\\&=\beta\delta_{K}{}^{K'}\{\tfrac{1}{2}((K+m)(K-m+1))^{\frac{1}{2}}\delta_{m-1}{}^{m'}\delta_{\sigma+1}{}^{\sigma'}\\&\qquad+\tfrac{1}{2}((K-m)(K+m+1))^{\frac{1}{2}}\delta_{m+1}{}^{m'}\delta_{\sigma-1}{}^{\sigma'}\\&\qquad+m\sigma\delta_{m}{}^{m'}\delta_{\sigma}{}^{\sigma'}\}.\end{aligned}$$

The characteristic values are: $E=\beta$ for $J=\frac{1}{2}$, $E=-\frac{1}{2}\beta$ for $J=1\frac{1}{2}$ arising from $K=1$; $E=1\frac{1}{2}\beta$ for $J=1\frac{1}{2}$, $E=-\beta$ for $J=2\frac{1}{2}$ arising from $K=2$, etc. The state of lowest energy[11] therefore has $J_0=1\frac{1}{2}$ and, since the energy is diagonal in K, $b_2=0$, $b_1=1$ (Eq. (2)).

[7] D. R. Inglis, Phys. Rev. **50**, 783 (1936).

[8] See D. R. Inglis, Phys. Rev. **50**, 784 (1936).

[9] Accelerations of the order of magnitude of the centrifugal terms will be neglected, since they depend on the square of the rotational angular momentum.

[10] The angular momenta given here and in the following correspond to the lowest rotational states as given in reference 2.

[11] This assumes that the separation between rotational levels is of the same order of magnitude of, or greater than, the spin-orbit interaction, so that rotational levels cannot be made to cross by this interaction.

Li^7, Be^7; $\Lambda=0$, $K=1$

In this case, the nuclei lack one neutron or proton of being two complete α-particles. This lack of a neutron or proton may be considered as an added neutron or proton "hole," where the hole is placed in the state from which the subtracted particle has been taken. The hole has a node between the two α-particles so that there is no body-fixed orbital angular momentum. In the complete system, there are then three neutrons (protons) with body-fixed orbital angular momentum equal to zero. Two of these particles are in the same state with antiparallel spin and give no contribution to the spin-orbit coupling energy. The third is coupled to rotation of the complete system since there is no body-fixed orbital motion. The interaction is again $V=-\beta(K\cdot S)$, $\beta>0$ so that the ground state has $J_0=1\frac{1}{2}$, $b_2=0$, $b_1=1$.

N^{15}, O^{15}; $K=1$

The system consists of four α-particles at the vertices of a tetrahedron plus a neutron or proton hole. The nucleus is then a spherical top and has no preferred axis; thus the angular momentum may be quantized along any body-fixed axis, but the rotational proper functions are degenerate in this quantum number, Λ.

Just as in the above case, there is one particle in a state of unsaturated spin which is entirely responsible for the interaction energy. However, the unsaturated particle moves relative to the α-particles and therefore gives rise to an orbital angular momentum which combines with rotation of the system as a whole to form the total angular momentum. Without a very detailed treatment, the question of how the total angular momentum is distributed between these two cannot be settled. It will be assumed that the two angular momenta contribute to the total angular momentum in the ratio $\theta/(1-\theta)$ where $0\leqq\theta\leqq 1$.

There are now two contributions to the energy; one due to rotation; $V_R=-\beta(K\cdot S)(1-\theta)$, and the other arising from orbital motion, $V_0=\pm\alpha(K\cdot S)\theta$. In order to determine the sign of V_0, it is necessary to consider the wave function of the hole in a little more detail.

Let $\psi_{l,\lambda}(k)$ be one of the possible orbital wave functions of the kth neutron or proton. Since a rotation by $2\pi/3$ about an axis through one α-particle and perpendicular to the plane of the other three permutes the three α-particles, these orbital functions must form a representation of this rotation. Therefore, under this rotation of $\Delta\omega=2\pi/3$, the $\psi_{1,\lambda}(k)$ must transform like $\exp(i\lambda\omega)$; $\lambda=0, 1, -1$. The fourth function, ψ_{00}, will be symmetric under all covering operations of the tetrahedron.

To get the lowest energy for the system, the hole is placed in a state of $|\lambda|=1$. Therefore the proper functions of the system may be taken to be

$$\Psi=\sum_P(-1)PP\psi_{00}(1)\alpha(1)\psi_{00}(2)\beta(2)\times\psi_{10}(3)\alpha(3)\psi_{10}(4)\beta(4)\psi_{1,-\lambda}(5)\alpha(5)\times\psi_{1,-\lambda}(6)\beta(6)\psi_{1,\lambda}(7)\begin{cases}\alpha(7)\\ \beta(7)\end{cases};\quad \lambda=\pm 1,$$

where P is the permutation operating on particles 1 to 7 and α and β are the usual spin wave functions.

If the entire system is rotated by $2\pi/3$ about the threefold axis and the neutrons (protons) by $-2\pi/3$ about the same axis, the proper functions of the complete system should remain unchanged since the α-particles form an Einstein-Bose system. This rotation multiplies the neutron (proton) proper function by $\exp 2\pi i\lambda/3$ and the rotational functions by $\exp 2\pi i\Lambda/3$, where Λ is the projection of K on the axis of rotation. The complete function is multiplied by $\exp 2\pi i(\Lambda+\lambda)/3$ which must be unity, and hence $\Lambda=-\lambda$. The only particle with unsaturated spin, that is, the only one that contributes to the spin-orbit energy, is in the state $\psi_{1,\lambda}$. For this particle, the projection of l, the orbital angular momentum, on the above threefold axis of symmetry is proportional to λ. Since the interaction energy is proportional to $-(l\cdot S)$, the equation $\Lambda=-\lambda$ indicates that the energy V_0 is given by $V_0=\alpha(K\cdot S)\theta$, $\alpha>0$.

The total interaction then becomes $V=V_0+V_R=(K\cdot S)[\alpha\theta-\beta(1-\theta)]=\gamma(K\cdot S)$. The sign of γ is determined by the ratio of rotational to orbital motion with $\gamma\leqq 0$ for $\theta/(1-\theta)\leqq\beta/\alpha$, respectively.

The quantity β may be assumed to be small as compared to α, since it gives the contribution to the energy due to rotation of the complete system, which corresponds to a much smaller

velocity than that of the orbital motion of the particle. Thus $\theta/(1-\theta)$ is probably greater than β/α and $\gamma>0$. According to the section on C^{13}, N^{13} the characteristic values of the interaction energy would then be $E=-\gamma$ for $J=\frac{1}{2}$ and $E=\frac{1}{2}\gamma$ for $J=1\frac{1}{2}$ arising from $K=1$. Thus the ground state would correspond to $J_0=\frac{1}{2}$ and, since K values are not mixed, $a_0=0$, $a_1=1$ (Eq. (2)).

For $\gamma<0$, the situation is exactly the same as for C^{13} etc., and $J_0=1\frac{1}{2}$, $b_2=0$, $b_1=1$.

Be^9, B^9; $\Lambda=1$, $K=1$

In this system, the proton or neutron has a node through the two α-particles; this corresponds to an angular momentum, $\Lambda=1$, about the body-fixed ζ axis. Therefore the greater part of the interaction energy is (since $\alpha\gg\beta$; see the section on N^{15}, O^{15}) $V=-\alpha(\Lambda\cdot S)$, $\alpha>0$.

In order to calculate this energy matrix, the spin vector, S, with components S_x, S_y, S_z in space must be projected on the body-fixed ζ axis by means of the direction cosines D (see Section 1). This projection, S_ζ, is given by

$$S_\zeta=\sum_{j=x,\,y,\,z}D_{\zeta j}S_j,$$

which yields

$$(\Lambda\cdot S)=\Lambda S_\zeta=\Lambda\sum_j D_{\zeta j}S_j$$

and

$$(K\ \ m,\Lambda,\sigma\,|\,(\Lambda\cdot S)\,|\,\sigma',\Lambda',m',K')=\delta_{\Lambda}{}^{\Lambda'}\Lambda\sum_j(K,m,\Lambda\,|\,D_{\zeta j}\,|\,\Lambda,m',K')(\sigma\,|\,S_j\,|\,\sigma'),$$

since $D_{\zeta j}$ is diagonal in Λ and σ and S_j is diagonal in K, m, Λ. The $(\sigma|S_j|\sigma')$ are the usual spin matrices and the matrix elements of $D_{\zeta j}$ may be obtained from the table of direction cosines.[6] From these and the fact that the energy must be Hermitian,

$$\begin{aligned}(K,m,\Lambda,\sigma\,|\,(\Lambda\cdot S)\,|\,\sigma',\Lambda,m',K+1)&=(K+1,m',\Lambda',\sigma'\,|\,(\Lambda\cdot S)\,|\,\sigma,\Lambda,m,K)\\&=\frac{\Lambda[(K-\Lambda+1)(K+\Lambda+1)]^{\frac{1}{2}}}{(K+1)[(2K+1)(2K+3)]^{\frac{1}{2}}}\\&\quad\times\{\tfrac{1}{2}[(K-m+1)(K-m+2)]^{\frac{1}{2}}\delta_{m-1}{}^{m'}\delta_{\sigma+1}{}^{\sigma'}\\&\quad-\tfrac{1}{2}[(K+m+1)(K+m+2)]^{\frac{1}{2}}\delta_{m+1}{}^{m'}\delta_{\sigma-1}{}^{\sigma'}\\&\quad+\sigma[(K-m+1)(K+m+1)]^{\frac{1}{2}}\delta_m{}^{m'}\delta_\sigma{}^{\sigma'}\},\end{aligned}$$

$$\begin{aligned}(K,m,\Lambda,\sigma\,|\,(\Lambda\cdot S)\,|\,\sigma',\Lambda,m',K)&=\frac{\Lambda^2}{K(K+1)}\{\tfrac{1}{2}[(K+m)(K-m+1)]^{\frac{1}{2}}\delta_{m-1}{}^{m'}\delta_{\sigma+1}{}^{\sigma'}\\&\quad+\tfrac{1}{2}[(K-m)(K+m+1)]^{\frac{1}{2}}\delta_{m+1}{}^{m'}\delta_{\sigma-1}{}^{\sigma'}\\&\quad+\sigma m\delta_m{}^{m'}\delta_\sigma{}^{\sigma'}\}.\end{aligned}$$

In accordance with Section 1, the energy matrix is to be transformed in such a way that it is labeled by J, M and K values. J and M values and those values of K for which $K\neq J\pm\frac{1}{2}$ are not mixed, therefore the matrix will split up into two-dimensional blocks corresponding to fixed values of J, M and to $K=J\pm\frac{1}{2}$. In particular if $V_{KK'}$ are the matrix elements of V corresponding to $K=J-\frac{1}{2}$, $K'=J+\frac{1}{2}$, then for $J=1\frac{1}{2}$, $M=1\frac{1}{2}$; $V_{11}=-\frac{1}{4}\alpha$, $V_{22}=\frac{1}{4}\alpha$, $V_{12}=V_{21}=-\frac{1}{4}3^{\frac{1}{2}}\alpha$.

In order to transform the energy matrix into diagonal form, it is necessary to calculate the a's and b's of Eqs. (1) and (2). The proper functions of the system may be written as $\Psi=b_K\psi_K+b_{K'}\psi_{K'}$. If H is the complete Hamiltonian of the system, and if $H=H_0-\alpha(\Lambda\cdot S)$, H_0 has the proper values E_K, $E_{K'}$ for $K=J-\frac{1}{2}$, $K'=J+\frac{1}{2}$, and the b's (or the a's) may be calculated by substituting $H_0\psi_K=E_K\psi_K$, $H_0\psi_{K'}=E_{K'}\psi_{K'}$ and $\Psi=b_K\psi_K+b_{K'}\psi_{K'}$ in the equation $H\Psi=E\Psi$. Multiplication by ψ_K, $\psi_{K'}$, respectively, and integration yields:

$$\begin{aligned}(V_{KK}-\delta)b_K+V_{K'K}b_{K'}&=0,\\V_{KK'}b_K+(V_{K'K'}-\delta-\epsilon)b_{K'}&=0,\qquad(6)\end{aligned}$$

with $\epsilon=E_K-E_{K'}$; $\delta=E-E_K$.

The condition that b_K, $b_{K'}$ be nontrivial determines the energy correction δ. This is

$$\begin{vmatrix}V_{KK}-\delta & V_{K'K}\\ V_{KK'} & V_{K'K'}-\delta-\epsilon\end{vmatrix}=0.\qquad(7)$$

The ground state has $J_0=1\frac{1}{2}$, for which the energy is given by

$$\delta=-\tfrac{1}{2}\epsilon-\tfrac{1}{2}[\epsilon^2-(\epsilon-\alpha)\alpha]^{\frac{1}{2}}.\qquad(8)$$

The coefficients in Eq. (1b) for this state depend on the ratio ϵ/α, and, since this ratio is not known, the calculations will be made for the extreme cases $-\epsilon\gg\alpha$, $-\epsilon\ll\alpha$.

For $-\epsilon\gg\alpha$ (set $\alpha\approx0$), $\delta\approx-\frac{1}{2}\epsilon-\frac{1}{2}|\epsilon|=0$ since ϵ is negative, and, by Eqs. (6), $b_2=0$. According

to Eq. (2), the normalized wave functions are given by $b_1=1$.

Similarly, Eqs. (6) and (8) may be solved for $\alpha \gg -\epsilon$ with the result that $b_1=\frac{1}{2}3^{\frac{1}{2}}$, $b_2=\frac{1}{2}$.

B^{11}, C^{11}; $\Lambda=1$, $K=1$

These nuclei are assumed to have three α-particles at the vertices of an equilateral triangle and a hole with a nodal plane intersecting the axis of figure. One particle in a state of unsaturated spin is again responsible for the spin-orbit interaction energy. Just as in the case of N^{15}, O^{15} the angular momentum is assumed to be divided between orbital motion in the body-fixed system and rotation of the system as a whole in the ratio $\theta/(1-\theta)$, $0 \leqslant \theta \leqslant 1$. There are then the two contributions to the energy $V_R=-\beta(K\cdot S)(1-\theta)$ and $V_0=\pm\alpha(\Lambda\cdot S)\theta$. The difference between the V_0 of N^{15}, O^{15} and the V_0 here is due to the fact that there is now a definite axis in the body, and the hole has its nodal plane through this axis, that is, its angular momentum about the axis. The sign of V_0 may be determined just as in the case of N^{15}, O^{15} with the simplification that only rotations about the axis of symmetry need be considered. The result is again $V_0=\alpha(\Lambda\cdot S)\theta$. The total interaction is

$$V=V_0+V_R=\alpha(\Lambda\cdot S)\theta-\beta(K\cdot S)(1-\theta).$$

The second term of the interaction energy has been calculated for C^{13}, N^{13} (β is to be replaced by $\beta(1-\theta)$) and it does not mix K values. Therefore the mixing of $K=J_0+\frac{1}{2}$ with $K=J_0-\frac{1}{2}$ will depend entirely on the first term, which has been treated for Be^9, B^9 (α to be replaced by $-\alpha\theta$).

There are again two possibilities for the lowest state; if the term $\alpha\theta(\Lambda\cdot S)$ is the more important term, $J_0=\frac{1}{2}$, and if $-\beta(K\cdot S)(1-\theta)$ is the predominant term, $J_0=1\frac{1}{2}$ for the ground state. These energies may be calculated as for Be^9, B^9; C^{13}, N^{13}, respectively, and the result is that the angular momentum for the ground state is $J_0=\frac{1}{2}$ or $1\frac{1}{2}$, according as $\theta>2\beta/(2\beta+\alpha)$ or $\theta<2\beta/(2\beta+\alpha)$, respectively.

If $\theta<2\beta/(2\beta+\alpha)$, $J_0=1\frac{1}{2}$ and the b's in Eq. (1b) must be calculated as in Eqs. (6) and (7). When $(-\alpha\theta)$ is substituted for α in Eq. (8):

$$\delta=-\tfrac{1}{2}\epsilon-\tfrac{1}{2}[\epsilon^2+(\epsilon+\alpha\theta)\alpha\theta]^{\frac{1}{2}},$$

where ϵ includes not only the separation of rotational levels but also the correction due to $\beta(1-\theta)(K\cdot S)$ or

$$\epsilon=-2\hbar^2/I-2\beta(1-\theta).$$

Eqs. (6) give:

$$b_1^2=\tfrac{3}{4}\frac{(\alpha\theta)^2}{(\alpha\theta)^2-2\alpha\theta\delta+4\delta^2};\quad b_2=-\frac{\alpha\theta-4\delta}{3^{\frac{1}{2}}\alpha\theta}b_1.$$

It seems reasonable to assume that the value of θ appearing here is approximately equal to the θ of N^{15}, O^{15}. It is experimentally known[15] that $J_0=\frac{1}{2}$ for N^{15}; this is possible only if $\theta>\beta/\alpha$. It is still possible, however, for the total angular momentum of B^{11}, C^{11} to be $1\frac{1}{2}$ if θ satisfies the condition $\beta/\alpha<\theta<2\beta/(2\beta+\alpha)$. Since β/α is small, the limits are narrow, and it may be assumed that $\theta=(4/3)\beta/\alpha$ (for convenience) with very little error. A value of θ of this order of magnitude is consistent with the fact that the exchange forces for a hole are small,[2] and therefore correspond to a small orbital velocity.

It is again necessary to know the ratio ϵ/α. For $-\epsilon \gg \alpha$, $b_1\approx 1$, $b_2\approx 0$; and for $-\epsilon\approx\beta\ll\alpha$, $b_1\approx 2/7^{\frac{1}{2}}$, $b_2\approx -(3/7)^{\frac{1}{2}}$. The actual values should lie between these two estimates which are valid for β/α not much greater than 0.1.

For $\theta>2\beta/(2\beta+\alpha)$, $J_0=\frac{1}{2}$ and the coefficients in Eq. (1a) become $a_0=0$, $a_1=1$.

4. Magnetic Moments

For the calculation of the magnetic moments, all that is needed now are the g factors. When these are given, they may be substituted in Eqs. (5a) or (5b) after applying the results of Section 3.

In order to calculate the g factors due to rotation, it will be assumed for simplicity that the added particle or hole is uniformly distributed over the system of α-particles with the result that the g factor for pure rotation of the system is given by the ratio of total charge to total mass. The g factor for orbital motion is one for a proton and zero for a neutron, and that for spin is given by twice the magnetic moment μ_τ or μ_σ as the case may be. The magnetic moments are given in the adjoining table in units of nuclear magnetons, $\mu_0=e\hbar/2M_0c$ (M_0 = mass of proton), but several require special attention.

The identification of the θ of N^{15}, O^{15} with that of B^{11}, C^{11} gave $\theta \approx (4/3)(\beta/\alpha)$ if $J_0 = \frac{1}{2}$ and $1\frac{1}{2}$ for N^{15}, O^{15} and B^{11}, C^{11}, respectively. Since β/α is small, θ has been assumed to be zero in giving the magnetic moments for this case. The g factors of these four nuclei depend on the distribution of angular momentum between orbital and rotational motion and are given by:

$$N^{15}: g_l = g_s = \theta + (7/15)(1-\theta),$$
$$O^{15}: g_l = g_s = (8/15)(1-\theta),$$
$$B^{11}: g_l = \theta + (5/11)(1-\theta),\ g_s = 5/11,$$
$$C^{11}: g_l = (6/11)(1-\theta),\ g_s = 6/11.$$

For B^{11}, C^{11} with $J_0 = 1\frac{1}{2}$, the magnetic moments have been listed for all ϵ between $-\epsilon = \beta$ and $-\epsilon \gg \alpha$.

The magnetic moments of Be^9, B^9 are given in Table I for $\alpha \gg |\epsilon|$, $\alpha \ll |\epsilon|$. The α-particle model then predicts that the actual magnetic moments should lie between these two extremes, and the experimental values may be used to determine the ratio ϵ/α.

5. F^{19}, Ne^{19}

The considerations of Hafstad and Teller did not include the nuclei F^{19}, Ne^{19}; since the magnetic moment of F^{19} has been measured,[12] it is of interest to extend the calculations to these nuclei, which consist of five α-particles minus a proton and neutron, respectively. The arrangement of the five α-particles is such that three are at the vertices of an equilateral triangle and the other two are placed one above and the other below the plane of the triangle. In order to set up the invariant wave functions of the hole, it is necessary to consider rotations of $2\pi/3$ about the axis connecting the two α-particles and reflection in the plane of the three α-particles.

If the three α-particles in the plane are labeled 1, 2, 3 and the other two, 4, 5, and if the proper function of the hole on the ith α-particle is φ_i, the orbitals for a given neutron (proton) may be written as

$$\psi_1 = \varphi_1 + \varphi_2 + \varphi_3,$$
$$\psi_2 = \varphi_1 + e^{2\pi i/3}\varphi_2 + e^{-2\pi i/3}\varphi_3,$$
$$\psi_3 = e^{2\pi i/3}\varphi_1 + e^{-2\pi i/3}\varphi_2 + \varphi_3,$$
$$\psi_4 = \varphi_4 + \varphi_5,$$
$$\psi_5 = \varphi_4 - \varphi_5.$$

Since ψ_1 and ψ_4 are invariant under rotation by $2\pi/3$ about the axis of symmetry and under reflection in the plane of symmetry, any linear combination of them is invariant under these operations. They will thus be mixed by the true Hamiltonian to form two states, one with no nodes and the other with two nodal planes, one above and one below the plane of symmetry. Since the other orbitals have one nodal plane and the hole is to be put into the state of highest

[12] J. M. B. Kellogg, I. I. Rabi, N. F. Ramsey, Jr., J. R. Zacharias, Bull. Am. Phys. Soc. **13**, 7, 10 (1938).

TABLE I. *Spins and magnetic moments of the light nuclei by the α-particle model. The last column contains the results of the Hartree model for the magnetic moments and for those values of J_0 (in parentheses) which are different in the two models. All magnetic moments are given in units of nuclear magnetons. The results of the Hartree model are taken from Rose and Bethe, reference 3, with the numerical values corrected to $\mu_s = 2.78$, $\mu_v = -1.75$.*

NUCLEUS	J_0	MAGNETIC MOMENT	α-MODEL	HARTREE MODEL
Li^7	$1\frac{1}{2}$	$\mu_s + 3/7$	3.21	3.08
Be^7,	$1\frac{1}{2}$	$\mu_s + 4/7$	−1.18	−1.05
Be^9	$1\frac{1}{2}$	$\mu_v + 2/9 < \mu < (3/5)\mu_v + 1/3$	$-1.53 < \mu < -0.7$	−1.40
B^9	$1\frac{1}{2}$	$(3/5)\mu_s + 0.87 < \mu < \mu_s + 7/9$	$2.55 < \mu < 3.56$	3.43
B^{11}	$\frac{1}{2}$	$-(1/3)\mu_s + (2/33)(3\theta+5)$	-0.44 $(\theta=1)$	
B^{11}	$1\frac{1}{2}$	$(1/3)\mu_s + 0.57 < \mu < \mu_s + 5/11$	$1.5 < \mu < 3.2$ $(\theta=0)$	3.43
C^{11}	$\frac{1}{2}$	$-(1/3)\mu_v + (2/11)(2-\theta)$	0.77 $(\theta=1)$	
C^{11}	$1\frac{1}{2}$	$\mu_v + 6/11 < \mu < (1/3)\mu_v + 0.68$	$-1.2 < \mu < 0.1$ $(\theta=0)$	−1.40
C^{13}	$1\frac{1}{2}$	$\mu_v + 6/13$	−1.29	1.05 $(J_0=\frac{1}{2})$
N^{13}	$1\frac{1}{2}$	$\mu_s + 7/13$	3.32	−0.73 $(J_0=\frac{1}{2})$
N^{15}	$1\frac{1}{2}$	$\mu_s + 7/15$	3.25	
N^{15}	$\frac{1}{2}$	$-(1/3)\mu_s + (2/45)(8\theta+7)$	-0.62 $(\theta=0)$	−0.26
O^{15}	$1\frac{1}{2}$	$\mu_v + 8/15$	−1.22	
O^{15}	$\frac{1}{2}$	$-(1/3)\mu_v + (16/45)(1-\theta)$	0.94 $(\theta=0)$	0.59
O^{17}	$\frac{1}{2}$	μ_v	−1.75	
F^{17}	$\frac{1}{2}$	μ_s	2.78	
F^{19}	$\frac{1}{2}$	μ_s	2.78	
Ne^{19}	$\frac{1}{2}$	μ_v	−1.75	

energy, which is the one with the greatest number of nodes, it will be in the second of the above mixed states. This state is nondegenerate and the orbital remains unchanged under a rotation around the figure axis. Since the total eigenfunction must be symmetric under all those rotations which correspond to an exchange of α-particles, it is seen that the state $\Lambda=0$, and therefore $K=0$ is allowed. Therefore $J_0=\frac{1}{2}$ and:

$$F^{19}: \mu=\mu_r,$$
$$Ne^{19}: \mu=\mu_r.$$

The experiments that have been made[12] on F^{19} give $J_0=\frac{1}{2}$, but the magnetic moment is somewhat smaller than predicted. In order to explain this by the pure α-particle model, a more detailed account must be taken of the spin-orbit interaction. The interaction that has been used here does not mix the state with angular momentum $J=\frac{1}{2}$ arising from $K=0$ with the state $J=\frac{1}{2}$ which arises from the higher rotational level $K=1$. However, if the centrifugal terms which have been neglected[9] are taken into account, these two states of the same symmetry may be mixed. Since the state $J=\frac{1}{2}$ arising from $K=1$ has a negative magnetic moment (just as for N^{15}, B^{11}), any slight mixing will decrease the magnetic moment in the ground state.

Conclusion

The numerical results in the table of magnetic moments are given for $\mu_r=2.78$ [12] and $\mu_p=-1.75$.[13] The results of the Hartree model as given by Rose and Bethe[14] are given in the last column of the table for comparison. The Hartree model gives the same angular momenta and approximately the same magnetic moments for all nuclei except C^{13}, N^{13}. Rose and Bethe give different angular momenta in the ground state for these nuclei with the result that the magnetic moments are much different. However, in the α-model, the state $J=\frac{1}{2}$ is very close to the ground state, $J_0=1\frac{1}{2}$, since the separation is of the order of magnitude of β.

It has already been pointed out[4] that the α-particle value of the magnetic moment of Li^7 is somewhat better than that given by the Hartree model. The two models agree with each other and with experiment in the case of F^{19}. The value of the spin of N^{15} also is in agreement with experiment,[15, 16] but the magnetic moment has not yet been measured.

The results of the α-model for B^{11}, Be^9 may be made to fit a large range of possible values by a suitable choice of θ and α/ϵ, whereas the results given for the Hartree model are unambiguous. However, it must be pointed out that the calculations[3] by the Hartree model do not take into account the mixing of P and S states due to spin-orbit coupling. This has been considered here and is completely responsible for the arbitrariness of the result.

The author wishes to thank Professor E. Teller for the suggestion of the problem and both Professor Teller and Dr. M. Goeppert-Mayer for many very valuable discussions.

Note added in proof.—The recent measurement of the magnetic moment of Be^9 by Kusch, Millman and Rabi[17] comes well within the range of possible values given by the α-model if the spin is assumed to be $1\frac{1}{2}$.

[13] This value is based on the mixing of S and D states in the deuteron as calculated by J. Schwinger, and makes use of the magnetic moments of the proton and deuteron as given in reference 12. The author wishes to express his appreciation to J. Schwinger for giving him this result before publication.

[14] See reference 3. Rose and Bethe assumed $\mu_r=2.85$, $\mu_p=-2.0$; however, the values given in Table II have been corrected to $\mu_r=2.78$, $\mu_p=-1.75$ for comparison.

[15] R. W. Wood and G. H. Dieke, J. Chem. Phys. **6**, 908 (1938).

[16] On the assumption that $\theta>\beta/\alpha$; see the section on N^{15}.

[17] P. Kusch, S. Millman and I. I. Rabi, Phys. Rev. **55**, 666 (1939).

The Inner, Initial, Magnetic Permeability of Iron and Nickel at Ultra-High Radiofrequencies

JUSTIN L. GLATHART
University of Chicago, Chicago, Illinois

(Received January 30, 1939)

A new method for the measurement of the ultra-high frequency, initial, inner permeability of ferromagnetic materials has been developed which gives much greater accuracy and is much faster than the older methods. The probable error is under one percent at a frequency of 197 megacycles per second, as contrasted with previous methods in which the error is of the order of 10 to 20 percent. This improvement is due to three factors: (1) the use of a coaxial cable instead of Lecher wires, (2) the use of a fine central wire and (3) correction for the influence of the finite conductivity of the resonance system. The magnetic permeability of high purity, commercial iron wire was found to be 53.8 ± 0.3 at 1.97×10^8 cycles per second, and 25°C. It was constant for all values of tension up to the breaking point of the wire at 980 grams force. It also remained constant for superimposed longitudinal magnetic fields up to 100 oersteds. The permeability of commercially pure nickel was found to be 3.61 ± 0.08 at the same frequency and temperature. As the temperature was raised the permeability increased to a value of 12.22 at 320°C, beyond which it dropped rapidly to unity at 370°C.

INTRODUCTION

THE magnetic properties of ferromagnetic materials at high radiofrequencies have been studied by a number of investigators.[1] The various methods used have proved to be both tedious and inaccurate; the precision in some cases is no better than 10–20 percent. With the object of alleviating these difficulties the method described below has been developed. With this method results accurate to within 0.5 percent can be obtained in a much shorter time.

A survey of the previous work in this field showed considerable discrepancies in the published values of initial permeability of iron and nickel in both the high frequency and the ultra-high frequency ranges. A number of factors might be responsible for these discrepancies, e.g., the purity of the sample, its previous heat and mechanical treatment as well as magnetic history, its tension, temperature, susceptibility to external magnetic fields, etc. The work reported here deals with the effect of external magnetic fields and changes in tension on the initial permeability of commercially pure iron wire, and the effect of temperature on the permeability of commercially pure nickel wire.

[1] (a) W. Arkadiev, Physik. Zeits. **22**, 511 (1921); (b) C. Gutton and Mme. I. Mihul, Comptes rendus **184**, 1234 (1927); (c) G. R. Wait, F. G. Brickwedde and E. L. Hall, Phys. Rev. **32**, 967 (1928); (d) J. B. Hoag and H. Jones, Phys. Rev. **42**, 571 (1932); (e) J. Müller, Zeits. f. Physik **88**, 143 (1934); (f) G. Potapenko and R. Sänger, Zeits. f. Physik **104**, 779 (1937).

Standing waves were set up in a coaxial cable resonating system by means of a frequency and intensity stabilized oscillator operating at approximately 197 megacycles per second. Two similar cable systems were used, in one of which the central conductor was a nonmagnetic wire (copper). In the other cable the central conductor was the magnetic wire (iron or nickel) whose permeability was to be determined. In the case of the latter, the resonance peaks were closer together than those obtained with the nonmagnetic cable. From this wave-length shortening and the known constants of the cable, such as tube and wire radii and electrical conductivity, the permeability of the magnetic sample could be deduced as follows.

THEORY

The coaxial cable has an inductance per unit length given by[2]

$$L = 2 \log (b/a) + (1/2\pi)[(\rho\mu/\nu a^2)^{\frac{1}{2}} + (\rho'\mu'/\nu b^2)^{\frac{1}{2}}] \text{ e.m.u./cm}, \quad (1)$$

where ν is the frequency of the electrical oscillations, a and b are the radii of the central wire and the outer tube, respectively, of the coaxial cable, ρ and μ are the electrical resistivity and magnetic permeability of the central wire, and ρ' and μ' are the corresponding quantities for the outer tube.

[2] J. J. Thompson, *Recent Researches in Electricity and Magnetism* (Clarendon Press, Oxford, 1893), p. 295.

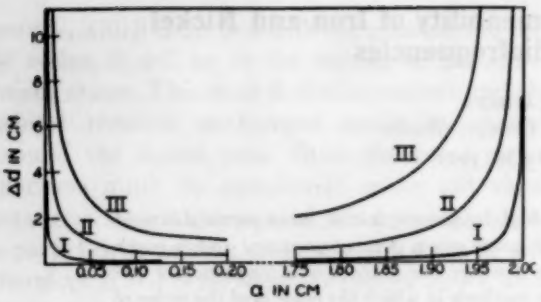

FIG. 1. The wave-length shortening as a function of the radius of the central iron wire of the coaxial cable. I, $d_0=25$ cm, $\mu=23$; II, $d_0=76$ cm, $\mu=53.8$; III, $d_0=150$ cm, $\mu=64$. In all cases $b=2$ cm, $\rho=10^4$.

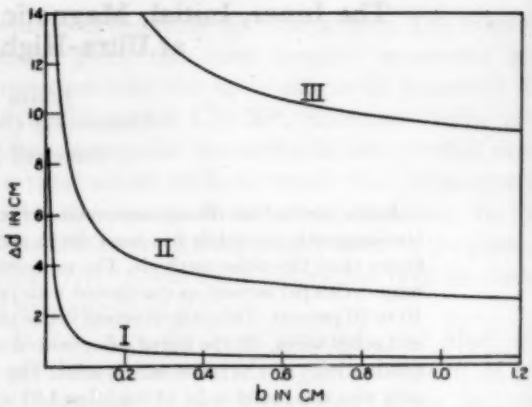

FIG. 2. The wave-length shortening as a function of the radius of the outer tube of the coaxial cable. I, $d_0=25$ cm, $\mu=23$; II, $d_0=76$ cm, $\mu=53.8$; III, $d_0=150$ cm, $\mu=64$. In all cases, $a=0.01$ cm, $\rho=10^4$.

Equation (1) may be written in the form

$$L=L_a+L_i, \tag{2}$$

where $L_a=2\log(b/a)$. This depends only on the cable dimensions, while L_i involves the resistivities and permeabilities in addition. From the equation for the velocity of electromagnetic waves in free space, $c=\nu\lambda_0$, and the equation for the velocity of propagation along the cable system, $v=1/(LC)^{\frac{1}{2}}$, together with the expression for the capacitance of the cable per unit length, $C=\epsilon/[2\log(b/a)]$, an equation may be derived for the *inner*, initial permeability of the central wire. When the outer tube is of nonmagnetic material, a term in this equation, $(a/b)(\rho'/\rho)^{\frac{1}{2}}$, may be neglected, provided the radius of the central wire, a, is small compared to that of the outer tube, b. In the actual cable used in the present investigation this term amounted to only 0.07 percent of the whole. Introducing the symbols $d_0=\lambda_0/2$ and $d=\lambda/2$ for the half-wavelengths in free space and along the cable, respectively, the final equation for the inner permeability may be written[3]

$$\mu=1.256\frac{a^2}{\rho}\left(\log_{10}\frac{b}{a}\right)^2\frac{(d_0^2-d^2)^2}{d_0d^4}\times10^{13}. \tag{3}$$

OPTIMUM CABLE DIMENSIONS

Since μ depends upon higher powers[4] of d and d_0-d, not only must the wave-lengths d and d_0 be accurately measured but also $d_0-d\equiv\Delta d$, the wave-length shortening, should be made as large as possible. As shown below, Δd depends upon the cable dimensions and can be made as large as necessary by a proper choice of a and b.

If Eq. (3) is solved for Δd we have

$$\Delta d=d_0\left\{1-\left[\frac{3.544a\log_{10}(b/a)\times10^6}{(\mu\rho d_0)^{\frac{1}{2}}+3.544\times10^6a\log_{10}b/a}\right]^{\frac{1}{2}}\right\}. \tag{4}$$

It can be seen that Δd approaches a maximum equal to d_0 itself as the term in the square brackets approaches zero. If ρ, μ and d_0 are taken as constants, this occurs as $a\to0$, $a\to b$, or $b\to0$.

Figure 1 shows Δd as a function of a for an outer tube radius of two cm.[5] The dependence of Δd upon b, the radius of the outer tube, is shown in Fig. 2. From these curves it can be seen that the best form of resonance cable, from the point of view of large Δd, would consist of a small capillary bore tube having an extremely fine wire stretched along its axis. From a practical standpoint, however, other factors enter the problem, such as the necessity for maintaining adequate insulation between the cable elements, the difficulty of insuring their accurate concentricity, the desirability of low electrical resistance, and the necessity for the introduction of a movable shorting piston.

The cable system finally adopted consisted of

[3] The analysis given here follows the same steps as that in the article by Hoag and Jones but is applied to a coaxial rather than a Lecher wire resonance system.

[4] When d is approximately equal to d_0 Eq. (3) reduces to

$$\mu=\frac{k(d_0-d)^2(d_0+d)^2}{d_0d^4}\doteq k'\frac{(\Delta d)^2}{d^2},$$

where k and k' are constants for a given cable.

[5] The values of μ used in computing Δd are the approximate values of Hoag and Jones, reference 1(d), and of Hoag and Gottlieb, Phys. Rev. 55, 410 (1939).

a conveniently large tube, nearly two cm in radius, along the axis of which was stretched a fine wire (radius 0.009 cm) of the material under test. This gave a value for Δd of about three cm in the case of iron, which could be measured with sufficient accuracy. Also such a cable fulfilled the practical requirements mentioned above and justified the neglect of the term $(a/b)(\rho'/\rho)^{\frac{1}{2}}$, which simplified the final equation.

Although, in this investigation, a single wave-length was used throughout, it is of interest to know the manner in which Δd varies with the wave-length. Fig. 3 shows this relationship for several selected values of a, when b remains equal to two cm in all cases. At wave-lengths of several meters the shortening amounts to 30 or 40 cm or more.

Determination of the Wave-Length of the Oscillator

A nonmagnetic coaxial resonance cable was used to obtain the true wave-length of the oscillator. However, the distance between successive resonance peaks is the half-wave-length in free space only when the cable system is of infinite conductivity. This is easily seen if Eq. (4) is written in the form

$$d_0-d=d_0\left[1-\left(\frac{k}{(\rho d_0)^{\frac{1}{2}}+k}\right)^{\frac{1}{2}}\right] \qquad (4')$$

where μ has been taken as unity, $k=3.544\times10^{6}a\log_{10}(b/a)$, and d_0-d is the half-wave-length shortening obtained with the nonmagnetic cable. Evidently $d=d_0$, i.e., the cable yields the true half-wave-length, only when $\rho=0$. This resistance shortening is appreciable even for a copper cable. Fortunately, however, Eq. (4') enables its value to be determined. The measured value, d, is related to the true half-wave-length by the equation

$$d=d_0\left(\frac{k}{(\rho d_0)^{\frac{1}{2}}+k}\right)^{\frac{1}{2}}. \qquad (5)$$

This can be computed for various values of d_0 and a curve plotted, from which the value of d_0 corresponding to any measured d can be read directly. For the cable described above, the difference between the measured and true values of the half-wave-length amounted to 0.21 cm at $d=76$ cm.

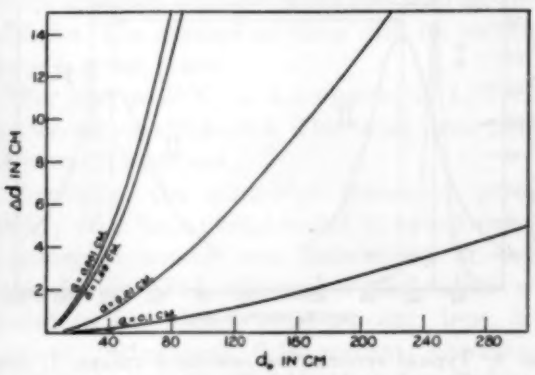

Fig. 3. The wave-length shortening as a function of the wave-length, for iron central wires of various radii. The outer tube radius is 2 cm in all cases.

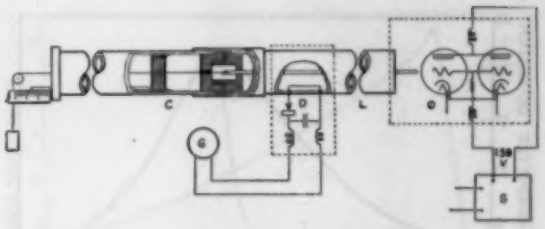

Fig. 4. Diagram of apparatus.

Apparatus

The arrangement of the apparatus used is shown in Fig. 4. The ultra-high frequency oscillator is shown at O. S is a voltage stabilizer used to maintain a constant plate voltage. The coaxial resonance cable, C, was coupled inductively to the oscillator by means of a concentric lead L, which contained a longitudinal slot for the introduction of the pick-up wire of the crystal detector circuit D. The latter was connected to a galvanometer whose deflections, plotted as a function of the position of the movable shorting piston in the resonance cable, yielded the desired resonance curves.

For measurements at high temperatures the resonance cable was surrounded along its entire length by a tubular, wire-wound, noninductive, resistance furnace, the temperature of which could be held constant at any desired value during the course of a run.

Discussion

The coaxial resonance system possesses, for this kind of work, a number of distinct advan-

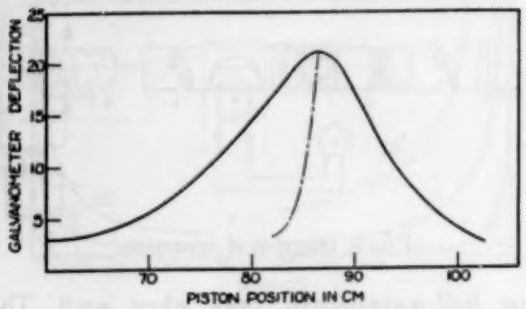

FIG. 5. A single resonance peak showing one type of asymmetry.

tages over an open type of system such as Lecher wires. The most important of these is that, if properly proportioned, it will yield large values of Δd, which enables a much greater accuracy to be attained than has hitherto been possible. The time required to take the necessary data and compute a result has been reduced from two or three hours to 30 or 40 minutes, because of the simple form of the final equation. Since a coaxial line causes less attenuation than an open system the successive resonance peaks do not decrease in height so rapidly nor broaden out so greatly as with an open wire line, thus again facilitating accurate location of the resonance peaks. The closed coaxial system eliminates difficulties caused by coupling between the resonance system and external objects in the room, and so has great stability. Practically perfect reflection of the waves can be attained with a simple form of metallic piston, obviating the necessity for large plate bridges or double bridges. Finally, the sample is used in the form of a single fine wire which is decidedly more convenient than the large rods required by previous methods.[6]

It was necessary that the oscillator be exceedingly stable, both as regards frequency and intensity. This was secured by stabilizing the plate potential by means of a Street and Johnson circuit,[7] with constants adjusted for the comparatively low voltage and large current required. When properly adjusted this stabilizer circuit held the plate potential constant at 158 volts even when the line voltage was changed by as much as 15 or 18 volts.

Because the resonance peaks, especially the second ones, were too broad to permit their tips to be located with the desired degree of accuracy, d_0 and d were determined by measuring the distance between the median lines of successive resonance peaks rather than the distance between their tips. This required that each of the peaks be symmetrical about a vertical line through its tip. Laville[8] has shown, for the similar case of Lecher wires, that this condition of symmetry is also necessary in order to get correct values for wave-length. The distance between the tips of successive peaks, if they are asymmetrical, is not the true half-wave-length. Fig. 5 shows one type of asymmetry encountered. Resonance curves showing asymmetry of this type (left-handed asymmetry) gave high values for d or d_0, while those having right-handed asymmetry yielded low values, with respect to the values obtained with symmetrical peaks. To attain this condition of symmetry required a careful adjustment of the relative positions of the various parts of the apparatus, especially of the detector circuit along the coaxial lead.

Figure 6 shows two typical resonance curves, each with two symmetrical peaks. Curve I is for a copper (nonmagnetic) coaxial cable and curve II is for one containing an iron central wire. The wave-length shortening is clearly evident. The intermediate portion of the scale of abscissae, where the galvanometer deflections were zero, has been omitted.

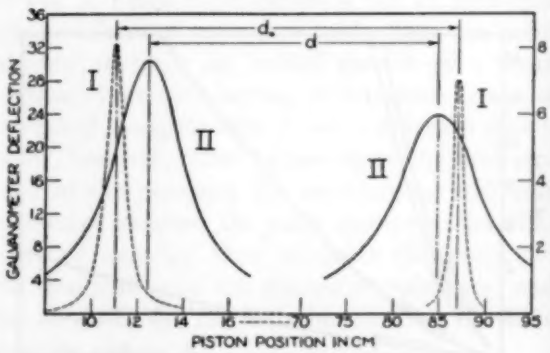

FIG. 6. Typical symmetrical resonance curves. I, nonmagnetic coaxial cable; II, cable with iron central wire.

[6] The method of Potapenko and Sänger, reference 1(j), uses only short wires.

[7] J. C. Street and T. H. Johnson, J. Frank. Inst. **214**, 155 (1932).

[8] G. Laville, Ann. de physique **2**, 328 (1924).

Effect of Changes in Tension

All data from which resonance curves were plotted were taken with the magnetic central wire under a constant tension of about 50 grams force, which was sufficient to keep the wire taut. In the case of iron wire an investigation was made of the effect of variation in tension upon the permeability. A number of runs were made with tensions ranging from 50 grams force to the breaking point of the wire at about one kilogram. The resonance curves at every value of the tension exactly superposed. No change in μ with tension in the range covered was detected.

Effect of an External Magnetic Field

To investigate the effect of an external longitudinal magnetic field upon the permeability of iron wire the resonance cable was completely surrounded by a large solenoid, and fields with intensities ranging from very nearly zero up to 100 oersteds were applied. Here again the resonance curves for all applied field strengths were identical. No change in permeability was noted in the range of field intensities used.

Results

Measurements were made of the permeability of both iron and nickel at room temperature. The iron wire was obtained from a commercial source and was found upon analysis to be 100 percent pure iron within 0.05 percent.

Five separate determinations of the permeability of this wire at room temperature were made at widely different times and with different samples. The average of these with its probable error is given below.

For iron at 25°C, at a frequency of 1.97×10^8 cycles/sec. $\mu=53.8\pm0.3$. This is an uncertainty of about 0.5 percent.

Similarly, the ultra-high frequency permeability of a high purity nickel obtained from a commercial source was determined at room temperature. The analysis of the nickel was found to be: nickel, 99.27 percent; iron, 0.14 percent; manganese, 0.10 percent; chromium, 0.0 percent; and cobalt, trace. In all, seven determinations of the permeability were made, on several different days and with different samples of this wire, which yielded as a mean $\mu=3.61\pm0.08$ for nickel at 27°C and a frequency of 1.97×10^8 cycles/sec. This is an uncertainty of 2.2 percent.

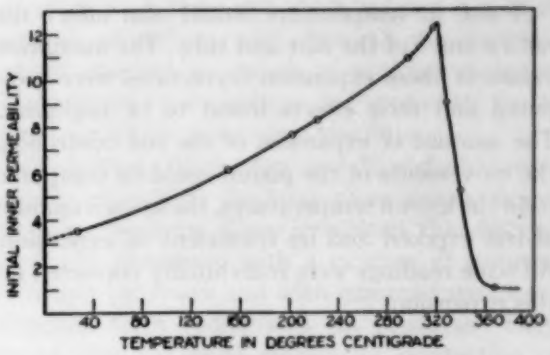

Fig. 7. Inner, initial permeability of nickel, at a frequency of 1.97×10^8 cycles per sec., plotted as a function of temperature.

Permeability of Nickel as a Function of Temperature

The nickel wire was subjected to temperatures ranging from 27°C to 368°C, the latter of which is beyond the Curie point for nickel, and the permeability measured at these and intermediate temperatures. The initial permeability as a function of temperature is shown by the curve of Fig. 7.

The points on this curve represent readings taken on two successive days with different samples of the nickel wire. The wave-length of the oscillator was measured several times during the course of these readings and although it was practically constant, each nickel resonance curve was compared with its corresponding copper curve. By assuming the slight variations in wave-length to be due entirely to experimental error in measurement, the wave-length λ_0 was found to be equal to 151.89 ± 0.04 cm. This is an uncertainty of 0.026 percent.

As may be seen from Eq. (3), the resistivity of the nickel wire had to be known for every temperature at which μ was to be determined. The resistivity *vs.* temperature curve was determined by a separate experiment. The wire was put in place in the cable and all conditions were made similar to those under which μ was measured.

A rise in temperature would also affect the radii a and b of the wire and tube. The maximum values of these expansion corrections were computed and their effects found to be negligible. The amount of expansion of the rod controlling the movements of the piston could be computed from the known temperatures, the known amount of rod exposed and its coefficient of expansion. All scale readings were individually corrected for this expansion.

Velocity of the Waves Along the Cable

From the accepted value for the velocity of the electromagnetic waves in free space, $c=2.99775\times10^{10}$ cm/sec., and the true wave-length of the oscillator, $\lambda_0=151.89$ cm, the frequency of the latter was found to be 1.9736×10^{8} cycles/sec. This combined with the measured wave-lengths along the cables containing copper, nickel and iron wires gave for the velocities of wave propagation along these cables at room temperature the following results. The velocity along the copper wire cable proved to be 2.993×10^{10} cm/sec., that along the nickel wire cable was 2.964×10^{10} cm/sec., and that along the iron wire cable was 2.936×10^{10} cm/sec. These differ from the wave-length in free space by 0.17 percent, 1.13 percent and 2.06 percent, respectively.

I wish to express my sincere appreciation to Professor J. Barton Hoag for suggesting this problem and for his encouragement and advice during the progress of the investigation. For the chemical analysis of the iron and nickel wire I am indebted to Mr. Alfred Klapperich.

MAY 1, 1939 PHYSICAL REVIEW VOLUME 55

On the Creation of Pairs or Positrons by Fast Electrons

H. R. Crane and J. Halpern
University of Michigan, Ann Arbor, Michigan

(Received March 20, 1939)

By means of the cloud chamber a search was made for the creation of pairs or positrons by electrons of energies between one and 12 Mev, in air, mica, lead and platinum. A total of 2588 traversals of electrons through solid materials, and a total track length of 628 meters in air were examined. The abnormally large cross section for the process, as reported in numerous papers by other workers, was not confirmed. The data found point toward agreement with the theoretical calculations. A test for an anomaly at the threshold (one Mev) was not attempted, because of the difficulty of making a decisive experiment in a cloud chamber under conditions in which the pairs formed would have very small energy. A resumé of the literature on the subject of pair and positron formation by electrons, and a rather full discussion of the possibilities for error in the experimental method are given.

Introduction

A NUMBER of papers are now on record in which it is stated by the authors that the cross section for the creation of pairs by electrons is much higher than that predicted by theory. During the course of experiments carried out in this laboratory[1–5] a great many cloud-chamber photographs have been accumulated which show the passage of high energy electrons through thin sheets of absorbing materials and through air. We have recently examined these photographs for the creation of pairs by the high energy electrons, and are in a position to compare our findings with those of other workers. Because the literature on the subject is rather scattered, the following resumé will be of convenience.

Experiments

Skobeltzyn,[6] in 1934, was the first to report the production of pairs by electrons. He observed

[1] J. J. Turin and H. R. Crane, Phys. Rev. **52**, 63 (1937).
[2] J. J. Turin and H. R. Crane, Phys. Rev. **52**, 610 (1937).
[3] A. J. Ruhlig and H. R. Crane, Phys. Rev. **53**, 618 (1938).
[4] D. S. Bayley and H. R. Crane, Phys. Rev. **52**, 604 (1937).
[5] M. M. Slawsky, Thesis, University of Michigan, 1938, unpublished.

[6] D. Skobeltzyn, Nature **133**, 23 (1934).

several pairs which were produced by the passage of electrons of slightly over one Mev energy through nitrogen gas in a cloud chamber. He concluded that the probability for the event was much greater than that given by the theory. The total track length observed was several hundred meters.

Alichanow and Kosodaew[7] measured the energies of electrons and positrons emitted from a Ra(B+C) source by means of a magnetic analyzer. They surrounded the Ra(B+C) with aluminum and determined the number of positrons as a function of the thickness of aluminum. They found that an appreciable number of positrons was produced by the action of the beta-rays on the aluminum, and that positrons were also produced by pair-internal conversion in the radioactive atoms. The number of positrons produced in the aluminum was estimated at 20 to 50 percent of the number produced by internal conversion, but no absolute cross section was given.

Skobeltzyn and Stepanowa[8] placed a radium source in a cloud chamber and surrounded it with a thin layer of glass and lead. They observed about 30 positrons, which was 0.02 to 0.04 positron per disintegrating atom in the source. Because this was far greater than expected theoretically they proposed that the positrons were produced by the action of the beta-rays on the material surrounding the radium, and that a new mechanism must be involved.

Skobeltzyn and Stepanowa,[9] in reporting a continuation of their experiments give evidence that the cross section for production of positrons by electrons of one to three Mev energy is of the order 10^{-22} cm^2 in lead and varies as the atomic number. This was based upon 130 positron tracks obtained in 1650 cloud-chamber photographs.

Skobeltzyn and Stepanowa,[10] in a further publication, reported that positrons were produced in abundance when fast electrons were allowed to strike a piece of carbon. They placed a carbon filter three mm thick in front of a small amount of radium, and observed the electrons which emerged by means of a cloud chamber. They found one positron for every 10 to 20 electrons which penetrated the filter.

Alichanow, Alichanian and Kosodaew[11] were unable to confirm the large cross section found by other workers. They irradiated thin foils of lead and aluminum with a mixture of gamma-rays and beta-rays and with gamma-rays alone, obtained from radon and its products. They found that the cross section for production of positrons (or pairs) by the gamma-rays of RaC was at least several times greater than the cross section for their production by the beta-rays of RaC, in both lead and aluminum. The experiment was done by means of a magnetic focusing apparatus and coincidence Geiger counters.

Champion[12] observed the passage of electrons through nitrogen gas in a cloud chamber, and in a total length of 200 meters of track along which the electrons had more than one Mev energy, he found no indication of the production of positrons.

Staub[13] carried out a cloud chamber experiment in which the beta-particles were preselected as to energy before entering the chamber, by means of an auxiliary magnet. He searched for pairs or positrons which might have been formed in the material which comprised the window of the cloud chamber. The mean energy of the electrons was 1.9 Mev. No positrons resulted from the passage of 565 electrons through lead weighing 0.23 g per cm^2, 675 electrons through aluminum weighing 0.27 g per cm^2 and 227 electrons through carbon weighing 0.23 g per cm^2. This indicates that the cross section is not larger than the order 10^{-24} for lead and 10^{-25} for aluminum and carbon.

Marques da Silva[14] performed an experiment with a cloud chamber and obtained a cross section of the order 10^{-22} cm^2 for the production of positrons by electrons of energy between 1.1 and 2.2 Mev passing through lead.

Skobeltzyn and Stepanowa[15] again reported

[7] A. I. Alichanow and M. S. Kosodaew, Zeits. f. Physik **90**, 249 (1934).
[8] D. Skobeltzyn and E. Stepanowa, Nature **133**, 565 (1934).
[9] D. Skobeltzyn and E. Stepanowa, J. de phys. et rad. **6**, 1 (1934).
[10] D. Skobeltzyn and E. Stepanowa, Nature **133**, 656 (1934).
[11] A. I. Alichanow, A. I. Alichanian and M. S. Kosodaew, Nature **136**, 719 (1935).
[12] F. C. Champion, Proc. Roy. Soc. **A153**, 353 (1935).
[13] Hans Staub, Helv. Phys. Acta **9**, 306 (1936).
[14] Marques da Silva, Comptes rendus **202**, 2070 (1936).
[15] D. Skobeltzyn and E. Stepanowa, Nature **137**, 272 (1936).

the results of a cloud-chamber experiment. In this instance the electrons from three to five millicuries of radium were pre-selected as to energy by a magnet outside the chamber, so that most of those entering had energies above two Mev. The electrons passed through sheets of lead 0.07 and 0.13 mm thick and of aluminum 0.5 and one mm thick at the center of the chamber. Ten pairs were found in about 1200 tracks. They concluded that beta-rays were more effective in producing pairs in lead than were gamma-rays of the same energy. They also confirmed the production of pairs by electrons in nitrogen gas.

Champion and Barber[16, 17] studied the tracks of electrons in a cloud chamber containing five percent mercury dimethyl vapor and 95 percent nitrogen. They observed the production of pairs, and concluded that it was due to the presence of the mercury, in view of the negative results obtained by Champion for pure nitrogen. The effective cross section for pair production by electrons of greater than one Mev energy in mercury was found to be about 3×10^{-22} cm^2. Their results also indicated that the cross section was greater for electrons having just slightly more than one Mev energy than for electrons of higher energy. They express the opinion that the cross section increases rapidly with atomic number.

Feather and Dunsworth[18] used a new and ingenious method of detecting the formation of low energy positrons by electrons. Beta-rays from *UX* were absorbed in lead, brass and aluminum. Since the materials used were thick, it was expected that most of the positrons formed would be stopped and annihilated within the materials. The resulting pairs of oppositely directed 0.5 Mev quanta were detected by means of coincidence Geiger counters set 180° apart. Their results indicated a cross section of about 1.4×10^{-22} cm^2 per atom of lead, when all electrons above the threshold (one Mev) were considered.*

TABLE I. *Some calculated cross sections for pair formation in lead.*

Energy (Mev)	1.5	2.5	5	10
Gamma-rays (10^{-25} cm^2)	6.5	30	83	144
Electrons (10^{-25} cm^2)	0.1	0.4	1.1	2.5

[16] F. C. Champion and A. Barber, Nature **140**, 105 (1937).
[17] F. C. Champion and A. Barber, Proc. Roy. Soc. **A168**, 159 (1938).
[18] N. Feather and J. V. Dunsworth, Camb. Phil. Soc. Proc. **34**, 435 (1938).

Theoretical values

A number of theoretical papers are available,[19–25] and they are in general agreement among themselves as to the cross section for production of pairs by electrons, under conditions in which the energies of the primary electron and of the pair are large compared to mc^2 and in which the energy of the primary electron is large compared to the energy of the pair formed. Although the extrapolation of the formulae to the comparatively low energies in which we are interested is not strictly permissible, it is to be expected that the cross section will decrease with decreasing energy over the whole range. This view is encouraged by the similarity of the formulae to those for the production of pairs by gamma-rays. It is known that in the latter case there is no anomaly at low energies, even at the threshold. Some calculated cross sections for pair formation in lead by both gamma-rays and electrons are given in Table I.

On the Choice of Experimental Conditions

In deciding upon the thicknesses of material and the energy range of the electrons with which to work, the following points should be kept in mind.

Chance that a pair will emerge from a material

The kinetic energy of a pair is expected to be less than that of the primary electron by *at*

* *Note added in proof.*—Since the time of writing, a paper by R. L. Sen Gupta has appeared (Proc. Phys. Soc. **51**, 355 (1939)) which deals mainly with the scattering of electrons in xenon gas. The author states that in a total track length of 330 meters in a gas mixture containing about 50 percent xenon at atmospheric pressure no pairs were formed. The energy of the electrons was 2.1 Mev ±10 percent.

[19] W. H. Furry and J. F. Carlson, Phys. Rev. **44**, 237 (1933).
[20] L. Landau and E. Lifschitz, Physik. Zeits. Sowjetunion **6**, 244 (1933).
[21] W. Heitler and L. Nordheim, J. de phys. et rad. **5**, 449 (1934).
[22] E. J. Williams, Nature **135**, 66 (1935).
[23] E. C. G. Stueckelberg, Helv. Phys. Acta **8**, 325 (1935)
[24] L. Nordheim, J. de phys. et rad. **6**, 135 (1935).
[25] J. J. Bhabha, Proc. Roy. Soc. **A152**, 559 (1935).

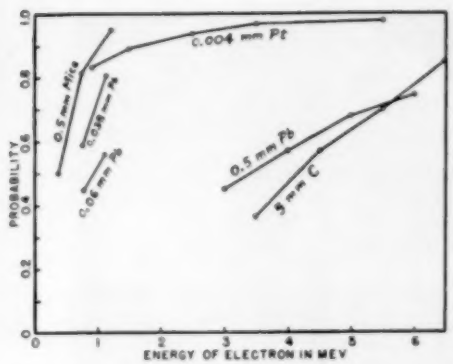

FIG. 1. The probability that an electron will emerge into the visible part of the cloud chamber if it starts at a given depth below the surface of the sheet of solid material and in an initial direction perpendicular to the surface. The kind of material and the depth at which it starts are given for each curve.

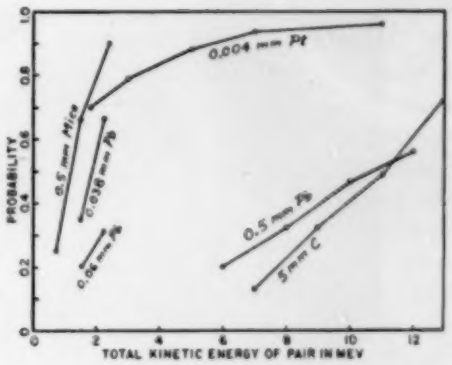

FIG. 2. The probability that both members of a pair will emerge into the visible part of the cloud chamber if the pair starts at a given depth below the surface of the sheet of solid material and in an initial direction perpendicular to the surface. The kind of material and the depth at which the pair starts are given for each curve.

least one Mev, and this is divided between the two members. Therefore if the pair is to have a reasonable chance of emerging from a solid material the primary electron must have much more than one Mev energy. We can give experimental data upon the chance that an electron will emerge, if it starts in a direction normal to the surface at a given depth below the surface. This is obtained by observing electrons which strike absorbing materials in a direction normal to the surface, and recording the relative numbers which apparently fail to pass through. The geometry of the cloud chamber is automatically taken into account, in that the few electrons which emerge in nearly the vertical direction are not seen and are recorded as not emerging. The chance of emergence for a single particle (Fig. 1) is easily transformed into the chance of emergence of both members of a pair in which the energy is divided equally between the two members (Fig. 2). Equal division of energy gives the greatest chance of emergence for the pair, so the curves in Fig. 2 must be considered as upper limits.

Double process

In thick absorbers of high atomic number a double process, in which the primary electron produces a gamma-ray quantum and the quantum produces a pair may become more probable than the direct production of a pair by the electron. Since the cross sections for the separate processes increase as Z^2, that of the double process will increase as Z^4. The probability of the double process will also increase roughly as the square of the thickness of the material (for small thicknesses) and will increase very rapidly with increasing energy of primary electron. A rough calculation indicates that for a 10-Mev electron passing through 0.5 mm of lead the probability of the double process is as large as

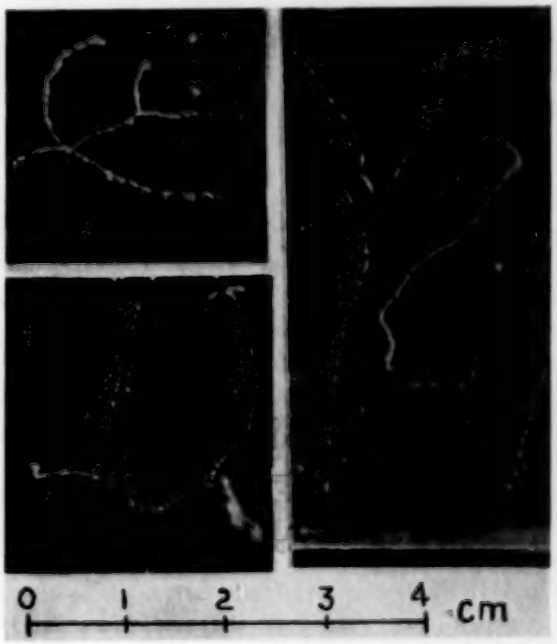

FIG. 3. Typical tracks of very low energy electrons, showing that the scattering by the gas largely masks the effect of the magnetic field. The chamber contained air at atmospheric pressure, and the strength of the field was 600 gauss.

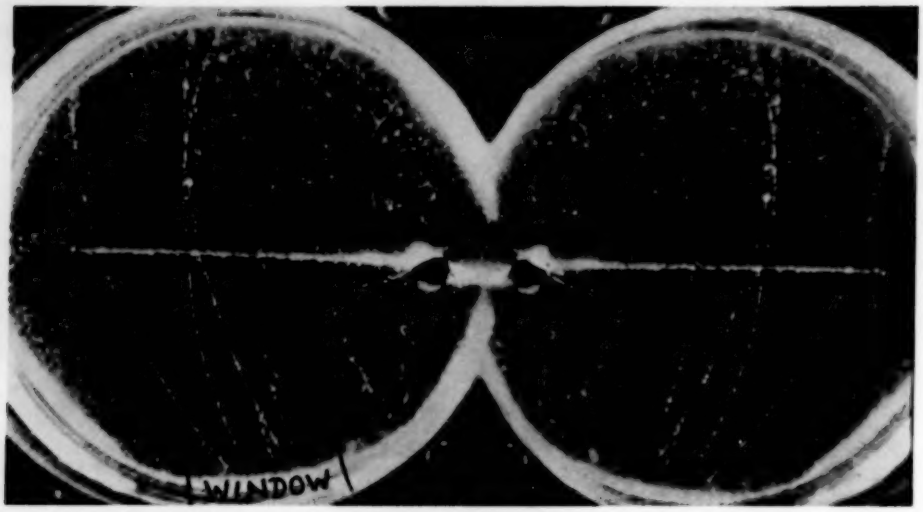

FIG. 4. Typical photograph of the tracks of electrons passing through a sheet of solid material in the center of the cloud chamber. A band of energies is selected by a slit system in the magnetic field outside the chamber. The electrons enter the chamber through a thin aluminum window. $H=1450$ gauss.

the probability of pair formation by the electron directly, as given in Table I. Thus the double process is important only for the highest energy electrons which we have observed (8 to 11 Mev, 0.5 mm lead), and there is no possibility that it could have introduced an error into the results so far reported by other workers.

Low energy pairs originating in a gas

Evidence[16, 17] has suggested an anomalously high probability for the formation of pairs of very low energy (a few thousand ev) by electrons of slightly over one Mev energy. We have decided against performing an experiment of this type ourselves, because of the difficulty of determining the sign of an electron of very low energy. It has been our experience that electrons having less than about two cm range in air ($\sim$33 kev) are so much scattered that the effect of a magnetic field of 500 to 1000 gauss is to a large extent masked. In fact many negative electrons are observed to have "curvatures" which indicate the opposite charge, under these circumstances. Some typical tracks of electrons of a few cm range in air are shown in Fig. 3. The field is 600 gauss, and it is seen that the electrons of higher energy are bent into smooth circles.

Negative electrons moving backwards

Electrons are very often reflected from the wall of the cloud chamber in such a way that they return to the source or to the emergent side of the absorbing material. Reflection coefficients range up to 20 percent for light materials and up to 50 percent for lead, depending, of course, upon the energy. Tracks of reflected electrons will have curvatures indicating that

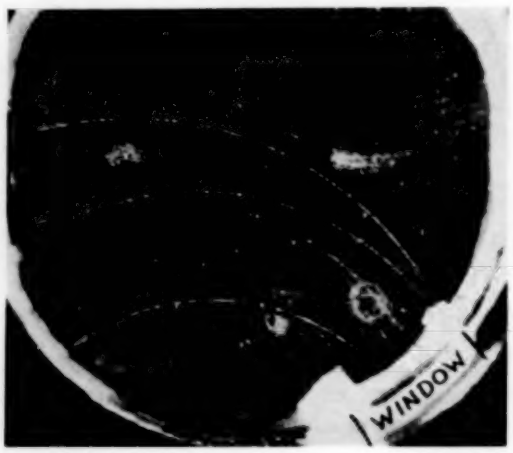

FIG. 5. Typical photograph used for determining the cross section for production of pairs by electrons in passing through air. The slit system and the window are the same as described under Fig. 4. $H=2850$ gauss.

they are positrons, and can easily be mistaken as such. The chance of making this mistake is greatly reduced if an arrangement is used in which the tracks are visible on both sides of the absorbing material, so that a positron or pair can be identified with the particular primary electron which produced it. For this reason we have not considered it worth while to repeat the type of experiment[8–10, 13, 14] in which the absorbing foil comprises part of the wall of the cloud chamber.

Gamma-rays and other confusing influences

When sources are used which emit both beta-rays and gamma-rays, it is difficult to keep the chamber clear of tracks which are due to the gamma-rays. Accidental coincidence in position of these tracks (especially the low energy ones) with the beta-ray tracks can easily indicate falsely the formation of pairs. The same is true even for a pure beta-ray source, if too many tracks are allowed on each picture. We have restricted our experiments to the use of sources which emit no appreciable gamma-radiation and have restricted the number of tracks per picture to between two and four, to avoid this kind of confusion as far as possible.

Experimental Method

Beta-rays from Li^8 or P^{32} were allowed to enter the cloud chamber through a thin aluminum window in the wall. A sheet of lead or other material was placed in the center of the chamber, so that the electrons passed through it nearly normal to the surface. The energy of each particle striking the material was determined by its curvature in the magnetic field. A slit system outside the cloud chamber placed very rough limits upon the energies of the electrons entering the chamber. This was done mainly to eliminate confusion by keeping the unwanted low energy electrons from entering, and not for the purpose of determining the energies, because the latter was done inside the chamber, on the tracks individually. The intensity of the source was so adjusted that only two to four electron tracks appeared on each photograph. Stereoscopic pairs of photographs were taken, by means of a mirror. In examining the photographs only very clear tracks were included in the data, and in order to select them in an unbiased way the following procedure was used for each photograph. A mask was placed over the far half of the chamber (the side on which the electrons emerged from the absorber), and those tracks which appeared to strike the absorber normally and which, particularly, were very clear in the neighborhood of the absorber were chosen. After the curvatures were measured, the mask was removed and the points of emergence on the other side of the absorber were examined for possible pairs or other secondaries.

In searching for pairs produced in the gas by electrons, the same arrangement was used except that no sheet of material was placed in the chamber. The electrons entered through the aluminum window and traveled completely across the chamber, each making a track about 15 cm long. Stereoscopic views of the chamber were not taken in this case.

Figures 4 and 5 show typical photographs taken with each of the two arrangements. These are shown because they give a good idea as to the geometrical conditions and also because it is of great importance in an experiment of this kind for the reader to know the general appearance, clarity and degree of confusion in the photographs, since this determines how easily a pair may escape notice, or how easily a "pair" may be seen where there is none.

Results

Platinum

Five hundred and forty-one electrons were observed to strike a platinum sheet 0.004 mm thick (8.3 mg/cm^2). The numbers of electrons in various energy ranges are given in Table II. No pairs or positrons were observed. It is difficult to place an upper limit upon the cross section when the number of pairs observed is zero. However, the following statement indicates the order of magnitude: We would expect, on the average, one pair to be formed by the

Table II. *Energy ranges of electrons striking platinum.*

Energy (Mev)	1–2	2–3	3–4	4–5	5–6	6–7
Number	73	144	158	86	53	27

TABLE III. *Energy ranges of electrons striking mica.*

Energy (Mev)	1–2	2–3	3–4	4–5	5–6	6–7	7–8
Number	67	59	117	200	167	67	33

TABLE IV. *Energy ranges of electrons passing through air.*

Energy (Mev)	6–8	8–10	10–12
Length (meters)	105	104	31

above group of tracks if the cross section in platinum were 7×10^{-23} cm².

Mica

A total of 710 electrons, having energies as shown in Table III were observed to strike a sheet of mica about 0.5 mm thick (150 mg/cm²). No indication of the formation of a pair or positron was found. We can give some idea as to the limit to be placed upon the cross section by stating that we should have expected one pair if the effective cross section were 4×10^{-25} cm². The mica used was of the form $H_2KAl_3\times(SiO_4)_3$, having an average atomic weight 19 and a density about 3.

Air

A large number of tracks produced by the beta-rays of Li^8 were examined for the production of pairs in air at atmospheric pressure. The total length of the tracks examined was 240 meters, distributed in energy according to Table IV. No pairs or positrons were found. The expectation would be one pair if the cross section were 1×10^{-24} cm². It should be remarked that also in those photographs in which the chamber contained a sheet of solid material, an examination was made for the formation of pairs in the gas, with negative results. The track length examined in this way was 388 meters, distributed in energy according to Table V. Combining the data of Tables IV and V, we can say that we should have found one pair if the effective cross section in air were 4×10^{-25} cm².

TABLE V. *Energy ranges of electrons passing through air.*

Energy (Mev)	1–2	2–4	4–6	6–8	8–10	10–12
Length (meters)	21	72	76	112	82	25

TABLE VI. *Energy ranges of electrons striking lead.*

Energy (Mev)	6–8	8–10	10–12
Number	625	548	164

Lead

We have examined a large number of photographs in which electrons strike a lead sheet 0.5 mm thick. According to Fig. 1 the probability that a pair will emerge from 0.5 mm of lead is very small unless it has several Mev energy. For this reason we have only examined those cases in which the energy of the primary electron is greater than six Mev. It should be kept in mind that the double process, which was mentioned earlier, may produce pairs under these conditions. 1337 tracks were examined, having energies according to Table VI. No pairs or positrons were found in these photographs. We should have expected one pair if the cross section in lead were 5×10^{-25} cm². However, because a pair or positron would not have more than a 50 percent chance of emerging from the lead, we must revise the above figure to about 1×10^{-24} cm².

CONCLUSIONS

As the above data show, we have been unable to find any indication that the cross section for pair formation by electrons is abnormally large, for energies below 12 Mev in substances of either low or high atomic number. The energies of the electrons we have used have, in the main, been greater than those used by the other experimenters. The use of electrons well above one Mev should, for many reasons, give a clearer test for the formation of pairs. However, this same choice of energies makes it impossible for us to offer any information concerning the possibility of an anomaly in the cross section at the threshold, one Mev.

We are grateful to the Rackham Endowment Fund for the financial support of this work.

Neutrons from the Breakup of He^5

H. STAUB* AND W. E. STEPHENS**
W. K. Kellogg Radiation Laboratory, California Institute of Technology, Pasadena, California
(Received March 9, 1939)

The energy spectrum of the neutrons from the disintegration of lithium by 0.8-Mev deuterons has been measured by the method of recoil particles in a high pressure cloud chamber at different stopping powers. A sharp drop in the number-energy curve at 3.8 Mev is interpreted as indicating the maximum energy of the neutrons from the two-stage reaction

$$Li^7+D^2\rightarrow He^4+He^5+14.3 \text{ Mev}, \quad (1)$$
$$He^5\rightarrow He^4+n^1+0.8 \text{ Mev}. \quad (1.0)$$

By measuring the alpha-particle spectrum with an ionization chamber-linear amplifier-counter, the relative number of alpha-particles from (1) gave the relative probability of reaction (1) and hence (1.0) in good agreement with the observed relative number of neutrons.

INTRODUCTION

THE investigation of the energy spectrum of the neutrons from the disintegration of lithium by deuterons is made difficult by the number of reactions taking place and the lack of homogeneity of the emitted neutrons. The following is a summary of the Li(d, n) reactions

$$Li^7+D^2\rightarrow He^5+He^4+14.3 \text{ Mev}, \quad (1)$$
$$He^5\rightarrow He^4+n^1+0.8 \text{ Mev}, \quad (1.0)$$
$$Li^7+D^2\rightarrow Be^8+n^1+15 \text{ Mev}, \quad (2.1)$$
$$^*Be^8+n^1+12 \text{ Mev}, \quad (2.2)$$
$$^{**}Be^8+n+5 \text{ Mev}, \quad (2.3)$$
$$[Li^7+D^2\rightarrow He^4+He^4+n^1+15.1 \text{ Mev}, \quad (3)]$$
$$Li^6+D^2\rightarrow He^5+He^3+0.8 \text{ Mev}, \quad (4)$$
$$He^5\rightarrow He^4+n^1+0.8 \text{ Mev}, \quad (4.0)$$
$$Li^6+D^2\rightarrow Be^7+n^1+3.1 \text{ Mev}, \quad (5)$$
$$[Li^6+D^2\rightarrow He^4+He^3+n^1+1.6 \text{ Mev}. \quad (6)]$$

Neutrons from these reactions were first observed by Crane, Lauritsen and Soltan.[1] Their energy was measured by Bonner and Brubaker,[2] who observed an apparent inhomogeneity of the neutrons except for one group of mono-energetic neutrons giving evidence for the reaction

$$Li^7+D^2\rightarrow Be^8+n^1+15 \text{ Mev}, \quad (2.1)$$

where Be^8 is left in its lowest (slightly unstable) level.[3] Later observations gave evidence for the same reaction with Be^8 left in a wide three-Mev level.[4]

$$Li^7+D^2\rightarrow ^*Be^8+n^1+12 \text{ Mev}. \quad (2.2)$$

Rumbaugh, Roberts and Hafstad[5] have observed neutrons from Li^6 separated targets and have also found evidence for the formation of Be^7 indicating the reaction

$$Li^6+D^2\rightarrow Be^7+n^1+3.1 \text{ Mev}. \quad (5)$$

In addition to these more or less discrete groups of neutrons, there have also been observed neutrons of apparently inhomogeneous energies from both Li^6 and Li^7 targets. These have usually been ascribed to the three-particle reactions

$$Li^7+D^2\rightarrow He^4+He^4+n^1+15.1 \text{ Mev} \quad (3)$$

and

$$Li^6+D^2\rightarrow He^4+He^3+n^1+1.6 \text{ Mev}. \quad (6)$$

While this mechanism of disintegration may

* Now at Stanford University, California. (International Exchange Student.)

** Now a Westinghouse Research Fellow, Westinghouse Research Laboratories, East Pittsburgh, Pennsylvania.

[1] Crane, Lauritsen and Soltan, Phys. Rev. **44**, 692 (1933).

[2] T. W. Bonner and W. M. Brubaker, Phys. Rev. **48**, 742 (1935).

[3] O. Laaf, Ann. d. Physik **32**, 743 (1938) has recently detected the coincidences of the alpha-particles from

$$Be^8\rightarrow He^4+He^4+<0.1 \text{ Mev}. \quad (2.01)$$

[4] W. E. Stephens, Phys. Rev. **53**, 223 (1938). $^*Be^8$ has been observed in other reactions: $B^{11}+H^1\rightarrow ^*Be^8+He^4+5.8$ Mev, Oliphant, Kempton and Rutherford, Proc. Roy. Soc. **150**, 241 (1935); P. I. Dee and C. W. Gilbert, Proc. Roy. Soc. **154**, 279 (1936); and $B^{10}+D^2\rightarrow ^*Be^8+He^4+15$ Mev, J. D. Cockcroft and W. B. Lewis, Proc. Roy. Soc. **154**, 246 (1936).

[5] Rumbaugh, Roberts and Hafstad, Phys. Rev. **54**, 657 (1938).

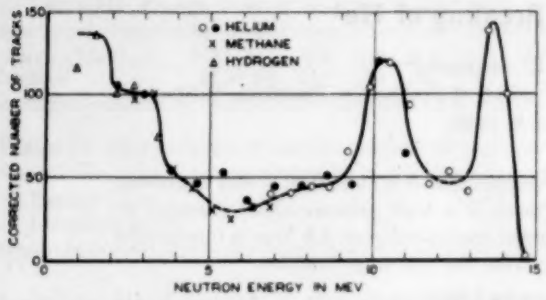

FIG. 1. Energy distribution of the neutrons from lithium bombarded with deuterons. The energy of the neutrons was measured by recoils in helium and hydrogen and the relative intensities corrected for geometry of the cloud chamber and scattering cross sections.

occur, it seems more reasonable to consider the reaction as mainly occurring in two stages

$$Li^7+D^2\rightarrow Be^8+n^1, \quad (2)$$

$$Be^8\rightarrow He^4+He^4, \quad (2.0)$$

and to consider the additional modes of disintegration[6]

$$Li^7+D^2\rightarrow He^5+He^4+14.3 \text{ Mev}, \quad (1)$$

$$He^5\rightarrow He^4+n^1+0.8 \text{ Mev} \quad (1.0)$$

and

$$Li^6+D^2\rightarrow He^5+He^3+0.8 \text{ Mev}, \quad (4)$$

$$He^5\rightarrow He^4+n^1+0.8 \text{ Mev}. \quad (4.0)$$

With this in mind, we reinvestigated the neutron spectrum resulting from the bombardment of lithium with deuterons to see if more accurate data would give any indications for reaction (1.0) and higher levels of Be^8. Preliminary results were reported in abstracts of the San Diego meeting of the American Physical Society.[7]

[6] Especially since the existence of reaction (1) has been established by Williams, Shepherd and Haxby, Phys. Rev. **52**, 390 (1937).

[7] H. Staub and W. E. Stephens, Phys. Rev. **54**, 236 (1938) and W. E. Stephens and H. Staub, Phys. Rev. **54**, 237 (1938).

EXPERIMENTS

Neutrons.—In measuring the neutron spectrum, we have followed the procedure already described[8] with one exception. The stopping power in each run was determined by replacing the Li target by a D_3PO_4 target and measuring the DD neutron recoils under the same conditions as the lithium neutron recoils. In calculating these stopping powers, the usual corrections[9] were applied to the extrapolated range of the DD neutron recoils as found in the cloud chamber, and this mean range was divided into the range as calculated from Bonner's[10] Q value of 3.29 Mev. The variation of stopping power with energy was taken from Livingston and Bethe[11] for hydrogen and methane and from Mano[12] for helium. The Cornell range-energy curves were used (revised 1938). The correction which was applied to the observed number of tracks for geometry was

$$K=(\pi/2)[\sin^{-1}\{1-(T/D)^2\}^{\frac{1}{2}} - (T/D)\{1-(T/D)^2\}^{\frac{1}{2}}]^{-1},$$

where T is the track length and D is the diameter of the cloud chamber. The neutron-proton scattering cross section was taken from Wigner's formula with $\epsilon_1=0.12$ Mev and $\epsilon_2=2.19$ Mev.[13] At high energies, the value of $(\sigma_{He}/\sigma_H)_{back}$ was assumed to be near unity.[14] The number of tracks

[8] W. M. Brubaker and T. W. Bonner, Rev. Sci. Inst. **6**, 143 (1935); T. W. Bonner and W. M. Brubaker, Phys. Rev. **47**, 910, 973 (1935); **48**, 742 (1935); **49**, 19 (1936); **50**, 308 (1936); Stephens, Djanab and Bonner, Phys. Rev. **52**, 1079 (1937); W. E. Stephens, Phys. Rev. **53**, 223 (1938).

[9] M. S. Livingston and H. A. Bethe, Rev. Mod. Phys. **9**, 289 (1937).

[10] T. W. Bonner, Phys. Rev. **53**, 711 (1938).

[11] M. S. Livingston and H. A. Bethe, Rev. Mod. Phys. **9**, 274 (1937).

[12] G. Mano, J. de phys. et rad. **5**, 628 (1934).

[13] $\sigma=5.15\times10^{-24}[\frac{1}{4}(\epsilon_1+E/2)^{-1}+\frac{3}{4}(\epsilon_2+E/2)^{-1}]$.

[14] H. Staub and W. E. Stephens, Phys. Rev. **55**, 131 (1939).

TABLE I. *Relevant data for the experiments on neutron energy distribution.*

Gas	Pressure Atmos.	Stopping Power For $D(d,n)$ Recoils	Stopping Power For ThC′ αs	Deuteron Bombarding Energy Mev	No. of Pictures	No. of Tracks	Energy Range Covered Mev
Methane	11.6	11.5		0.8	5,000	1,026	3 to 7
Hydrogen	12.5	2.89		1.0	2,500	714	1 to 3
Helium	6.3	1.38		0.8	12,000	746	3 to 10
Helium	11.9		2.6	0.93	9,000	1,034	7 to 15
				Total	28,500	3,520	1 to 15

counted was first changed from range intervals to energy intervals and then corrected for geometry and cross section. The resulting number-energy curves were then fitted at about three Mev and six Mev and gave Fig. 1. Table I gives the relevant data on the different runs. Included in this are the data taken with high pressure helium already reported.[4] The different runs were made in order to cover the whole spectrum most conveniently and the different runs were overlapped sufficiently to eliminate uncertainties in corrections.

Alpha-particles.—To make sure that reaction (1.0) was probable enough at our bombarding energies to be observable, we have measured the number range curve for the alpha-particles from lithium disintegrated by 0.8-Mev deuterons.[15] An absorption chamber was placed between the target and a four-mm ionization chamber. This latter was coupled to a linear amplifier of the Wynn-Williams type.[16] The output was put through a biased single thyratron to actuate a telephone counter. As the resolving power of the counter was about 300 counts per minute, care was taken that the counting rate was low compared to this. Special care was taken to make the mechanical coupling of the chamber to the target

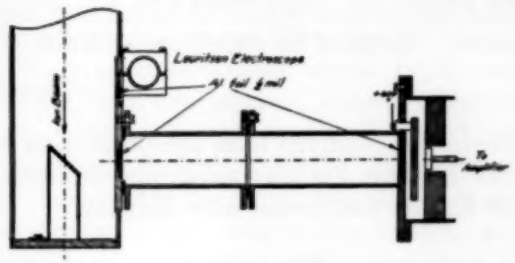

FIG. 2. Diagram of target tube, absorption tube, ionization chamber and monitor electroscope for measuring the number-range curve for the α-particles from lithium bombarded with deuterons.

tube insensitive to the vibration of the target tube, which thus prevented an increase in the counter noise level.

The absorption chamber was calibrated with ThC and C′ and Po alpha-particles. With the Po alpha-particles, number-bias curves for different

[15] This curve is similar to Williams, Shepherd and Haxby, reference 6, but taken at our higher bombarding energy.

[16] Baldinger, Huber and Staub, Helv. Phys. Acta **11**, 247 (1937).

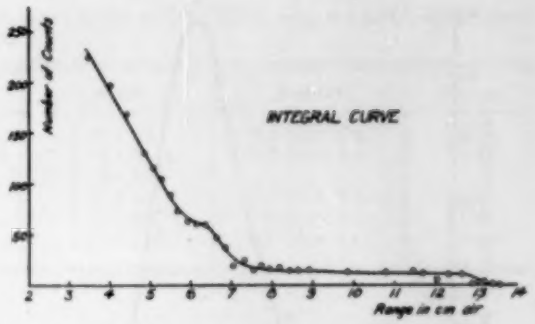

FIG. 3. Integral number-range curve of the α-particles from lithium bombarded with deuterons.

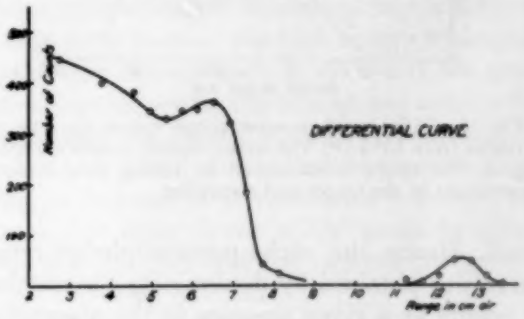

FIG. 4. Differential number-range curve of the α-particles from lithium bombarded with deuterons.

absorption were run to determine the bias for maximum ionization,[17] and it was determined that for differential counting the bias was about 98 percent of this maximum bias. For integral counting, the bias was put at 36 percent of the maximum and all particles entering the chamber were counted. The noise level was estimated to be about nine percent of the maximum alpha-particle ionization.

As a measure of primary intensity, we have used a Lauritsen electroscope[18] with a small ionization chamber mounted as shown in Fig. 2. Alpha-particles of over four cm range coming from the target could enter the electroscope and gave a deflection proportional to the total number of alpha-particles. By interposing foils between the electroscope and target it was found that most of the ionization in the electroscope was due to alpha-particles from the target. Because of the small size of the electroscope chamber, the effect of x-rays, γ-rays, etc., was

[17] A very clear discussion of these procedures is given in M. G. Holloway and M. S. Livingston, Phys. Rev. **54**, 18 (1938).

[18] C. C. Lauritsen and T. Lauritsen, Rev. Sci. Inst. **8**, 438 (1937).

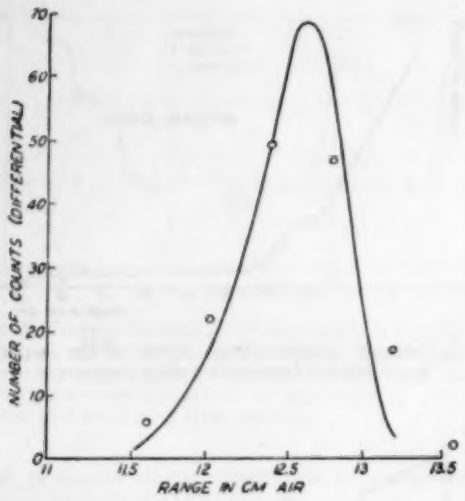

FIG. 5. Differential number-range curve for the α-particles from Li^6+D^2. The experimental points are from Fig. 4. The curve is calculated by taking into account penetration in the target and straggling.

small. Hence the alpha-particle-number-range curve was obtained by determining the number of counts at a given pressure in the absorption cell for a standard deflection of the electroscope. This deflection corresponded to about 3000 alpha-particles. Both an integral and a differential curve were taken and are shown in Figs. 3 and 4. The seven-cm group of alpha-particles ascribed to the reaction

$$Li^7+D^2\rightarrow He^5+He^4+14.3 \text{ Mev} \qquad (1)$$

is not completely resolved, but is clearly evident. Its width is greater than that found by Williams, Shepherd and Haxby[6] because of the increased energy of the incident deuterons which gives a greater energy spread in the disintegrating deuterons (and a possible difference in chamber depth and percent bias). A calculation of the distribution in range of the 13-cm group of alpha-particles based on Eq. (801) of Livingston and Bethe[9] gives the curve of Fig. 5. The experimental points fit quite well, indicating the line is no wider than would be expected. A reasonable guess at the shape of the seven-cm group gives a width slightly greater than that of the 13-cm group in agreement with Williams, Shepherd and Haxby[6] and probably indicates a natural width of the level in He^5 of the order of 0.1 or 0.2 Mev. The alpha-particle intensities and ranges taken from these curves are shown in Table II.

This ratio of 1 : 5 : 55 is for alpha-particle intensities. Changing it to disintegration intensities, we get 1 : 10 : 55 at 0.8-Mev a.c. for a thick lithium target. In Table III are given comparisons with other data on the ratio $Li^6(d,\alpha)\alpha$: $Li^7(d,\alpha)He^5$: $Li^7(d,\alpha)\alpha, n+Li^7(d,\alpha)He^5$ for a lithium target.

The ratio in which we are interested is

$$\frac{Li^7(d,\alpha)\,He^5}{Li^7(d,\alpha)\,He^5+Li^7(d,\alpha)\alpha n}=\frac{10}{55}=\frac{10}{10+45},$$

since it gives the ratio we are seeking,

$$\frac{Li^7(d,\alpha)He^5}{Li^7(d,\alpha)\alpha n}=\frac{1}{4.5}=\frac{He^5(\ ,n)\alpha}{Li^7(d,n)\alpha\alpha}.$$

Hence[10]

$$\frac{He^5(\ ,n)}{Li(d,n)}=\frac{He^5(\ ,n)\alpha}{Li^7(d,n)Be^8+He^5(\ ,n)\alpha+Li^6(d,n)}$$

$$=\text{about }\tfrac{1}{6}.$$

Hence the neutrons from the breakup of He^5 should be about $\frac{1}{6}$ of the total number of neutrons from lithium bombarded with deuterons.

DISCUSSION

The neutron spectrum shown in Fig. 1 can be interpreted as follows: The high energy group

[10] About 8 percent of the total neutrons are from Li^6 according to reference 5.

TABLE II. *Alpha-particle intensities and ranges.*

REACTION	INTENSITY (RELATIVE) DIFFERENTIAL	INTEGRAL	AV.	RANGES IN CM OBS.	CALC.
$Li^6(d,\alpha\alpha)$	11.1	12	1	12.95	12.85
$Li^7(d,\alpha)He^5$	47 to 56	44	5	7.3 to 7.6	7.68
$Li^7(d,\alpha\alpha)+He^5(\alpha)n$	537 to 546	414	50	Max. 7.7 to 8.1	8.10
$Li^7(p,\alpha\alpha)$				8.70	8.68
$Li^7(d,\alpha\alpha)+He^5(\ ,\alpha)n+Li^7(d,\alpha)He^5$			55		

TABLE III. *Values for the ratio of disintegration intensities* $Li^6(d,\alpha)\alpha : Li^7(d,\alpha)He^5 : Li^7(d,\alpha)\alpha$, $n+Li^7(d,\alpha)He^5$ *for a lithium target.*

REFERENCE	RATIO	ENERGY	TARGET
Oliphant, Kinsey and Rutherford[1]	1 :— : 10	0.2 Mev d.c.	Thick
Williams, Shepherd and Haxby[2] taken from published curve	1 : 2 : 8	0.2 Mev d.c.	Thick
Published ratio	2 : 3 : 400		
Rumbaugh, Roberts and Hafstad[3]	1 :— : 15	0.2 Mev d.c.	Thin
	1 :— : 100	0.8 Mev d.c.	Thin
Staub and Stephens[4]	1 : 10 : 55	0.8 Mev a.c.	Thick

[1] Oliphant, Kinsey and Rutherford, Proc. Roy. Soc. **141**, 722 (1933).
[2] Williams, Shepherd and Haxby, Phys. Rev. **52**, 390 (1937).
[3] Rumbaugh, Roberts and Hafstad, Phys. Rev. **54**, 657 (1938).
[4] This ratio neglects the contribution of the $Li^6(d,\alpha)He^3$ reaction, and is further uncertain due to the extrapolation to zero energy.

of neutrons is from reaction (2.1). While most evidence[4] indicates that the lowest state in Be^8 is slightly unstable, some recent work has suggested that it is 0.3 Mev unstable.[20] The wider group at 10.5 Mev is from reaction (2.2).[4] Since evidence[5] has been found for

$$^{**}Be^8 \rightarrow He^4 + He^4 + 10 \text{ Mev}, \qquad (2.03)$$

the neutrons around five Mev may be due to reaction (2.3). It would be expected that a ten-Mev level in Be^8 would be wider even than the three-Mev level (which is about one Mev wide). This widening of the levels may account for the overlapping of the neutron groups.

The point at 5.5 Mev obtained with helium recoils is the only point where the helium and hydrogen recoils disagree. Whether this is due to statistical or observational errors or is some departure from the assumed smoothly varying neutron scattering cross section is not known. The curve was drawn through the hydrogen recoil points because the hydrogen cross section is considered more reliably smooth. The helium recoil points above eight Mev were not checked by hydrogen recoils because of the difficulty of getting pressures high enough to make the hydrogen recoils short enough for accuracy. Hence the high energy part of the curve is still uncertain because of the lack of knowledge of the neutron-helium forward scattering cross section. The only available evidence concerning this comes from comparing the neutron spectrum of boron bombarded by deuterons as measured in helium and methane.[21] This comparison is subject to large error because the high energy hydrogen recoils were slowed down in mica and the geometrical correction for this is large and uncertain. It is further not known whether He^5 has higher levels which would give resonance neutron scattering in helium. It is reasonable however, to assume that higher levels of He^5 would be quite broad and not give spurious neutron groups.

In a two-stage reaction

$$M_0 + M_1 \rightarrow M_3 + M_2 + Q_1,$$
$$M_3 \rightarrow M_5 + M_4 + Q_2,$$

the intermediate nucleus M_3 can come off at almost any angle and still disintegrate to emit a particle M_4 at 90° to the incident particle M_1. Since the energy of recoil depends on the angles, the emitted particle (at 90°) has a spread in energy and this spread can be calculated by the formula:[22]

$$E_4 \gtrless [(Q_2 M_2 M_4/M + M_0 M_2 M_4 E_1/M^2)^{\frac{1}{2}} \pm (Q_2 M_5)^{\frac{1}{2}}]^2/M_3 - M_4 M_1 E_1/M^2.$$

In this case, using $Q_2 = 0.8$ Mev, $E_1 = 0.8$ Mev and $Q_1 = 14.3$ Mev for the reactions (1) and (1.0), we get 0.1 Mev $< E_4 <$ 3.8 Mev. Hence the neutrons would be expected to have a spread in energy from 0.1 Mev to 3.8 Mev. Therefore the sharp rise in number of neutrons at 3.8 Mev in Fig. 1 is interpreted as the high energy end of the neutron continuum from reaction (1.0). Making reasonable guesses as to the distribution of these neutrons, we estimate them to be $\frac{1}{3}$ to $\frac{1}{6}$ of the total number of neutrons, in excellent agreement with the ratio calculated from the alpha-particle

[20] Allison, Graves, Skaggs and Smith, Bull. Am. Phys. Soc. **13**, 14 (1938).
[21] T. W. Bonner and W. M. Brubaker, Phys. Rev. **50**, 308 (1936); H. Staub and W. E. Stephens, Phys. Rev. **53**, 212 (1938). Also reference 14.
[22] M. S. Livingston and H. A. Bethe, Rev. Mod. Phys. **9**, 280 (1937).

intensities. This estimate depends on the $(\sigma_{He}/\sigma_H)_{back}$ ratio which is, as we have said, not very well known at energies greater than six Mev. Also the background of neutrons from other modes of disintegration is not well known. Hence the agreement is only valid in order of magnitude, but to this extent supports our interpretation.

These experiments indicate that present data may be explained on the assumption that two-stage reactions are much more probable than three-particle reactions. However, they do not give a decisive answer as to whether three-particle reactions occur with any measurable probability or not. The relative probabilities of a three-particle reaction compared to a two-stage reaction might be gotten by accurately measuring the neutron spectrum of separated Li^6 bombarded by deuterons.[23] If the reaction goes in two stages

$$Li^6+D^2\rightarrow He^5+He^3+0.8 \text{ Mev}, \quad (4)$$

$$He^5\rightarrow He^4+n^1+0.8 \text{ Mev}, \quad (4.0)$$

the neutrons will have a spread in energy from 0.18 Mev to 1.22 Mev (for 0.8 Mev bombarding energy) while if the three-particle reaction occurs

$$Li^6+D^2\rightarrow He^4+He^3+n^1+1.6 \text{ Mev}, \quad (5)$$

the neutrons will have energies from 0 to 1.85 Mev. In addition, the maximum energy of the neutrons will vary much faster with bombarding energy in the case of the three-particle reaction than the two-stage reaction.

We wish to thank Mr. Tom Lauritsen for the electroscope, the Seeley W. Mudd Fund for financial support, and Dr. C. C. Lauritsen for continued encouragement. One of us (H. Staub) is very much indebted to the "Stipendienfond" and the "Jubilaumsfond der Eidgenossischen Technischen Hochschule" Zurich, Switzerland for a grant.

[23] Rumbaugh, Roberts and Hafstad, reference 5, have measured this neutron spectrum, but not accurately enough for this purpose.

MAY 1, 1939 PHYSICAL REVIEW VOLUME 55

The Magnetic Rotation Spectra of SO_2 and CS_2 in the Ultraviolet

P. KUSCH* AND F. W. LOOMIS
University of Illinois, Urbana, Illinois

(Received March 15, 1939)

The apparatus previously used for the study of magnetic rotation spectra in the visible and infra-red has been modified for use in the ultraviolet. The object was to see whether the simplification often found in magnetic rotation spectra will help in the analysis of the complicated spectra associated with electronic transitions of polyatomic molecules, most of which occur in the ultraviolet. The spectra of this type which have been found are those of CS_2, SO_2 and formaldehyde. In each case the band spectrum is replaced by sharp lines which may readily be correlated to band heads. These spectra occur for only limited regions of the absorption spectrum, in which the band heads are rather sharp and present a regular appearance. In the region where the band heads are irregular and confused in appearance, no effect occurs. In no case is the magnetic rotation spectrum sufficiently extensive to permit a vibrational analysis of the band system to be made, nor to give any material aid in its analysis.

INTRODUCTION

THE magnetic rotation spectrum of a gas is the spectrum of light transmitted by a gas between crossed polarizing prisms when the gas is placed in a magnetic field parallel to the direction of propagation of the light beam. Several types of magnetic rotation spectra have been observed. The most usual type occurs in the region of the $^1\Pi\leftarrow{}^1\Sigma$ absorption systems of the alkali metal molecules and consists of a number of fairly sharp lines which lie near the band heads of the corresponding absorption system. These magnetic rotation spectra have been observed[1] for all

* Now at Columbia University.

[1] F. W. Loomis and R. E. Nusbaum, Phys. Rev. **38**, 1447 (1931); **39**, 89 (1932); **40**, 380 (1932). F. W. Loomis and M. J. Arvin, Phys. Rev. **46**, 286 (1934). P. Kusch, Phys. Rev. **49**, 218 (1936).

the alkali metal molecules with the exception of Cs_2. This type of magnetic rotation spectrum occurs only for electronic band systems in which the molecule has a magnetic moment in at least one of the two electronic states involved in the transition. It occurs because the Zeeman splitting of the rotational lines, and hence the rotation, by the molecule, of the plane of polarization of incident plane polarized light of a frequency near to that of the rotational lines, is large for rotational lines of low quantum number but decreases rapidly with increasing rotational quantum number. It may be predicted from theoretical considerations that for the case of the $^1\Pi \leftarrow {}^1\Sigma$ systems of the alkali metal molecules the rotation just outside an R line should be positive and just outside a P line negative. When, as in the case of the $^1\Pi \leftarrow {}^1\Sigma$ systems of the alkali metal molecules, the head of a band appears at low rotational quantum numbers, the effect of the many closely spaced lines in the band head is superimposed and a bright line is observed just outside the head where the effect of reabsorption is small. Under very prolonged exposures of photographic plates the magnetic rotation due to individual lines of rather high J, which do not lie in the band head, may be observed[1] but the lines so observed are not of an intensity comparable to that of the composite line near the band head. This apparent simplification of the absorption spectrum permits a very complete vibrational analysis to be made, since band heads are easily located and weak bands are not obscured by the structure of intense neighboring bands. Extrapolations of the very extensive data which may be obtained from such analyses yield more accurate values of the energies of dissociation of the alkali metal molecules than could be obtained from an analysis of the absorption spectra alone.

Unperturbed $^1\Sigma \leftarrow {}^1\Sigma$ systems should show no magnetic rotation spectrum since the molecule has a magnetic moment in neither of the two electronic states involved in the transition, and hence exhibits no Zeeman splitting. If a system which is known to result from a $^1\Sigma \leftarrow {}^1\Sigma$ transition does show a magnetic rotation spectrum, it may be inferred that one of the states involved in the transition has acquired a magnetic moment due to perturbation effects. The magnetic rotation lines observed for such a system do not correspond in any simple way to the absorption heads, nor do any obvious regularities occur in the arrangement of the lines. The magnetic rotation spectrum of the $^1\Sigma \leftarrow {}^1\Sigma$ system of Na_2 was first observed by Wood and Hackett.[2] Fredrickson and Stannard[3] have analyzed this magnetic rotation spectrum on the basis of the hypothesis that some levels of the magnetically insensitive upper $^1\Sigma$ state are perturbed by some unknown magnetically sensitive state, so that a molecule occupying these levels acquires a magnetic moment and rotational lines resulting from transitions to these levels show magnetic rotation effects. A similar spectrum of K_2 has been observed by Carroll[4] and has been explained by him in terms of perturbations of the upper state.

A magnetic rotation spectrum has been observed[5] for I_2. Modern theory ascribes this to a magnetic moment acquired by the molecule in the upper state and caused by a rotational distortion. The magnetic moment becomes large only for high rotational speeds and hence the magnetic rotation lines observed for I_2 correspond to absorption lines of high rotational quantum number. Serber[6] and Carroll[4] have given theoretical accounts of these magnetic rotation phenomena in diatomic molecules.

Because the method of magnetic rotation offers an important method of investigation of the spectra of certain diatomic molecules, this investigation was undertaken in the hope that the magnetic rotation spectra of the electronic band systems of polyatomic molecules would present a useful simplification of the enormously complicated structure observed in the corresponding absorption spectra. Since the present work was inaugurated Carroll[4] has pointed out that the probabilities of success are small and that the magnetic rotation spectra, when observed, might well exhibit the complexities rather than the simplicities of the band structure.

---

[2] R. W. Wood and F. E. Hackett, Astrophys. J. **30**, 339 (1909).
[3] W. R. Fredrickson and C. R. Stannard, Phys. Rev. **44**, 632 (1933).
[4] T. Carroll, Phys. Rev. **52**, 822 (1937).
[5] R. W. Wood and G. Ribaud, J. de phys. et rad. **4**, 378 (1914).
[6] R. Serber, Phys. Rev. **41**, 489 (1932).

Experimental

Only very few polyatomic molecules exhibit absorption spectra due to electronic transitions in the visible region of the spectrum. A good many such molecules do, however, possess absorption spectra in the near ultraviolet. It was, therefore, necessary to modify the magnetic rotation technique, heretofore used only in the visible and infra-red regions of the spectrum, for use in the ultraviolet.

Since the rotations which are produced by the Zeeman splittings of the rotational lines are usually very small, the intensity of magnetic rotation lines is usually weak compared to that of the corresponding absorption spectrum. A very intense source of continuous radiation is, therefore, necessary as a background for the observation of this type of spectrum. A water-cooled hydrogen discharge tube of a type described by Lawrence and Edlefsen[7] was used. When a current of about four amperes at 4400 volts was sent through the tube, it gave a very intense continuum in the ultraviolet region of the spectrum. The use of this source and a Hilger E1 quartz spectrograph permitted satisfactory plates of the magnetic rotation spectra to be obtained in exposure times varying from 15 minutes to six hours. The corresponding absorption spectra could be photographed in a few seconds.

The polarizing and analyzing prisms consisted of a pair of quartz Rochon prisms with components in optical contact. Since the angle separating the two beams of light, polarized in planes at right angles to each other, which leave the polarizing prism is only about 0.5° at 3500A, it was necessary to have a well collimated beam of light incident on the prism, so that the two polarized beams might be resolved. A lens of long focal length was used to collimate the light from the discharge tube, and the aperture of the beam was reduced by suitable diaphragms. Sufficient resolution of the beam was then obtained so that the extraordinary, refracted beam could be stopped by means of a screen and only the ordinary, unrefracted ray sent through the absorption tube. Since all the optical adjustments were made by observations on the visible light produced by the discharge tube, or, on occasion, by observations on the ultraviolet light as viewed on a fluorescent screen, the two beams often overlapped to some degree in the ultraviolet, or else the beam transmitted through the tube was improperly collimated so that reflections occurred from the inside walls of the absorption tube. Either of these two difficulties prevented extinction from being obtained in the ultraviolet and at once obviated the possibility of observing magnetic rotation spectra below about 2700A.

It is necessary that the windows of the absorption tube be free from strains so that extinction may be obtained between the Rochon prisms in the absence of a magnetic field. Fused quartz windows were entirely unusable because of the strains. Corex windows were found to be satisfactory down to about 3000A, but at shorter wave-lengths they began to absorb strongly. Eventually two crystal quartz windows of identical thickness, one of right-handed and the other of left-handed quartz, and cut with their surfaces perpendicular to the optic axis were found to be satisfactory.

The solenoid used in this work has been previously described by Loomis and Nusbaum.[1] It produced a field of about 1800 gauss under working conditions.

The magnetic rotation spectra were observed at a number of different pressures for each of the gases investigated. Since the vapor pressures at room temperatures were, in all the cases investigated, much greater than the pressures required to give well-developed absorption spectra, the pressure could easily be adjusted by pumping the tube down to suitable pressures.

Carbon disulphide

CS_2 has an absorption spectrum in the region 3900–2750A. Wilson[8] has published an extensive list of wave-lengths of band heads in this region, but has given no analysis of the system. Watson and Parker[9] have given a formula to represent the bands in this system, but the formula cannot represent a true analysis since the vibrational frequencies given for the ground state do not agree with results obtained from later work on the Raman effect of CS_2.

[7] E. O. Lawrence and N. E. Edlefsen, Rev. Sci. Inst. **1**, 45 (1930).

[8] E. D. Wilson, Astrophys. J. **69**, 34 (1929).

[9] W. W. Watson and A. E. Parker, Phys. Rev. **37**, 1013 (1931).

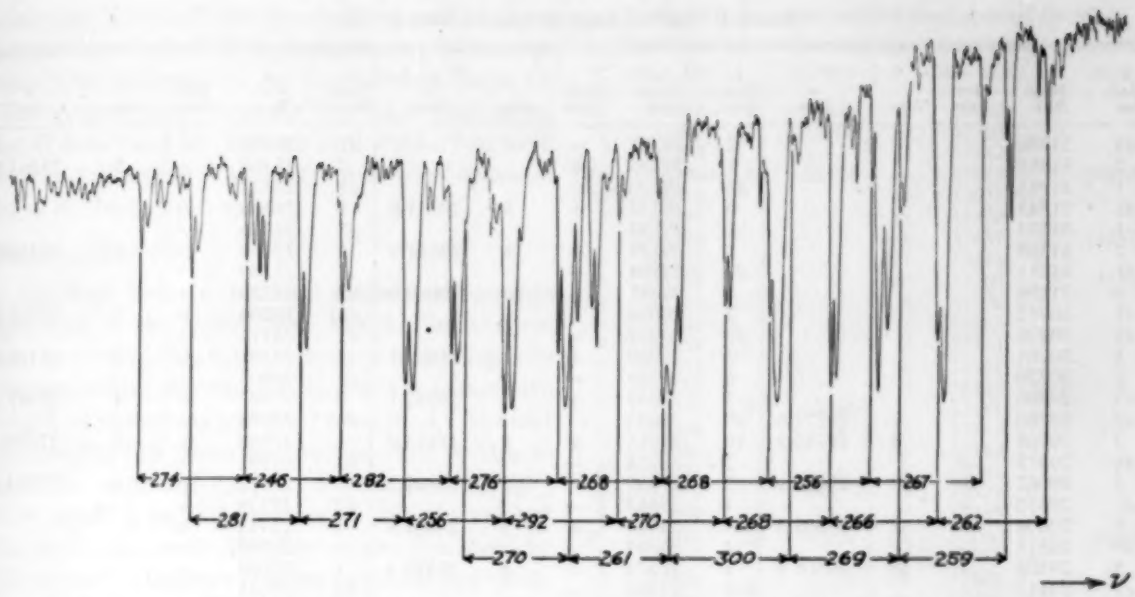

FIG. 1. Microphotometer record of the magnetic rotation spectrum of CS_2. Pressure = 6 cm.

We have found an intense magnetic rotation spectrum in the region 3355–3640A, and a very much weaker spectrum in the region 3125–3250A, the region of most intense absorption. No magnetic rotation was observed to shorter wavelengths. A weak spectrum may, of course, exist, but if it does it is of such low intensity that it cannot be observed against the weak background transmitted by the optical system. It is noteworthy that the magnetic rotation spectrum occurs in that region where the absorption bands are sharp and well defined. At short wavelengths, where the absorption bands are diffuse and irregular in appearance no effect is observed.

A microphotometer trace of the magnetic rotation spectrum in the region 3355–3640A is reproduced in Fig. 1. The most obvious feature of the spectrum is that it consists of a number of doublets, the components of each of which are separated by about 17 cm^{-1}, and in which the low frequency component is sharper than the high frequency component. This doublet structure is not apparent in the much weaker magnetic rotation spectrum observed to shorter wavelengths. Because the magnetic rotation spectrum was quite intense it was possible to take photographs of the spectrum for settings of the analyzing Rochon prism at small angles on either side of the extinction position without admitting enough background to obscure the spectrum. By comparison of several photographs taken in this manner it was possible to determine the direction of rotation of the plane of polarization at each line, since the intensity of a line relative to the background decreases as the analyzing prism is rotated in the same direction as the rotation of the plane of polarization. This effect could be observed for the more intense lines by a visual examination of the plates, and by the use of microphotometer traces, the direction of rotation could readily be determined for all the lines shown in Fig. 1 with the exception of a few very weak ones which were obscured by the continuous background admitted by the analyzing Rochon. In all cases the direction of rotation of the plane of polarization is positive for the sharp, low frequency component and negative for the diffuse, high frequency component. A positive rotation is defined as that which occurs when the rotation is in the same direction as the current producing the field, if the field itself is in the same direction as the direction of propagation of the light beam.

The absorption spectrum of CS_2 was photographed in the first order of a 21-ft. grating under a dispersion of about 1.25A/mm. This permitted the accurate measurement of absorption edges, a good many of which are very sharp. The usual

TABLE I. *Observed magnetic rotation lines of* CS_2.

i MAG. ROT.	ν MAG. ROT.	ROT. SIGN	i ABS.	ν ABS.	i MAG. ROT.	ν MAG. ROT.	ROT. SIGN	i ABS.	ν ABS.	i MAG. ROT.	ν MAG. ROT.	ROT. SIGN	i ABS.	ν ABS.
*d*4	31986				2	29297	−			*d*1	28383	−		
2	31955				1	29284	+			2	28368	+	5	28367.2
1	31945				*d*6	29250	−			*d*1	28323			
*d*1	31543				6	29237	+	8	29234.6	1	28308			
1	31533				1	29152	−			*d*5	28286	−		
2	31369				1	29139	+	5	29141.9	4	28269	+	7	28269.9
*d*1	31211				*d*9	29104	−			1	28250			
0	31196				4	29081	+	10	29080.9	*d*2	28220	−		
*d*1	30912				2	29056				*d*2	28206	+	5	28205.8
*d*1	30898				*d*3	28982	−			*d*7	28171	−		
1	30781				3	28969	+	5	28968.7	6	28151	+	7	28154.4
1	30770				4	28856	−			*d*3	28005	−		
*d*2	29800				3	28839	+	4	28837.7	3	27987	+	4	27987.1
*d*2	29780		7	29777.6	*d*9	28832	−			*d*4	27896	−		
2	29765		4	29765.2	10	28813	+	8	28815.8	4	27880	+	4	27878.4
*d*4	29679	−			2	28714	−			*d*3	27792	−		
3	29667	+	10	29666.1	2	28699	+	3	28697.2	3	27776	+	4	27774.4
*d*1	29618	−			4	28643	−			*d*2	27759	−		
1	29604	+	8	29605.3	3	28628	+	3	28632.9	2	27741	+		
*d*8	29518	−			4	28594	−			1	27709	−		
5	29503	+	10	29500.6	4	28578	+	4	28579.4	1	27694	+		
*d*2	29417	−			*d*10	28563	−			*d*2	27615	−		
2	29408	+	9	29407.2	5	28545	+	10	28543.5	2	27599	+	5	27599.7
*d*4	29377	−			*d*2	28449				*d*2	27527	−		
7	29355	+	6	29360.4	*d*10	28427	−			2	27508	+	3	27507.5
2	29337		10	29336.6	9	28407	+	7	28408.1	*d*2	27484	−		
										2	27467	+	4	27467.1

intensity variation observed in absorption bands is not in evidence, and many of the observed features have more nearly the character of absorption lines. An excellent correlation exists between the sharp, low frequency member of the magnetic rotation doublets and the sharp absorption edges. No absorption edges were observed corresponding to the high frequency component of the doublets, nor was it possible to find absorption edges which correspond to the weaker magnetic rotation lines in the region 3125–3250A. The frequencies of the observed magnetic rotation lines, their estimated intensities, directions of rotation, and the frequencies of the corresponding heads measured in absorption are given in Table I.

The obvious regularities in the magnetic rotation spectrum and the excellent correlation which may be established between the sharp magnetic rotation lines and the absorption heads indicate that this spectrum is of the type observed for the $^1\Pi \leftarrow {}^1\Sigma$ systems of the alkali metal molecules. That is, the molecule possesses a magnetic moment along the axis of the molecule in the upper of the two electronic states involved in the transition. The ground state can possess no magnetic moment since CS_2 is known to be diamagnetic. The rotational lines are, therefore, subject to a Zeeman splitting and a large rotation of the plane of polarization results near the band head where the effect of many closely spaced lines is superimposed and the effect of reabsorption is small. The occurrence of the diffuse components of the doublets is rather puzzling; from the fact that the diffuse components do not correspond to structure in the bands in a manner similar to that observed for the sharp components and from the different directions of rotation of the plane of polarization by the molecules for the two components, it may be inferred that the diffuse and sharp components have their origins in a different type of structure in the band. Until a detailed analysis of the structure of the absorption spectrum is available, no explanation of these observed magnetic rotation effects seems possible.

The observed magnetic rotation lines fall into several progressions. These are marked in Fig. 1 and it is seen that the intensities in most of the progressions vary smoothly. The differences between successive members of these progressions are about 270 cm^{-1} and converge to high fre-

quencies. Jenkins[10] has pointed out one of these progressions which is very prominent in absorption. The progressions are tabulated in Table II. The frequency of about 270 cm^{-1} has been noted by Wilson[8] and by Watson and Parker[9] as well. It seems probable that this frequency corresponds to ν_1 in the excited state.

Sulphur dioxide

Sulphur dioxide has an intense absorption spectrum in the region 2600–3900A. This absorption system of SO_2 is much more intense than the corresponding system of CS_2. For the same path length of absorbing gas the pressure of CS_2 must be roughly ten times as great as that of SO_2 to give the same absorption. Watson and Parker[11] have made a partial analysis of this system but the analysis is untenable for reasons discussed by Clements.[12] Clements has investigated the variation of the intensities of the bands in absorption as a function of temperature and has proposed an analysis on the basis of his results. Asundi and Samuel[13] have proposed an alternative analysis which disregards the results of the temperature variation and has other defects discussed by Price and Simpson.[14]

A magnetic rotation spectrum has been found in the region 2939–3164A. The intensity of this spectrum is much lower than that of the magnetic rotation spectrum of CS_2 for a gas density such that the absorption spectra of the two are of about equal intensity. As in the case of CS_2, the magnetic rotation spectrum occurs in the low frequency region of the absorption spectrum where the absorption edges are fairly sharp and well defined and in which the bands appear quite regular. At higher frequencies, where the bands appear confused and irregular, no magnetic rotation spectrum has been observed of an intensity great enough to permit of its observation against the continuous background transmitted by the optical system. No effect was observed at longer wave-lengths where the bands are regular but appear only at much higher gas pressures.

TABLE II. *Progressions in the magnetic rotation spectrum of* CS_2.

28308	27599	27467
270	*281*	*274*
28578	27880	27741
261	*271*	*246*
28839	28151	27987
300	*256*	*282*
29139	28407	28269
269	*292*	*276*
29408	28699	28545
259	*270*	*268*
29667	28969	28813
	268	*268*
	29237	29081
	266	*256*
	29503	29337
	262	*267*
	29765	29604

TABLE III. *Magnetic rotation lines observed for* SO_2.

i	ν(MAG. ROT.)		ν(ABS.)	i	ν(MAG. ROT.)		ν(ABS.)
2	34017	*L*	34030	3	32782		
2	33800	*J*	33760	3	32763		
2	33792			3	32742		
*d*6	33336	*G*	33313	*d*1	32632	*D*	32607
2	33314			*d*1	32621		
5	33298			*d*1	32579		
4	33286			*dd*1	32457	*C*	32377
4	33272			*dd*1	32421		
4	33257			*d*5	32200	*B*	32161
4	33241			4	32194		
4	33223			2	32183		
4	33203			3	32174		
2	33182			1	32162		
2	33157			3	32153		
1	33076	*F*	33080	1	32141		
1	33066			3	32127		
1	33050			3	32112		
1	33034			3	32093		
1	33017			3	32077		
1	32999			2	32057		
*d*6	32878	*E*	32850	*d*3	31960	*A*	31949
3	32868			*d*3	31950		
2	32860			*d*2	31681		
4	32849			*d*2	31661		
2	32838			1	31636		
3	32827			2	31613		
3	32812			1	31592		
3	32797						

The frequencies of the lines observed in magnetic rotation are given in Table III. The relative intensities were estimated from visual observations made while the plates were measured in the comparator. No measurements were made in absorption, but the frequencies which Clements[12] has published for the band heads, together with the symbol which he used to designate them are included in the table. Clements remarks that his frequencies of the

[10] F. A. Jenkins, Astrophys. J. **70**, 191 (1929).
[11] W. W. Watson and A. E. Parker, Phys. Rev. **37**, 1484 (1931).
[12] J. H. Clements, Phys. Rev. **47**, 224 (1935).
[13] R. K. Asundi and R. Samuel, Proc. Ind. Acad. Sci. **2**, 30 (1935).
[14] W. C. Price and D. M. Simpson, Proc. Roy. Soc. **A165**, 272 (1938).

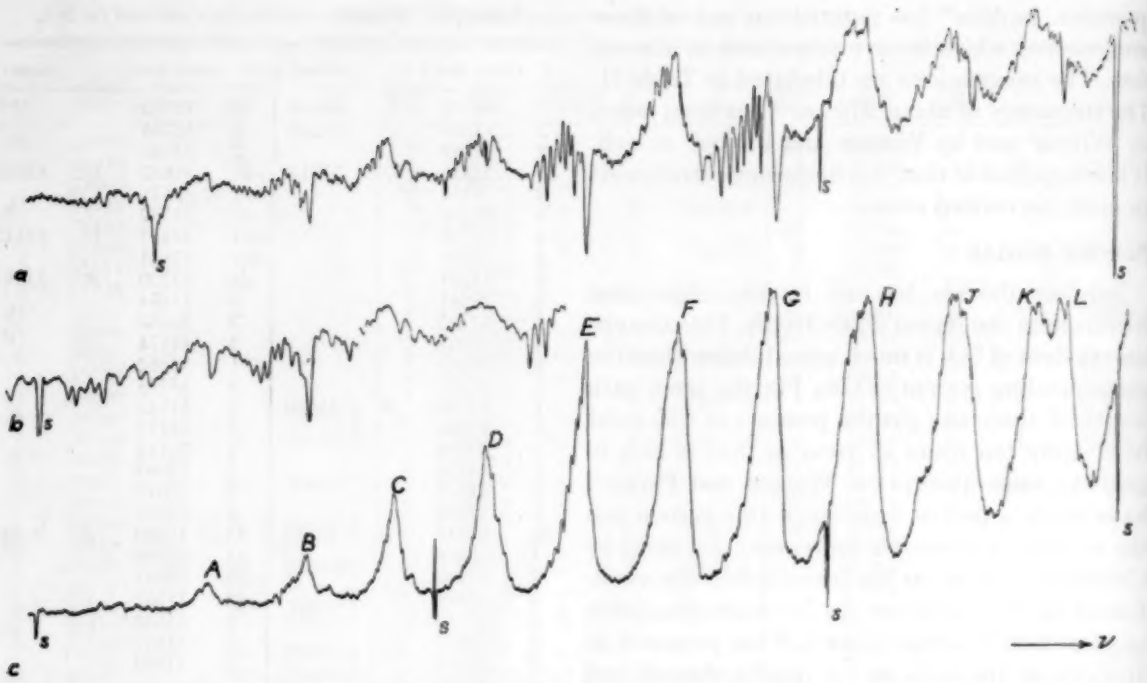

FIG. 2. (*a*) Microphotometer record of the magnetic rotation spectrum *od* SO_2. Pressure = 0.5 mm. (*b*) Pressure = 3 mm. (*c*) The absorption spectrum of SO_2. Pressure = 4 mm.

band heads as determined from different plates are consistent to about 15 cm^{-1}. In the present case, where it is possible to measure fairly sharp lines instead of broad bands, the frequency measurements are consistent to about 2 cm^{-1}.

Microphotometer traces of the magnetic rotation spectrum of SO_2 are reproduced in Fig. 2(*a*) and (*b*). These were observed at pressures of 0.5 and 3 mm, respectively. The corresponding absorption spectrum, at a pressure of 4 mm is shown in Fig. 2(*c*). Reference scratches, accidental scratches, and other plate defects are marked with an *s*. The letter designating the band head is the same as that used by Clements. Because of the long exposure time required to photograph the magnetic rotation spectrum, the absorption spectrum produced by the background transmitted by the polarizing apparatus is present with a considerable intensity.

Since the magnetic rotation spectrum is so weak, it has not been possible to determine the direction of rotation of the plane of polarization for the lines. Any small rotation of the analyzing Rochon introduced enough background to obscure the magnetic rotation spectrum quite effectively.

The most obvious feature of the magnetic rotation spectrum is the appearance of the bands *B*, *E* and *G*. In each of these cases an intense diffuse line appears at the position of the band head. To the long wave-length side of this line appears a series of sharp lines which corresponds to the subheads in the absorption bands. The intervals between successive subheads increases to low frequencies; in the case of the band *G* they increase from 12 cm^{-1} near the band head to 25 cm^{-1} between the two furthest subheads measured. It is evident from the traces that the absorption subheads are best defined in the case of those bands which show the subheads in magnetic rotation most clearly. The band *F*, whose absorption subheads are not as well defined than those of *B*, *E* and *G*, shows a somewhat similar magnetic rotation spectrum consisting of several faint lines whose spacing increases to low frequencies. The intense line which occurs near the band heads, *B*, *E* and *G* does not occur for *F*. The frequencies of the lines in *F*, listed in Table III, were obtained from the microphotometer traces since the lines are too weak to be measured from the original plates.

Magnetic rotation structure of some sort

occurs for all the other bands in Fig. 2 as well. In some cases it is sharp enough to be measured, and otherwise its presence may be inferred by noting the difference between the intensity distribution in the absorption spectrum and in the absorption background transmitted by the analyzing prism.

The series of bands, $A-KL$, in which the magnetic rotation spectrum occurs has been assigned by Clements[12] as the $(000)''-(0v_20)'$ progression in which the band A is the $(000)''-(000)'$ band. This progression is partly overlapped by the $(000)''-(1v_20)'$ progression whose first member is the band G. The frequency $\nu_2{}^1$ is approximately 225 cm^{-1}. From the point of view of the present work it is difficult to see why bands lying in a single progression should show such widely varying magnetic rotation spectra. It is, of course, impossible to place bands which do show similar structure, such as B, E and G, into a single progression because the separations between such bands vary too greatly to represent a vibrational frequency. It does not seem likely that the structure can be explained on the basis of perturbations because of the great regularity in the appearance of the spectrum.

Other molecules

An electronic band spectrum due to formaldehyde appears in the region 2750–3750A. Dieke and Kistiakowsky[13] have given a complete rotational analysis of this system. A magnetic rotation spectrum was found for the 3260A band only. This consists of a number of lines which do not fall into any regular series and among which no other regularities are apparent. No correlation can be established between the observed lines and the structure observed in absorption. Evidently the appearance of the spectrum precludes the possibility that it arises from a magnetic moment characteristic of the upper state, for in that case a somewhat similar structure might be expected for several bands. It seems probable that the observed effect is due to a perturbation of the upper state by some unknown state which does possess a magnetic moment. Dieke and Kistiakowsky have found perturbations in some of the bands but the band at 3260A is entirely regular in its behavior. Presumably the perturbation does not disturb the rotational energy levels sufficiently to permit of its detection by an observation of the displacement of the rotational levels. The frequencies of the lines and their estimated relative intensities are listed in Table IV.

TABLE IV. *Magnetic rotation lines of formaldehyde.*

i	ν	i	ν	i	ν
6	30719	1	30637	10	30557
1	30709	1	30632	3	30531
$d5$	30695	8	30617	$d2$	30515
$d1$	30691	0	30604	2	30489
5	30679	6	30563		

Two other molecules, acetaldehyde and acrolein, of the same general type as formaldehyde, have well-defined absorption spectra in the near ultraviolet which have been investigated by Eastwood and Snow.[16] Neither of these two molecules show any sign of magnetic rotation. Ozone, which shows a strong absorption spectrum in the region 2900–3660A, has no observable magnetic rotation spectrum.

NO_2 is known to have a magnetic moment in the ground state and Wood and Dieke[17] have found an intense magnetic rotation spectrum. This spectrum was readily obtained but consisted of an apparently hopeless confusion of structure which gave no useful simplification of the absorption spectrum.

It seems difficult to obtain any useful information about the absorption spectrum of a polyatomic molecule from a study of its magnetic rotation spectrum for the cases here investigated. A complete understanding of the magnetic rotation spectrum seems rather to require a more detailed knowledge of the structure of the absorption spectrum than seems at present available.

[13] G. H. Dieke and G. B. Kistiakowsky, Phys. Rev. **45**, 4 (1934).

[16] E. Eastwood and C. P. Snow, Proc. Roy. Soc. **A149**, 434, 446 (1935).

[17] R. W. Wood and G. H. Dieke, Nature **128**, 545 (1931).

Influence of Atomic Electrons on Radiation and Pair Production*

JOHN A. WHEELER, *Princeton University, Princeton, New Jersey*

AND

WILLIS E. LAMB, JR., *Columbia University, New York, New York*

(Received March 8, 1939)

A fast electron passing through matter will radiate at a greater rate than would be expected if the atoms traversed presented to the electron simply a static field of force. This follows because of the additional possibility of collisions in which an atom is excited. In a similar way energetic quanta will produce pairs at a greater rate. Consequently the unit of length characteristic of the multiplicative production of showers will be decreased by a factor which in the case of air amounts to 17 percent. The probabilities of radiation and pair formation are not proportional to the square of the nuclear charge but are supplemented by terms linear in atomic number (mass absorption law).

INTRODUCTION

THE probability for the deflection of a fast electron by a nucleus of charge Ze can be calculated in the Born approximation in terms of the scattering of a plane wave by a medium whose scattering power at each point is proportional to the potential at that point. Thus the amplitude of the wave scattered at an angle θ to the original direction will be determined by

$$\int d\tau(Ze/r)\exp\{i(\mathbf{p}_1-\mathbf{p}_2)\cdot\mathbf{r}\}=4\pi Ze/q^2, \quad (1)$$

where $q=|p_1-p_2|=2p_1\sin\theta/2$ is the momentum transferred to the nucleus in the collision.[1]

At a sufficiently great speed, the electron will in addition have a large probability of radiation. When a particle of energy E_1mc^2 emits a quantum of energy νmc^2, the nucleus will take up a momentum qmc, where q lies between the limits $q_{\min}$ and $q_{\max}$. For large values of E_1 and ν we have approximately

$$q_{\min}=\nu/2E_1(E_1-\nu); \quad q_{\max}=2E_0. \quad (2)$$

The probability of such a radiative process will again contain the factor $(4\pi Ze/q^2)^2$. The total probability of radiating quanta of energy νmc^2 in such collisions will arise principally from processes in which the momentum transfer is small. The probability will be finite for a given value of the primary energy but for increasing E_1 it will rise indefinitely as $a\ln E_1+b$, where a and b are constants. This follows because of the growing contribution of small momentum transfers.

The orbital electrons, however, will screen the field of the nucleus and reduce the probability of small momentum transfers. With Z electrons located at points $\mathbf{r}_1, \mathbf{r}_2, \cdots\mathbf{r}_z$, we shall have for the probability amplitude for a given momentum transfer the expression

$$\int\exp(i\mathbf{q}\cdot\mathbf{r})\left\{\frac{Ze}{r}-\sum_i\frac{e}{|\mathbf{r}-\mathbf{r}_i|}\right\}d\tau = (4\pi e/q^2)\{Z-\sum_i\exp(i\mathbf{q}\cdot\mathbf{r}_i)\}. \quad (3)$$

This must now be averaged over all positions of the electrons. The result is

$$(4\pi e/q^2)\int\Psi_0^*(\mathbf{r}_1,\cdots\mathbf{r}_z)\{Z-\sum_i\exp(i\mathbf{q}\cdot\mathbf{r}_i)\} \times\Psi_0(\mathbf{r}_1,\cdots\mathbf{r}_z)d\tau_1\cdots d\tau_z = (4\pi Ze/q^2)\{1-F(q)\}, \quad (4)$$

where $ZF(q)$ is the same atomic form factor as that which describes the elastic scattering of x-rays. For small values of q, $1-F(q)$ approaches zero as q^2. Thus the probability of small momentum transfers is bounded and the probability for the radiation of a quantum with energy νmc^2 approaches a finite upper limit with increasing energy of the primary electron. This upper limit

* Publication assisted by the Ernest Kempton Adams Fund for Physical Research of Columbia University.

[1] We are using relativistic units $\hbar/mc$, mc^2, mc for length, energy and momentum.

has been calculated by Bethe and Heitler[2] by adopting the form factor for a Fermi-Thomas model atom. They obtain for the differential cross section the expression

$$\Phi(\nu)d\nu=(Z^2/137)(e^2/mc^2)^2(d\nu/\nu)(4/E_1^2)\times\{(E_1^2+E_2^2-2E_1E_2/3)\times\ln(183/Z^{\frac{1}{3}})+E_1E_2/9\}, \quad (5)$$

where $E_2=E_1-\nu$. This follows directly by integrating over all momentum transfers q an expression of the form

$$(4\pi Ze/q^2)^2\{1-F(q)\}^2G(q,\nu,E_0)dq, \quad (6)$$

in which the factor[3] $G(q,\nu,E_1)$ contains all effects arising from the light quantum and the electron, while the other factors express the entire influence of the system which takes up the impulse.

In addition to radiative processes in which the atom is left unexcited, there will, however, occur collision[4] in which the momentum transfer to an atomic electron excites the atom to a state Ψ_n. Radiative processes of this kind, analogous to the inelastic or Compton scattering of x-rays, may be divided into two groups, as follows.

Small Momentum Transfers

The probability of a momentum transfer qmc, where q is small compared with unity, will be determined by squaring the absolute value of

$$(4\pi Ze/q^2)\int\Psi_0^*(\mathbf{r}_1,\cdots,\mathbf{r}_z)\{Z-\sum\exp(i\mathbf{q}\cdot\mathbf{r}_i)\}\times\Psi_n(\mathbf{r}_1,\cdots,\mathbf{r}_z)d\tau_1\cdots d\tau_z, \quad (7)$$

multiplying by $G(q,\nu,E_0)$, and summing over all excited states Ψ_n. A free electron would receive an energy $(qmc)^2/2m$ in the encounter, and therefore only those states Ψ_n would give a contribution whose energies are exactly equal to this value. When we allow for the binding of the electrons, it will still be true that the only appreciable effect will come from excitation energies small compared with mc^2. Therefore retardation and other possible relativistic corrections will not arise from the motion of the atomic electron, and we shall be justified in considering $G(q,\nu,E_1)$ in the summation as a factor independent of Ψ_n. Adding to the sum the contribution of the elastic radiation process considered by Bethe and Heitler, and using the completeness theorem for the orthogonal states Ψ_n, we obtain

$$(4\pi e/q^2)^2\int\Psi_0^*(\mathbf{r}_1,\cdots\mathbf{r}_z)|Z-\sum\exp(i\mathbf{q}\cdot\mathbf{r}_i)|^2\times\Psi_0(\mathbf{r}_1,\cdots\mathbf{r}_z)d\tau_1\cdots d\tau_z \quad (8)$$

for the factor which determines the total probability (elastic plus inelastic) for the atom to take up a recoil of magnitude qmc.

The above result may be understood as follows: The time required for the primary electron to traverse the atom is short in comparison with the period of the motion of the atomic electrons. Therefore we may visualize the process in terms of an instantaneous photograph, in which we find the Z electrons respectively at positions $\mathbf{r}_1,\cdots,\mathbf{r}_z$. The probability that this field of force will take up a recoil qmc is determined by the quantity

$$(4\pi e/q^2)^2|Z-\sum\exp(i\mathbf{q}\cdot\mathbf{r}_i)|^2. \quad (9)$$

In a repetition of the experiment, the position of the electrons will be different; averaging over many experiments, we obtain just the expression (8). From this point of view, the validity of the result depends upon the energy of the primary being sufficiently high and the recoil momentum being sufficiently small so that the motion of the atomic electron during the passage of the primary can be neglected. This condition will be satisfied to a good approximation for primary energies large in comparison with mc^2.

The production of pairs by energetic gamma-radiation is closely related to the radiative effect just considered. All the arguments referring to the relative probability of momentum transfers of various magnitudes can be taken over the simple changes, as will be seen in more detail below.

---

[2] H. Bethe and W. Heitler, Proc. Roy. Soc. **A146**, 83 (1934).

[3] G is given by H. Bethe, Proc. Camb. Phil. Soc. **30**, 524 (1934).

[4] The possibility of pair production as well as radiation in the field of atomic electrons was first pointed out by F. Perrin, Comptes rendus **197**, 1100 (1933).

Large Momentum Transfers

In radiative and pair production processes where the recoil momentum is comparable with or larger than mc, the atomic electron may be treated as free (no screening). The total cross section (including all momentum transfers) for the production of pairs in the field of a free electron can be obtained by inverting a type of argument due to Williams. Racah[5] has calculated the cross section Q according to quantum electrodynamics for the production of pairs in the impact of an electron of energy E_0mc^2 on a heavy nucleus of charge Z_1:

$$Q(E_0)=(Z_1e^2/137mc^2)^2(1/\pi)\cdot\{(28/27)\ln^3E_0 +[(28/9)\ln 2-178/27]\ln^2 E_0+d\ln E_0+f\}. \quad (10)$$

Here d and f are numerical constants, given by Racah, the values of which are slightly different in the two cases where the incident particle is an electron or a heavy particle. If we now consider the process in the frame of reference in which the electron is initially at rest, Q will represent the cross section for the production of pairs in the impact of a nucleus of charge Z_1 moving with the original velocity $(1-1/E_0^2)^{\frac{1}{2}}c$ toward the electron, considered to be initially at rest. The field of the passing nucleus can be replaced by an equivalent radiation field, in which the number of quanta in the spectral range $\nu mc^2/h$ to $(\nu+d\nu)mc^2/h$, after summing over all impact parameters, is[6]

$$N(\nu, E_0)d\nu=(2Z_1^2/137\pi)(d\nu/\nu)\ln kE_0/\nu, \quad (11)$$

provided ν is less than $E_0(\gg 1)$. The limitations of the semi-classical argument involved make it impossible to give a precise value to the numerical constant k, which is of the order of magnitude unity.

Let us suppose for the moment that we know the cross section $\sigma(\nu)$ for the production of pairs by a light quantum of energy νmc^2 in the field of a free electron. Then, subject to the limitations of the method of virtual light quanta, we shall have for Q, the expression

$$Q(E_0)=\int_0^{E_0}\sigma(\nu)N(\nu, E_0)d\nu =(2Z_1^2/137\pi)\int_0^{E_0}\sigma(\nu)\ln(kE_0/\nu)d\nu/\nu. \quad (12)$$

Conversely, knowing Q, we may find $\sigma(\nu)$ by differentiating (12) twice with respect to $\ln E_0$ and integrating the resultant first-order differential equation:

$$\sigma(\nu)=(137\pi/2Z_1^2)\exp(-\ln\nu/\ln k)(1/\ln k) \cdot\int_{-\infty}^{\ln\nu}\exp(\ln E_0/\ln k)\frac{\partial^2 Q}{\partial(\ln E_0)^2}d(\ln E_0). \quad (13)$$

Upon insertion of Racah's result in (13), we obtain for $\sigma(\nu)$ a value which is independent of the mass of the particle in whose field the gamma-ray is absorbed, since the constants d and f in (10) fall out on the differentiation:

$$\sigma(\nu)=(1/137)(e^2/mc^2)^2\{(28/9)\ln\nu +(28/9)\ln(2/k)-178/27\}. \quad (14)$$

Except for the difference in charge and the indeterminacy in the constant term of (14) due to the lack of definition of k, the cross section obtained agrees with the formula of Bethe and Heitler for pair production in the field of an unscreened heavy nucleus. It also agrees with what our calculations give just from a consideration of momentum transfers small compared with mc, but large in comparison with the momentum of an atomic electron in its orbit. Therefore we conclude that momentum transfers large compared with mc give a contribution to the total cross section, either for pair production or for radiation, which is small (since k is of the order of magnitude unity) and enters only as a part of the constant term in (14).

Pair production processes involving large recoils of the atomic electron ("triplet production") and the analogous radiation effects can only be treated by a systematic application of quantum electrodynamics. Since there is a clear cut distinction between them and the processes discussed in this paper, we shall not consider them further here. We shall therefore in the following calculate the probabilities for pair production and radiation by integrating only over momentum transfers up to mc.

[5] G. Racah, Nuovo Cimento **14**, 112 (1937).
[6] E. J. Williams, Kgl. Dansk. Videnskab. Selskab. **13**, No. 4 (1935).

TABLE I. *Incoherent scattering factor, defined by Eq. (17), as calculated from the Fermi-Thomas atom model. The values for $v>0.04$ are due to Bewilogua. For small values of v, $S(v)=13.8v-55.4v^3$. The momentum transfer qmc (which for the incoherent scattering of x-rays would be represented by $(2h/\lambda)\sin\theta/2$) is reduced to Fermi-Thomas units by the substitution $v=(6\pi)^{\frac{1}{3}}137qZ^{-\frac{1}{3}}$.*

v	$q/Z^{\frac{1}{3}}$	S	v	$q/Z^{\frac{1}{3}}$	S
0.00	0.00000	$13.8v$	0.3	0.0066	0.776
0.01	0.00022	0.097	0.4	0.0088	0.839
0.02	0.00044	0.169	0.5	0.0110	0.880
0.03	0.00066	0.227	0.6	0.0132	0.909
0.04	0.00088	0.277	0.7	0.0154	0.929
0.05	0.00110	0.319	0.8	0.0176	0.944
0.10	0.00219	0.486	0.9	0.0197	0.954
0.20	0.00440	0.674	1.0	0.0219	0.963

EVALUATION OF CROSS SECTION

The contribution of the inelastic radiative and pair production processes is best calculated by returning directly to the expression (7) which determines the probability of a recoil q in a transition from the state o to an excited state n. The term with Z may be omitted from the integrand because of the orthogonality of the two wave functions Ψ_0 and Ψ_n. With the help of the completeness relation, we obtain after summation the factor determining the intensity of the incoherent radiative processes:

$$(4\pi e/q^2)^2\left\{\sum_{i,j}\int\Psi_0^*\exp\left[i\mathbf{q}\cdot(\mathbf{r}_i-\mathbf{r}_j)\right]\Psi_0 d\tau - \left|\int\Psi_0^*\sum_i\exp\left(i\mathbf{q}\cdot\mathbf{r}_i\right)\Psi_0 d\tau\right|^2\right\}. \quad (15)$$

We write Ψ_0 as a determinant built from Z single particle wave functions $\psi_{i\alpha}(\mathbf{r})$ where $i=1, 2, \cdots, Z$, and $\alpha=1, 2$ gives the two spin components of each function. Expression (15) then reduces to

$$(4\pi e/q^2)^2 ZS(q), \quad (16)$$

where $S(q)$ is a quantity analogous to the atomic form factor, and is defined by

$$ZS(q)=Z-\sum_{i,j}\int\psi_{i\alpha}^*(\mathbf{r})\psi_{j\beta}(\mathbf{r}')\exp\left[i\mathbf{q}\cdot(\mathbf{r}-\mathbf{r}')\right]\times\psi_{j\alpha}(\mathbf{r})\psi_{i\beta}(\mathbf{r}')d\mathbf{r}d\mathbf{r}'. \quad (17)$$

The values of $S(q)$ range from $S=0$ for small values of q (recoil not sufficient to excite the atom), to $S=1$ for $q\gg\hbar/$(atomic radius) (i.e., electrons effectively free, and random phase relations between the contributions of different electrons). Heisenberg[7] has shown how the incoherent scattering factor $S(q)$ can be computed on the basis of the Fermi-Thomas atom model. The numerical values are given by Bewilogua. We have extended his calculations to smaller values of q. The results of Bewilogua[8] thus supplemented are given in Table I.

For the cross section $\Phi(E_1, v)dv$ for emission of a quantum of energy between vmc^2 and $(v+dv)mc^2$ in an incoherent radiative process, we obtain the general expression

$$dv\int(4\pi e/q^2)^2 ZS(q)G(q, v, E_1)dq, \quad (18)$$

where $G(q, v, E_1)$ is already known from the theory of the coherent radiative processes. Evaluating (18) on the basis of the Fermi-Thomas model, we find in the limit of primary energies very great in comparison with mc^2 (complete screening)

$$\Phi_{\text{inelastic}}(E_1, v)dv=(Z/137)(e^2/mc^2)^2(dv/E_1^2v)\cdot\{(E_1^2+E_2^2)(29.1-8/3\ln Z)-(2E_1E_2/3)(28.4-8/3\ln Z)\}. \quad (19)$$

Here $E_2=E_1-v$.

The cross section for production of a pair of particles with energies E_1mc^2 and E_2mc^2 is obtained in a similar way in the case $v\gg1$:

$$\Phi_{\text{inelastic}}(v, E_1)dE_1=(Z/137)(e^2/mc^2)^2(dE_1/v^3)\cdot\{(E_1^2+E_2^2)(29.1-8/3\ln Z)+(2E_1E_2/3)(28.4-8/3\ln Z)\}. \quad (20)$$

In order to have a check on the accuracy of this application of the Fermi-Thomas model, we have also carried through the integration of (18) for nitrogen in the limiting case of high energies, by using atomic wave functions,[9] and for hydrogen, for all energies. The results are given in Fig. 1.

Radiative and pair production processes in the fields of atomic electrons will make themselves very noticeable in the multiplicative production

[7] W. Heisenberg, Physik. Zeits. **32**, 737 (1931).
[8] L. Bewilogua, Physik. Zeits. **32**, 740 (1931).
[9] Morse, Young and Haurwitz, Phys. Rev. **48**, 948 (1935). We are indebted to Professor Morse for supplying us with the tables employed in computing the wave functions for nitrogen.

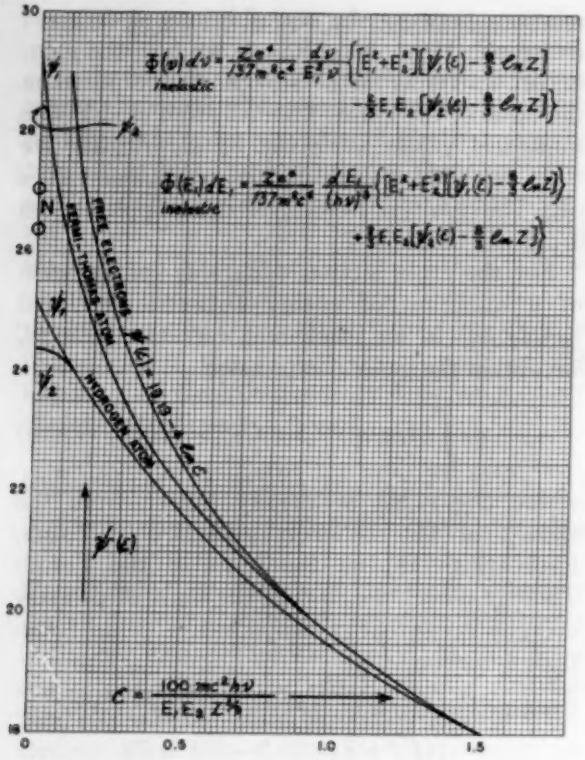

FIG. 1. Screening factors for inelastic pair production and radiative processes. The two points marked N give the factors ψ_1 and ψ_2 as calculated for nitrogen from atomic wave functions. For free electrons $\psi_1=\psi_2=\psi$.

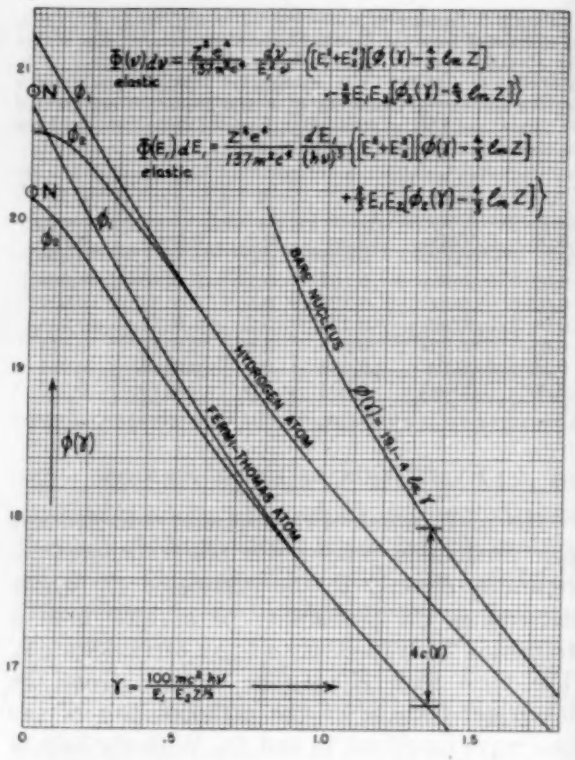

FIG. 2. Screening factors for pair production and radiative processes which leave the atom unexcited. The points N are for nitrogen. The two curves marked "Fermi-Thomas atom" are taken from the paper of Bethe and Heitler, where a table is also given for larger values of γ of the quantity $c(\gamma)$ which determines the difference between the curves for the Fermi-Thomas atom and a bare nucleus.

of cosmic-ray showers in substances of low atomic weight, such as air and water.[10] In order to make it possible to compare their importance for light elements with the corresponding elastic processes considered by Bethe and Heitler, we have supplemented the calculations of the latter authors, based on the Fermi-Thomas atom, with computations for nitrogen and hydrogen, by using atomic wave functions (Fig. 2).

Taking air as an example, and basing our choice of screening constants on the values obtained for nitrogen, we obtain for the integrated cross section for production of pairs by a very high energy quantum the result

$$\Phi_{\text{pairs}}=\Phi_{\text{elastic}}+\Phi_{\text{inelastic}}$$
$$=(41.9+6.94)\times10^{-26}\ \text{cm}^2. \qquad (21)$$

[10] L. Landau and G. Rumer (Proc. Roy. Soc. **A166**, 213 (1938)) have taken this effect into account in a preliminary way by replacing Z^2 in the formula of Bethe and Heitler by $Z(Z+1)$.

CONCLUSION

Because of the possibility of collisions in which an atom is excited, a fast electron passing through matter will radiate at a greater rate than would be expected if the atoms traversed presented to the electron simply a static field of force. In a similar way, energetic quanta will produce pairs at a greater rate. Consequently the unit of length characteristic of the multiplicative production of cosmic-ray showers will be decreased by a factor which in the case of air amounts to 17 percent (Eq. (21)). In addition, the probabilities of radiation and pair formation are not entirely proportional to the square of the atomic number of the absorbing material, but are supplemented by terms linear in the atomic number (mass absorption law).

Packing Fraction Differences Among Heavy Elements

ALVIN C. GRAVES
Ryerson Physical Laboratory, University of Chicago, Chicago, Illinois
(Received March 10, 1939)

A group of new packing-fraction-difference measurements are reported for the following elements: chromium, gadolinium, gold, lutecium, molybdenum, osmium, platinum, ruthenium, strontium, tantalum, tin, uranium, ytterbium and zirconium. By combining these differences with known packing fractions a number of new packing fractions are deduced. These are plotted on a packing-fraction curve. Atomic weights of osmium and lutecium are calculated. The atomic weight of osmium is still below the chemical value, while that of lutecium is shown to be the same as a recent chemical determination.

THE work of many investigators on mass spectra and nuclear disintegrations has established the shape and general aspects of the packing fraction curve. Many gaps exist in the curve for which no points have been measured and many of its details are masked by experimental errors. This work was undertaken in an attempt to check the shape and position of the curve and to establish accurate points in the region of heavy elements.

METHOD

If there are in the source of a mass spectrograph two isotopes of masses $m_1=n_1i_1(1+f_1)$ and $m_2=n_2i_2(1+f_2)$, m_1 and m_2 will form a doublet if $i_1=i_2=i$. In these expressions n_1 and n_2 are integers representing ionic charges, n_1i_1 and n_2i_2 are integers known as mass numbers and f_1 and f_2 are packing fractions defined by the above expressions. The mass difference between m_1 and m_2 can be determined from the separation of the members of this doublet if there are lines on the photograph to determine a mass scale. Let I and $I+k$, where k is a small integer, be the mass numbers of isotopes used for determining the mass scale. If $x-x'$ is the separation of these isotopes and x_2-x_1 is the doublet separation, the required packing fraction difference is given by,[1]

$$f_2-f_1=\frac{2}{i^{\frac{1}{2}}}\frac{(x_2-x_1)}{(x-x')}[(I+k)^{\frac{1}{2}}-I^{\frac{1}{2}}]. \qquad (1)$$

It is preferable to bracket one isotope between two isotopes of a second element when no two sufficiently small charges, n_1 and n_2, can be found to satisfy the relation $n_1i_1/n_1=n_2i_2/n_2$ (=mass/charge) or when isotopes with which the element can be doubled are lacking, rare, or for other reasons inconvenient. Moreover, the dissymmetry introduced in the field of view by the second member of a close doublet is known to influence the setting of a comparator cross hair on the first.[2] In bracketing, larger separations reduce this last effect to a minimum. By this method two isotopes of masses $n'i_1(1+f_1)$ and $n'i_2(1+f_2)$ appear as lines on either side of an isotope of a second element of mass $ni(1+f)$ which appears on the plate at the position of mass $i(1+f)$. If the positions of the lines are x_1, x_2 and x, respectively, Dempster has shown that if we calculate,[1]

$$a=\frac{(x-x_1)}{(x_2-x_1)}(i_2^{\frac{1}{2}}-i_1^{\frac{1}{2}}) \qquad (2)$$

and
$$\Delta m=(i^{\frac{1}{2}}+a)^2-i, \qquad (3)$$

then
$$\frac{\Delta m}{i}=f-\frac{(i^{\frac{1}{2}}-i_1^{\frac{1}{2}})}{(i_2^{\frac{1}{2}}-i_1^{\frac{1}{2}})}f_2-\frac{(i_2^{\frac{1}{2}}-i^{\frac{1}{2}})}{(i_2^{\frac{1}{2}}-i_1^{\frac{1}{2}})}f_1. \qquad (4)$$

For cases discussed in this paper Eq. (4) reduces to one of the following approximations.

$$\Delta m/i=f-\tfrac{1}{2}(f_1+f_2), \qquad (5)$$

$$\Delta m/i=f-\tfrac{1}{3}(2f_1+f_2), \qquad (6)$$

$$\Delta m/i=f-\tfrac{1}{4}(3f_1+f_2). \qquad (7)$$

Equation (5), (6) or (7) is selected depending upon whether the ratio of $x-x_1$ to x_2-x_1 is approximately one-half, one-third or one-fourth,

[1] A. J. Dempster, Phys. Rev. **53**, 64 (1938).

[2] C. E. St. John and L. W. Ware, Astrophys. J. **44**, 17 (1916).

respectively. Approximations made in deriving the above formulae introduce no error larger than the experimental error.

Procedure

Plates used in these determinations were taken on Dempster's double-focusing mass spectrograph[3] and measured visually on a Gaertner comparator. The comparator, when checked for periodic error by measurements of a scale ruled on the ruling engine of Professor H. G. Gale, showed no appreciable error in the region of the screw used for these measurements. Microphotometer traces were taken of a number of exposures as a check on visual measurements. Since the screw of the microphotometer was not reliable, a trace of an accurate scale was made on the same film and doublet separations were compared with these known distances. Results obtained in this way checked the visual measurements but were not as self consistent and were not used in the results reported. For each set of elements studied, many exposures were taken and those to be measured were carefully selected on the basis of sharpness of focus, equality of intensity and symmetry of lines. This procedure accounts to a large extent for the accuracy obtained. Line intensities were equalized by varying the spark potential and by proper choice of an alloy.

Platinum-ruthenium-osmium

By using electrodes of an alloy of platinum, ruthenium and osmium in a high frequency arc source, excellent doublets were obtained at two masses. One at mass number 96 was singly charged ruthenium and doubly charged osmium; the other at mass number 99 was singly charged ruthenium and doubly charged platinum. Nineteen measurements were made on the first of these doublets and twenty-six on the second and packing fraction differences of $(+7.65\pm0.14)10^{-4}$ and $(+7.92\pm0.10)10^{-4}$, respectively, were obtained. With the same electrodes the platinum lines at 194, 195 and 196 were bracketed between ruthenium (96) and (99) and were measured on twelve, thirteen and twelve exposures, respectively. The differences obtained were $(+7.72\pm0.17)10^{-4}$, $(+7.71\pm0.20)10^{-4}$ and $(+7.69\pm0.20)10^{-4}$, respectively.

Platinum and osmium packing fractions

The packing fraction for the platinum line at 195 is known[1] to be $(+2.03\pm0.3)10^{-4}$. Hence, one can deduce the mean packing fraction of ruthenium (96) and (99) to be $(-5.68\pm0.36)10^{-4}$. If it is assumed that the weighted mean for these two elements as given in Eq. (6) is the same as that given in Eq. (5), the packing fractions for platinum (194) and (196) can be deduced. Results of this calculation are $(+2.04\pm0.4)10^{-4}$ and $(+2.01\pm0.4)10^{-4}$, respectively, which are nearly the same as Dempster's value for platinum (195). If the packing fraction of ruthenium (96) is assumed to be $(-5.68\pm0.36)10^{-4}$, the packing fraction of osmium (192) becomes $(+1.97\pm0.4)10^{-4}$. If in addition the platinum (194) value deduced above is assumed, the osmium (190) packing fraction becomes $(+2.00\pm0.4)10^{-4}$. In the table of masses submitted by the atomic committee of the International Union of Chemistry,[4] the packing fraction of osmium is given as -1×10^{-4}. This is below the packing fraction curve and would place elements whose packing fractions are compared with osmium in this paper below the curve. Therefore the fraction for osmium should probably be raised. The atomic weight of osmium, with 2×10^{-4} for the packing fraction and Nier's[5] value of the relative abundances for osmium, becomes 190.38. The agreement with the chemical value of 191.5 is better but leaves much to be desired.

Uranium-tin

With one electrode of uranium and one of tin, a doublet consisting of singly charged tin (119) and doubly charged uranium (238) was formed. Line intensities could be varied relative to each other by varying the spark voltage so that lines of equal intensity were obtained. The doublet was well separated and easily measured on twenty-six exposures. The mean value obtained was $(+10.12\pm0.09)10^{-4}$. The bracket of uranium (238) between tin (118) and (120) was measured on fourteen exposures as a check on the doublet

[3] A. J. Dempster, Phys. Rev. **51**, 67 (1937).

[4] O. Hahn, Ber. d. D. Chem. Ges. **71A**, 1 (1938).

[5] A. O. Nier, Phys. Rev. **52**, 885 (1937).

measurement and was found to give a value of $(+10.12\pm0.13)10^{-4}$.

The known packing fraction for uranium,[6] $(+5.56\pm0.1)10^{-4}$, gives for tin (119) the value $(-4.56\pm0.13)10^{-4}$ from the doublet, and for tin (118) and (120) an average value of $(-4.56\pm0.23)10^{-4}$ from bracket measurements. Dempster[6] has given values for tin which are within the experimental errors given.

Gold-molybdenum

The gold-molybdenum bracket was obtained with one electrode of gold and one of molybdenum. The lines obtained were sharp and easy to measure. Eleven exposures of doubly charged gold (197) bracketed between molybdenum (97) and (100) were measured and checked by calculating the bracket of gold (197) between molybdenum (98) and (100) on twelve exposures. The mean differences obtained were $(+7.95\pm0.06)10^{-4}$ and $(+8.13\pm0.07)10^{-4}$, respectively.

The packing fraction for gold (197) is[1] $(+2.0\pm0.4)10^{-4}$ which gives as a mean packing fraction for molybdenum (97) and (100), $(-5.95\pm0.4)10^{-4}$ and for molybdenum (98) and (100) a mean value of $(-6.13\pm0.4)10^{-4}$. Dempster[1] has compared molybdenum with platinum at masses 97 and 98 and with osmium at masses 95 and 96. By using his results in conjunction with the values for platinum and osmium obtained in a previous section of this paper, the packing fractions of molybdenum (95), (96), (97) and (98) are found to be $(-5.76\pm0.5)10^{-4}$, $(-5.61\pm0.5)10^{-4}$, $(-5.66\pm0.5)10^{-4}$ and $(-5.67\pm0.5)10^{-4}$, respectively.

Tantalum-zirconium

Doubly charged tantalum (181) was bracketed between singly charged zirconium (90) and (91) when metallic electrodes of these elements were used. Six exposures were measured to determine a mean packing fraction difference of $(+7.71\pm0.09)10^{-4}$. The bracket of tantalum (181) between zirconium (90) and (92) was also measured on six exposures. The difference obtained from this bracket was $(+7.77\pm0.08)10^{-4}$.

Aston[7] gives an estimate of the packing fraction of tantalum of $(-4\pm3)10^{-4}$. This value is about 5 units below the curve and would place zirconium about the same distance below the curve. This is improbable and no attempt to deduce a packing fraction for either of these elements will be made until a more accurate value for one of them has been obtained.

Gadolinium-chromium

Many exposures with different types of electrodes were taken of these two elements in getting equal intensities. The large number of electrodes used permitted four different measurements to be made with optimum intensities for each. For one set of plates an electrode was made by packing a nickel tube with gadolinium oxide and filings of neodymium. The second electrode was of Nichrome wire for some plates and stainless steel for others. Other plates were made with both electrodes of nickel tubes filled with 25 mg of gadolinium oxide, 25 mg of lanthanum and from 0.5 to 5.0 mg of chromium filings. Eighteen measurements were made on the triply charged gadolinium (156), singly charged chromium (52) doublet. This measurement was checked by the bracket of chromium (52) between gadolinium (155) and (157) on sixteen exposures. The differences obtained were $(+6.37\pm0.11)10^{-4}$ and $(-6.39\pm0.09)10^{-4}$, respectively. Chromium (53) was bracketed between gadolinium (158) and (160) on ten exposures and on six exposures gadolinium (160) was bracketed between chromium (53) and (54). The results measured on these brackets were $(-6.38\pm0.13)10^{-4}$ and $(+6.33\pm0.26)10^{-4}$, respectively.

Recently Aston[8] has reported a value for the packing fraction of chromium (52) of -8.18×10^{-4} with an error in mass units of 0.0008 which corresponds to an error in his packing fraction of 0.15×10^{-4}. If this value is assumed, the packing fraction of gadolinium (156) is $(-1.81\pm0.19)10^{-4}$ and the average value for gadolinium (155) and (157) is $(-1.79\pm0.18)10^{-4}$. The assumed packing fraction of chromium and those values deduced from it are below the packing fraction curve.

Ytterbium-strontium

For ytterbium and strontium determinations, electrodes were nickel tubes filled with 25 mg

[6] A. J. Dempster, Phys. Rev. **53**, 872 (1938).
[7] F. W. Aston, *Mass Spectra and Isotopes* (Edward Arnold & Co., 1933), pp. 141, 235.
[8] F. W. Aston, Nature **141**, 1096 (1938).

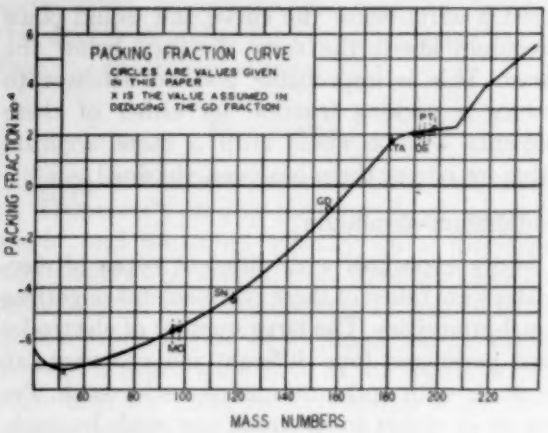
PACKING FRACTION CURVE
CIRCLES ARE VALUES GIVEN IN THIS PAPER
X IS THE VALUE ASSUMED IN DEDUCING THE GD FRACTION
PACKING FRACTION ×10⁴
MASS NUMBERS

FIG. 1.

of ytterbium oxide, 25 mg of lanthanum and varying amounts of strontium. Plates were taken using 10, 15, 30 and 60 mg of strontium filings. Twenty-four measurements were made of the doublet formed by doubly charged ytterbium (172) and singly charged strontium (86) to give a mean packing fraction difference of $(+6.20\pm0.15)10^{-4}$. Ten measurements of the doublet between ytterbium (174) and strontium (87) were made with a mean result of $(+6.18\pm0.14)10^{-4}$. In addition strontium (86) was bracketed between ytterbium (171) and (173) on thirteen exposures. The measured difference was $(-6.48\pm0.19)10^{-4}$. A strong line was found at the position of mass 175. The only isotope of this mass number is lutecium which was present as an impurity in the ytterbium. Seven measurements were made on the strontium (87) line bracketed between ytterbium (173) and lutecium (175) and the difference measured was $(-6.37\pm0.16)10^{-4}$. A comparison of this result with other results discussed in this section indicates that there can be no large difference in the packing fractions of lutecium and ytterbium. This was checked by making ten measurements of the lutecium line compared with ytterbium (173) and (174). The results of this and a different calculation on the same measurements were $(0.00\pm0.34)10^{-4}$ and $(+0.05\pm0.20)10^{-4}$, respectively.

That the packing fraction of lutecium is about the same as that of ytterbium is of interest in view of the recent atomic weight determination

TABLE I. *Summary of doublets and brackets measured. I is the mass number at which the comparison is made; n is the number of exposures measured; $f=(m-I)/I$ is the packing fraction if m is the mass and I is the mass number of the ion. In the description of the function measured in the last column, the f's are in order of the ions in column 3.*

COMPARISON NUMBER	I	IONS COMPARED (PART 1)	n	$(f_1-f_2)10^4$
1	52	Gd(156)−Cr(52)	18	+6.37±0.11
2	86	Yb(172)−Sr(86)	24	+6.20±0.15
3	87	Yb(174)−Sr(87)	10	+6.18±0.14
4	96	Os(192)−Ru(96)	19	+7.65±0.14
5	99	Pt(198)−Ru(99)	26	+7.92±0.10
6	119	U(238)−Sn(119)	26	+10.12±0.09
		(PART 2)		$[f_1-\frac{1}{2}(f_2+f_3)]10^4$
7	52	Cr(52)−Gd(155), Gd(157)	16	−6.39±0.09
8	53	Cr(53)−Gd(158), Gd(160)	10	−6.38±0.13
9	86	Sr(86)−Yb(171), Yb(173)	13	−6.48±0.19
10	87	Sr(87)−Yb(173), Lu(175)	7	−6.37±0.16
11	90.5	Ta(181)−Zr(90), Zr(91)	6	+7.71±0.09
12	96	Ru(96)−Os(190), Pt(194)	5	−7.70±0.11
13	97.5	Pt(195)−Ru(96), Ru(99)	13	+7.71±0.20
14	98.5	Au(197)−Mo(97), Mo(100)	11	+7.95±0.06
15	119	U(238)−Sn(118), Sn(120)	14	+10.12±0.13
16	174	Yb(174)−Yb(173), Lu(175)	10	+0.05±0.20
		(PART 3)		$[f_1-\frac{1}{3}(2f_2+f_3)]10^4$
17	53.3	Gd(160)−Cr(53), Cr(54)	6	+6.33±0.26
18	97	Pt(194)−Ru(96), Ru(99)	12	+7.72±0.17
19	98	Pt(196)−Ru(99), Ru(96)	12	+7.69±0.20
20	175	Lu(175)−Yb(174), Yb(173)	10	+0.00±0.34
		(PART 4)		$[f_1-\frac{1}{4}(3f_2+f_3)]10^4$
21	90.5	Ta(181)−Zr(90), Zr(92)	6	+7.77±0.08
22	98.5	Au(197)−Mo(98), Mo(100)	12	+8.13±0.07

TABLE II. *New packing fraction determinations. By using packing fraction differences given in Table I and assuming a packing fraction for one element, the packing fraction for a second element can be determined. The comparison numbers of the first column correspond to those in Table I.*

COMPARISON NUMBER	$f\times10^4$ ASSUMED		$f\times10^4$ DEDUCED	
13	Pt(195)	+2.03±0.3	Ru(96), (99)	−5.68±0.36
18	Ru(96), (99)	−5.68±0.36	Pt(194)	+2.04±0.4
19	Ru(96), (99)	−5.68±0.36	Pt(196)	+2.01±0.4
5	Ru(99)	−5.68±0.36	Pt(198)	+2.24±0.4
12	Ru(96)	−5.68±0.36		
	Pt(194)	+2.04±0.4	Os(190)	+2.00±0.4
4	Ru(96)	−5.68±0.36	Os(192)	+1.97±0.4
6	U(238)	+5.56±0.1	Sn(119)	−4.56±0.13
15	U(238)	+5.56±0.1	Sn(118), (120)	−4.56±0.23
14	Au(197)	+2.00±0.4	Mo(97), (100)	−5.95±0.4
22	Au(197)	+2.00±0.4	Mo(98), (100)	−6.13±0.4
Mo−Os[1]	Os(190)	+2.00±0.4	Mo(95)	−5.76±0.5
Mo−Os[1]	Os(192)	+1.97±0.4	Mo(96)	−5.61±0.5
Mo−Pt[1]	Pt(194)	+2.04±0.4	Mo(97)	−5.66±0.5
Mo−Pt[1]	Pt(196)	+2.01±0.4	Mo(98)	−5.67±0.5
1	Cr(52)	−8.18±0.15	Gd(156)	−1.81±0.19
7	Cr(52)	−8.18±0.15	Gd(155), (157)	−1.79±0.18

of Hönigschmid[9] on lutecium. He obtained an atomic weight of 174.98 and by assuming a packing fraction of -4×10^{-4} he deduced an atomic weight from physical measurements of 174.91. When this was corrected for an isotope reported by Gallnow[10] from spectroscopic evidence to be present at 173 or 177, he obtained an atomic weight of 174.96 if the higher isotope was present to about 2.5 percent. From the present curve it is improbable that the packing fraction of lutecium is lower than 0.5×10^{-4}. This corresponds to an atomic weight of 174.96 and if there is an isotope present at 177 its relative abundance must be less than one percent.[11]

[9] O. Hönigschmid, Naturwiss. **25**, 748 (1937).
[10] H. Gallnow, Zeits. f. Physik **103**, 443 (1936).
[11] J. Mattauch and H. Lichtblau (Zeits. f. Physik **111**, 514 (1939)) report an isotope of lutecium at 176 with a relative abundance of 2.58 percent. This yields an atomic weight of 174.99 in good agreement with Hönigschmid's value.

SUMMARY

Results discussed above are summarized in Tables I and II, and in Fig. 1. Table I is divided into four parts. Part 1 gives the results obtained when the function of the packing fraction given by Eq. (1) is calculated. Similarly, Parts 2, 3 and 4 are calculations from Eqs. (5), (6) and (7). Plus and minus values appended are probable errors.

The author wishes to express his appreciation to Professor A. J. Dempster for permission to use his mass spectrograph, for suggesting the problem and for his many helpful suggestions in completing the above investigation.

Diurnal and Sidereal Effects and the Meteorologic Influences on Shower and Vertical Intensity of Cosmic Rays

J. Barnóthy and M. Forró
Institute for Experimental Physics, University of Budapest, Budapest, Hungary
(Received February 24, 1939)

During the period of a year we have measured three million shower coincidences with counters arranged in a triangle and a threefold coincidence apparatus. The results were analyzed by the method of multiple correlation for a possible influence of meteorologic and magnetic factors on shower intensity and through harmonic analysis for the existence of a diurnal and sidereal periodicity. Table I shows the results obtained.

The major part of the showers we observe at sea level is produced by electrons which originate from the disintegration of mesotrons in the lower portion of the atmosphere, in a layer of about 170 g/cm² thickness. The intensity of the showers will therefore depend on the number of the mesotrons reaching the lower region of the atmosphere and also on how many of these mesotrons will decay in that layer of 170 g/cm² thickness, from where the cascade electrons can still arrive at the apparatus. If the vertical extension of this layer is altered, through a variation in the barometric pressure or the temperature, then the number of the mesotrons disintegrating in the layer will change because of the change which occurs in the length of their path in the layer. Therefore the barometric and temperature effect on the shower intensity is equal to the barometric effect or temperature effect on the mesotron intensity in addition to the barometric effect or temperature effect on the probability of disintegration of the mesotrons in the layer producing the observed shower intensity. The first part, that is the barometric effect or temperature effect on the mesotron intensity can be determined with a vertical arrangement. As the aperture of a triangle arrangement is rather wide, for comparison we have put in Table I column 3 the corresponding data obtained with a vertical arrangement of wide aperture.[1, 2]

A decrease of 1 mm Hg in the barometric pressure will have as a consequence the extension by about 0.14 percent of the layer in which the observed showers are formed. Hence the barometric effect on the shower intensity should be greater than the barometric effect of the vertical intensity by this amount.

An increase of 1°C in the air temperature will be followed by an extension of the lower region of the atmosphere by about 0.35 percent, and a corresponding increase in the intensity of the showers. This effect alone would induce a positive temperature effect, and therefore it must be subtracted from the negative temperature effect of the vertical intensity to obtain the proper value of the temperature effect for the measured shower intensity. By calculating the temperature effect from hourly means, we must still take into consideration that—as meteorologic observations attest—the daily temperature variation does not extend over 1.5 to 2 km height (corresponding to a layer of material about 170 g/cm² thick). Therefore the average daily variation of the temperature in this layer 170 g/cm² thick will be less than the variation observable at the earth's surface. By assuming that the amplitude of the temperature variation declines linearly with height and attains zero value at 2 km, one would be obliged to calculate with half as great a variation of the average temperature as that which is practically observable. But on account of the absorption of the showers, the contribution of the mesotrons to the observed shower intensity will be greater the nearer to the counters their decay takes place. As a first approximation the shower intensity is assumed to decline linearly with height. Then we find that only two-thirds of the observed temperature variation will be efficacious and the temperature effect of the showers, calculated from the hourly means, should differ from the temperature effect of the vertical intensity only by

[1] J. Barnóthy and M. Forró, Zeits. f. Physik **100**, 742 (1936).
[2] J. Barnóthy and M. Forró, Zeits. f. Physik **104**, 534 (1937).

TABLE I. *Variations of shower and vertical intensities.*

	SHOWER INTENSITY	VERTICAL INTENSITY	DIFFERENCES	
			MEASURED	CALCULATED
Barometric effect Percent per mm Hg	−0.42 ±0.03	−0.29 ±0.03	−0.13±0.04	−0.14
Temperature effect from hourly means Percent per °C	−0.10 ±0.08	−0.42 ±0.07	+0.33±0.11	+0.35
Temperature effect from hourly means Percent per °C	+0.14 ±0.01	−0.10 ±0.02	+0.24±0.02	+0.23
Magnetic effect Percent per 10^{-5} gauss	+0.004±0.004	−0.056±0.003		
Sideral time periodicity Amplitude Percent Time of the Max. S.T.	0.15 16^h 17′	0.40 9^h 13′		
Diurnal variation Amplitude Percent Time of the Max. M.E.T.	0.41 15^h	0.49 10^h		

two-thirds of 0.35 percent, that is by 0.23 percent.

For vertical radiation and small aperture we have not found a temperature effect and for wide aperture the experimental value of the temperature effect was very small when determinations were made from the hourly means.[2] This is comprehensible on the basis of the explanation given by Blackett[3, 4] for the temperature effect of the vertical radiation; that is, the daily temperature variation does not extend beyond a height of 2 km, and the levels where the mesotrons are formed do not alter their distance from the earth, and hence the intensity of the mesotrons remains unchanged. The positive temperature effect of the shower surpasses the small negative temperature effect of the mesotrons and will furnish finally for shower intensity the positive value of the temperature effect which is found experimentally. From columns 4 and 5 in Table I we can see that the above calculated differences agree well with the observed differences.

The diurnal variation of the shower intensity seems to be a consequence of the daily variation of the air temperature[5] and not, as was shown in the case of the vertical radiation,[2] a consequence of the daily fluctuation of the intensity of the earth's magnetic field.

The sidereal time periodicity is apparently also for shower intensity a consequence of the galactic rotation. We have shown elsewhere[6, 7] that the maximum of the intensity does not occur at the time when the direction of motion of our solar system is culminating (20^h40^m), but it is displaced to later hours. It appears that this phase shift would be an inference of the magnetic deflectibility of the rays, since we found that the displacement is smaller for more inclined directions corresponding to greater mean energy of the incoming rays. For the same reason the observed displacement will be less for an apparatus with wide aperture.

We may assume that the production of showers in the lower region of the atmosphere by mesotrons of different energy will be proportional to the probability of their disintegration and so inversely proportional to their energy. Furthermore it seems very probable that greater energy of the mesotrons is associated with greater energy of the incoming primaries, so that the primaries of the observed shower should be softer than those of the vertical intensity observed with an apparatus of large aperture. The experimental records fit well with these assumptions, as we have found for the vertical arrangement a phase shift of 12^h and in case of the shower a phase shift of 19^h.

We should expect an increase of the intensity in the direction of the motion for three main reasons: (1) change in the number of the in-

[3] P. M. S. Blackett, Nature **142**, 992 (1938).
[4] P. M. S. Blackett, Phys. Rev. **54**, 973 (1938).
[5] M. Forró, Nature **139**, 633 (1937).
[6] J. Barnóthy and M. Forró, Nature **139**, 1064 (1937).
[7] J. Barnóthy and M. Forró, *Réunion International de physique, chimie, et biologie*, (Paris, October, 1937), p. 166.

coming particles[6] (0.3 percent); (2) decrease of the probability of disintegration of the mesotrons by increase of their energy (0.1 percent); (3) change in the radius of curvature of the rays through increase of their energy, which effect is equal to that produced by a decrease of the intensity of the earth's magnetic field.[6, 7] This portion of the change can be calculated from the value of the magnetic effect and is always proportional to it. To calculate from these three components the amplitude to be expected for the sidereal wave, we have still to multiply their sum by a factor F, which depends on the maximum and minimum value of the angle between the direction of the translatory motion and the direction of the incoming rays. In our latitudes (47° 30′) and for apparatus with wide aperture F has the mean value 0.2. Hence we obtain finally as the amplitude to be expected with a vertical arrangement of wide aperture 0.3 percent and with a shower arrangement 0.06 percent, since for showers only part (1) is efficacious as (3) is ineffective because of the missing magnetic effect and (2) is compensated through the simultaneous diminution in the shower production. We can see that these values agree fairly well with the experimental results.

The experiments were performed with the kind assistance of the Hungarian Council for Natural Science and the Szécheny Scientific Society.

[6] A. H. Compton and I. A. Getting, Phys. Rev. **47**, 817 (1935).

MAY 1, 1939 PHYSICAL REVIEW VOLUME 55

Cosmic-Ray Particles at Great Depth

J. BARNÓTHY AND M. FORRÓ
Institute for Experimental Physics, University of Budapest, Budapest, Hungary

(Received March 13, 1939)

DURING the year 1938 we have performed measurements of cosmic radiation in a coal mine at 980 meters water-equivalent depth.

We have determined the twofold and threefold counting rates for the same distance between the top and bottom G-M tube when the entire absorber between the tubes consisted only of the tube walls and was equivalent to 0.4 cm Pb. Because of the good resolving time of the circuit employed ($\vartheta = 1.4 \times 10^{-6}$ sec.) the accidental counts were, even for the twofold coincidences, less than $\frac{1}{10}$th of the recorded counts. The efficiency of the G-M tube was found to be 5 percent, whereas at sea level it was nearly 100 percent. This can be explained by assuming that the major part of the radiation, measured with twofold coincidences and with only thin layers of material between the tubes, consists of feebly ionizing rays.

The solid curve of Fig. 1 represents the data and their probable error obtained with twofold coincidences when the thickness of the absorbing layer between the tubes was varied from 0.2 cm Pb up to 1.4 cm Pb. The arrangement was shielded from both sides with 15 cm Pb. The number of the accidental counts and those produced through showers (6/hour) were subtracted from the values obtained. The whole curve was measured three times and the positions of the maximum and minimum were always found at the same thickness of lead. The same experiment was then repeated with the whole arrangement turned through 90°. In this case only horizontal rays or rays deviating therefrom not more than 40° could produce coincidences. The dotted line represents the results obtained. We observe: (1) that the value of the intensity and its decrease with interposed lead is equal to that of the vertically incident rays; and (2) that there is apparently no trace of a maximum.

These results, together with those found in connection with the efficiency of the counters, lead to the conclusion that the absorption corresponding to the dotted line is due in both cases to photons, which have, as it is well known, an efficiency of 2 or 3 percent, and it seems not unlikely that they are of radioactive origin. On

the other hand, the maximum must be regarded as a characteristic feature of the vertical radiation and perhaps is caused by γ-rays produced by cosmic radiation. If there is no lead between the counters, the efficiency of these rays in producing twofold coincidences will be very small, but in a sufficiently thick layer of lead they are able to create cascade electrons. Thus the counting rate increases considerably, since now the feebly ionizing γ-radiation is obliged only to discharge the upper counter. The lower counter is discharged by the electrons. This may explain the maximum found for 0.7 cm Pb. The whole phenomenon can be described by a Rossi curve but the maximum of the intensity is found at half as great thickness of lead as at sea level. This result is consistent with our previous conclusions drawn from our experiments performed two years ago,[1] namely that at great depth the majority of the ionizing radiation consists of shower particles, which are softer than the particles of the showers at sea level.[2]

Figure 2 represents the data obtained by means of threefold coincidences. A total of 7000 coincidences were registered in 4000 hours. The thickness of the interposed lead was varied from 0 to 120 cm. We may see from Fig. 2 (full line) that when lead was placed only between the two lower tubes the intensity decreased rapidly until a thickness of 10 cm had been reached. We seem to detect the same decrease in the measurements

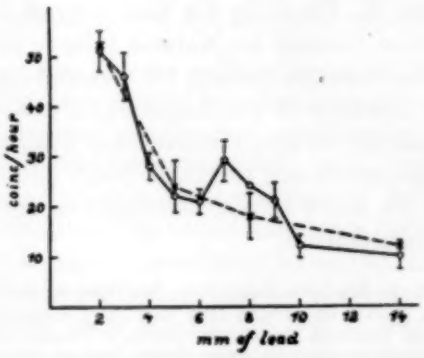

FIG. 1. Absorption of cosmic rays at 980 m depth in thin layers of lead between a twofold coincidence counter.

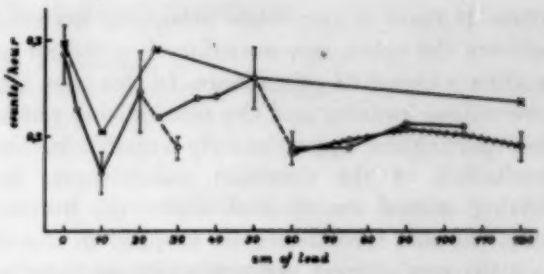

FIG. 2. Absorption of cosmic rays at 980 m depth in lead obtained with three counters. The line with crosses represents the measurements of V. C. Wilson. Full line: No lead between two upper tubes, varying thickness between lower tubes. Dotted line: 20 or 50 cm of lead between the center and bottom tubes; additional lead is placed between the upper tubes. Crossed line: 60 cm of lead between the top and center tubes, additional lead between the lower tubes.

performed by Volney C. Wilson[3] at 300 m water-equivalent depth, although he did not take into consideration the point at 10 cm Pb. In Fig. 2 we have drawn the curve corresponding to his measurements but have taken into account the point at 10 cm Pb; the two curves were adjusted at 50 cm Pb. If lead is placed between the top and center tubes, when 20 cm or 50 cm of Pb is in position between the lower tubes, the intensity again decreases considerably until an additional thickness of 10 cm has been placed between the upper tubes. (See dotted lines.) But if lead is placed between the two lower tubes when 60 cm Pb was between the top and center tube, the additional increase of lead between the lower tubes does not alter remarkably the intensity (crossed line).

In our opinion this behavior may be due to the following circumstances: great depth can be attained by an ionizing radiation (most probably mesotrons or perhaps protons) and by a non-ionizing radiation (neutrinos or neutrettos[4]). The greater the depth, the more important the non-ionizing component becomes and at 1000 m depth it may strongly exceed the number of the ionizing particles. The non-ionizing radiation produces along its path secondaries (photons, electrons) which give rise to a cascade shower. In this way the non-ionizing radiation is always accompanied, in a certain small percentage of its range, by ionizing particles and so it is able to discharge, but with small probability, the G-M

[1] J. Barnóthy and M. Forró, Nature **138**, 325 (1936); Zeits. f. Physik **104**, 744 (1937).
[2] J. Clay and P. H. Clay, Physica **2**, 1042 (1935) were the first to show that shower particles are to be found even at greater depth.
[3] V. C. Wilson, Phys. Rev. **55**, 6 (1939).
[4] N. Arley and W. Heitler, Nature **142**, 158 (1938).

tubes. If there is very little absorbing material between the tubes, one secondary is sufficient to produce a threefold coincidence. In this case, the penetrating ionizing and the non-ionizing radiation participate approximately equally in the production of the threefold coincidences. By putting several cm of lead above the bottom tube, the soft secondaries are stopped in it and now the non-ionizing ray needs two secondaries to be able to produce a threefold coincidence; accordingly the coincidence rate corresponding to the non-ionizing component will decrease to a small fraction of its original value. We will find the same behavior when lead is put above the center tube, no matter what thickness of lead is already between the center and the bottom tube, because now a non-ionizing ray is not able to discharge the two upper tubes with only one soft secondary. In a thicker layer of lead, however, the probability that a non-ionizing ray makes an encounter with a nucleus increases considerably and through transformations described by Heitler[5] or multiple processes discussed by Heisenberg[6] it can produce one or more heavy ionizing particles, which are able to penetrate through large thickness of lead. Here, we believe, lies the explanation of the increase of the intensity after the minima. In the second case, with 50 cm Pb between the lower tubes, the increase is less, as now only mesotrons of greater energy are able to discharge the apparatus.

The intensity variation corresponding to the crossed line should be attributed to heavy ionizing particles, most probably to mesotrons. It is possible that these mesotrons are created by non-ionizing particles, but in this case it is necessary to assume, that all of them have a range of several meters of lead, because the intensity does not decrease considerably between 60 cm and 120 cm Pb. This supposition does not seem to be likely. A second interpretation would be to assume that the non-ionizing radiation produces coincidences with the help of three soft secondaries. This seems unlikely too, because if the whole intensity should be attributed to a non-ionizing radiation, the rather small decrease up to 10 cm Pb (corresponding to a change from one to two secondary rays) would indicate that the non-ionizing ray is accompanied on half of its path by ionizing secondaries. The third explanation would be that these ionizing particles are primaries. It is true that a particle loses through ionization only approximately 4×10^{11} e-volts energy until it can attain 980 m depth. From the energy statistics of Blackett[7] we know that 2 percent of the rays to be found at sea level have a greater energy than 4×10^{10} e-volts. Assuming an energy distribution decreasing with the square of the energy, one can compute that 0.2 percent have greater energies than 4×10^{11} e-volts. This agrees well with the observation that the intensity at 980 m depth and with 120 cm Pb between the tubes was found to be only 0.15 percent of the total intensity at sea level. This explanation seems to be the most probable, even though for such great energies the radiative losses become appreciable[8] also for heavy particles.

We think that the most important question would be to determine the efficiency of the radiation at great depth when the thickness of the interposed lead absorber is very great (such measurements are now being made).

The authors wish to express their gratitude to Professor K. Tangl for his kind interest, to the Hungarian Council for Natural Science and the Szecheny Scientific Society for financial support, to the directors of the Salgotarjani Coal Mine Company for making the coal mine available for the experiments and to Mr. D. Nagy and Mr. Z. Ozorai for much helpful assistance in obtaining the measurements.

[5] W. Heitler, Proc. Roy. Soc. **166**, 529 (1938).
[6] W. Heisenberg, Zeits. f. Physik **101**, 533 (1936).
[7] P. M. S. Blackett, Proc. Roy. Soc. **159**, 1 (1937).
[8] If it should be proved that this third explanation is right, our previous statement (Zeits. f. Physik **104**, 744 (1937)) namely that at great depth the number of the penetrating ionizing particles is to be neglected besides the number of the soft shower particles, must be amended.

Symmetry Properties of Variational Functions

H. M. JAMES AND A. S. COOLIDGE
Department of Physics, Purdue University, Lafayette, Indiana, and Division of Chemistry, Harvard University, Cambridge, Massachusetts

(Received March 11, 1939)

IN A previous treatment of the ^2S ground state of lithium[1] we have employed variational functions which, we have since noticed, are not of pure doublet symmetry. In this note we wish to indicate the significance of this fact and the rôle which such symmetry properties play in general in the variational treatment of atomic systems.

To describe the ground state of lithium we have employed wave functions of the form

$$\psi(1,2,3)=(1/3)^{\frac{1}{2}}\{\varphi(1,2,3)\delta(\beta/\sigma_1)\delta(\alpha/\sigma_2)\delta(\alpha/\sigma_3)+\varphi(2,3,1)\delta(\beta/\sigma_2)\delta(\alpha/\sigma_3)\delta(\alpha/\sigma_1)+\varphi(3,1,2)\delta(\beta/\sigma_3)\delta(\alpha/\sigma_1)\delta(\alpha/\sigma_2)\},$$

with the only general restriction on φ that $\varphi(1,2,3)=-\varphi(1,3,2)$. Such a function describes a state of the atom with spin component $M_s=\frac{1}{2}$, which, however, might be a doublet or a quartet state, or a hybrid. For a pure quartet state $\varphi(1,2,3)$ must be antisymmetric to any interchange of the three variables, while for a doublet state it must be orthogonal to any such function. The functions φ can all be divided into pure doublet and quartet parts as follows:

$$\varphi=\varphi_d+\varphi_q,$$
$$\varphi_d(1,2,3)=\tfrac{1}{3}\{2\varphi(1,2,3)-\varphi(2,3,1)-\varphi(3,1,2)\},$$
$$\varphi_q(1,2,3)=\tfrac{1}{3}\{\varphi(1,2,3)+\varphi(2,3,1)+\varphi(3,1,2)\}.$$

If $\varphi=\varphi_d+\varphi_q$ were to be determined for the ground state of lithium by minimizing the energy in a variational procedure of complete flexibility, a pure doublet function would result, with the quartet part automatically eliminated. But when the flexibility of the varied function is limited by its restriction to a particular form, the function of lowest energy may contain a quartet part, unless the form of the function is especially chosen to assure pure doublet symmetry. For instance, the "separate orbital" functions of our paper, with

$$\varphi(1,2,3)=K'(1)\{K(2)L(3)-K(3)L(2)\},$$

are not pure doublet functions unless $K'=c_1K+c_2L$. It is easy to show that the "separate orbital" function of lowest energy does not meet this requirement, is not a pure doublet function, though it provides the "best" approximation of the given form to a pure doublet function. This function can, of course, be further improved (energy being still the criterion of goodness) by removing the high energy quartet part, but the residue,

$$\varphi_d(1,2,3)=\tfrac{2}{3}K'(1)\{K(2)L(3)-K(3)L(2)\}-\tfrac{1}{3}K'(2)\{K(3)L(1)-K(1)L(3)\}-\tfrac{1}{3}K'(3)\{K(1)L(2)-K(2)L(1)\},$$

is not then of the form to which the function has been restricted. If, however, we extend the definition of "separate orbital" functions to include all expressible as linear combinations of $K'(1)K(2)L(3)$ with the other functions arising from permutations of the electrons, then the best separate orbital function *is* of pure doublet type; for the quartet part of any such function can be eliminated with a resultant decrease in the energy of the function (provided only that φ_d has a lower energy than φ_q), and this without carrying the function out of the separate orbital class. The situation with respect to the "separate shell" functions of our paper is essentially similar.

In constructing more accurate functions of the Hylleraas series type we used terms some of which contain quartet parts. As these quartet parts are all expansible in the series used they would have been eliminated automatically from a wave function computed with the complete infinite variation series. Since instead we employed a limited number of these terms the elimination of the quartet parts was not complete. For instance, the ten-term function given in that paper contains a small quartet part arising from the terms $f(0001)$ and $h(0001)$, which would vanish if the coefficients of the two terms were the same. An approximate quantitative treatment of the situation indicates that the

[1] H. M. James and A. S. Coolidge, Phys. Rev. **49**, 688 (1936).

improvement of the energy attainable by subtracting the quartet part of this function would be entirely negligible. A pure doublet function could also be obtained by a variation process in which the coefficients of $f(0001)$ and $h(0001)$ were restricted to equal values. This decrease in the flexibility of the function would make the computed energy worse by some 0.0004 ev; conversely one might make similar improvements by relaxing the restriction to equality of the coefficients of such terms as $g(1010)$ and $g(1100)$, thus permitting a further increase in the quartet part of the functions. From the smallness of these changes it appears that we would not have been justified in undertaking the considerable labor which would have been required to eliminate the quartet parts of the trial functions without reduction of their flexibility; on the other hand, we might have assured doublet symmetry with a loss of flexibility of little importance in the computation, by imposing equality of certain coefficients.

This raises the question as to whether the possession by an approximating function of the symmetry properties of the exact function is an indication of goodness which would justify some sacrifice of accuracy in the computed energy. To avoid involvement with the well-understood use of symmetry properties in simplifying the treatment of excited states we shall restrict attention to the cases of the ground states of Li and H_2^+.

The practical use of variational wave functions is of course not in the deduction of selection rules or other properties of the system which depend essentially on symmetry, but in computations the accuracy of which depends on smallness of the mean-square-error q^2, the mean-square-energy-deviation δ^2, etc., of the wave function.[2] Taking q^2 as our criterion of accuracy, we have

$$q^2 \gtrsim \epsilon/(E_2-E_1).$$

[2] H. M. James and A. S. Coolidge, Phys. Rev. **51**, 860 (1937).

Here ϵ is the energy error, E_1 the correct ground state energy, and E_2 the energy of the lowest excited state having the symmetry of the approximating function—the first excited state if this function has no special symmetry. In the case of H_2^+ the first state above the $^2\Sigma_g$ ground state is a $^2\Sigma_u$ state, the next $^2\Sigma_g$ state lying considerably higher. Given two approximate functions with the same energy, the first possessing the g symmetry of the exact function, the second no special symmetry, the upper limit on q for the first will be considerably lower than that for the second. But in the case of Li all the low states are doublet states, and the upper limit placed on q is not lowered by giving the approximate function the exact doublet symmetry of the ground state function.

That the natural expectation of accuracy corresponds to the value of the upper limit on q may be seen thus: Let the approximating function ψ be expanded in terms of the exact functions.

$$\psi = a_1\psi_1 + a_2\psi_2 + \cdots.$$

The presence in this series of the small term $a_n\psi_n$ introduces a root-mean-square error in ψ of the order of a_n^2, and an energy error of the order of $a_n^2(E_n-E_1)$. Thus the larger E_n-E_1 the more sensitive is the energy to introduction of a given root-mean-square-deviation in ψ by addition of $a_n\psi_n$. If a restriction on the symmetry of ψ would eliminate the possibility of error to which the energy is insensitive (as in H_2^+), the symmetry of ψ is a useful additional criterion of its goodness. But if restriction of the symmetry eliminates errors to which the energy is sensitive in favor of those to which it is not sensitive it is not reasonable to sacrifice goodness of the computed energy to assure a definite symmetry. This is the case with Li; for practical purposes the use of the computed energy as the single criterion of goodness in a treatment of the ground state is thus justified.

LETTERS TO THE EDITOR

Prompt publication of brief reports of important discoveries in physics may be secured by addressing them to this department. Closing dates for this department are, for the first issue of the month, the eighteenth of the preceding month, for the second issue, the third of the month. Because of the late closing dates for the section no proof can be shown to authors. The Board of Editors does not hold itself responsible for the opinions expressed by the correspondents.

On Stability in the Sense of Poisson for Orbits of Cosmic Rays, and Magnetic Storms

The question of stability of the orbits of cosmic rays presents great physical interest. In a forthcoming paper to appear in a mathematical journal we shall prove that all bounded orbits of charged particles in the field of a magnetic dipole are not stable in the sense of Poisson.[1] This conclusion contradicts a theorem already announced by Schremp,[2] without thereby affecting either his theorems 1 and 2, from which he thought the theorem in question could be deduced, or his other theorems.

To begin with we prove that the regions of stability[3] around stable periodic orbits are infinitesimal. This is a consequence of the fact that the potential energy[4] of the motion in the meridian plane $-P(x, \lambda; \gamma_1)$ contains positive and negative powers of the distance to the dipole. The convergence of the Hamiltonian function K which enters into the variational equations of the periodic orbit therefore holds only in an annular region. The study of the successive approximations of these equations shows that this region should be divided by n when one stops at the nth approximation. If n is taken greater and greater, that is, if the time increases, the region of stability becomes smaller and smaller. When the distance is infinitesimal, the time required for all particles to leave the vicinity of the periodic orbit must be infinite.

In the second place our problem may be reduced to the problem of the motion of molecules of an incompressible liquid in an appropriate force field and in an *infinite* container. We shall than have an integral invariant[5] $\int\int\int dx d\lambda d\eta$ (in the notation used by Lemaitre and Vallarta[4]). Stability in the sense of Poisson has been proved[1] in this case, but only for a finite vessel, that is, when the integral invariant extended to the entire domain of variation of x, λ, η remains finite. Is it possible to introduce a change of independent variable defined by

$$d\sigma/d\sigma' = M(x, \lambda, \eta) \gtrless 0$$

in such a way that the integral invariant

$$\int\int\int M dx d\lambda d\eta$$

remains finite throughout the infinite domain of variation of x, λ, η? If so, the analytic continuations of the orbits, in terms of the old variable, will be stable in Poisson's sense. But it is impossible to find such a function, for the same reason that reduced the size of the region of stability of the periodic orbits to an infinitesimal domain. Nevertheless, the integral invariant

$$\int\int\int M dx d\lambda d\eta$$

remains finite for all bounded orbits which do not reach the dipole. If such orbits exist in a region of stability then they are stable in Poisson's sense, with the exception of orbits of zero measure such as asymptotic orbits. Isolated bounded orbits do not satisfy this condition of stability, because if they returned near their starting point they could be considered as new orbits, since the time origin is arbitrary. But in such a case the bounded orbit would no longer be isolated. It is therefore clear that Poisson's stability exists only in regions of stability which do not contain stable periodic orbits. Such regions, if they exist, must possess on their boundary at least one unstable periodic orbit.

It seems therefore that stable periodic orbits in the case of terrestrial magnetism will play an insignificant role as far as the external magnetic field is concerned. But a weak perturbation which keeps unaltered the qualitative characteristics of the problem (axial symmetry, etc.) may, in accordance with Poincaré's theorem of analytic continuation, enlarge to a great extent the regions of stable periodic orbits, and thus cause magnetic perturbations. Further this weak perturbation may bring and retain for a brief time charged particles on unstable periodic orbits,[6] and in regions of stability of which such orbits may be on the boundary. This would account for the fact that a magnetic storm begins abruptly and disappears slowly. But the perturbation on the other orbits, due to the presence of charged particles on these periodic orbits, does considerably affect the angle η (zenith angle) while scarcely changing the angle θ (angle with the meridian plane). Since, by Liouville's theorem, the intensity of cosmic radiation depends essentially on the shape of the cone of allowed directions (η, θ), it is seen that weak magnetic perturbations may cause relatively large changes in the intensity of cosmic radiation.

This paper arose from discussions with Professor M. S. Vallarta, to whom I wish to express my indebtedness.

O. GODART*

Massachusetts Institute of Technology,
Cambridge, Massachusetts,
December 3, 1938.

* Fellow of the Belgian American Foundation.

[1] H. Poincaré, *Méthodes Nouvelles de la Mécanique Célest*, Vol. 3 (1899) Chap. 26, hereafter referred to as M. N.

[2] E. J. Schremp, Phys. Rev. **54**, 154 (1938).

[3] H. Poincaré, M.N., Vol. 3, p. 156, Sec. 298.

[4] G. Lemaitre and M. S. Vallarta, Phys. Rev. **49**, 719 (1936), to which reference may also be made for other necessary definitions.

[5] H. Poincaré, M.N., Vol. 3, Chap. 22; G. D. Birkhoff, Mem. Pont. Acad. Scient. Novi Lyncaei, Ser. 3, Vol. 1, p. 91.

[6] A preliminary examination of this question has been made by S. Kusaka, S.M. Thesis, M.I.T., 1938.

Delayed Neutron Emission from Uranium

Further measurements have been made on the neutron emission observed by Roberts, Meyer and Wang[1] after uranium is exposed to neutrons. In our experiments these delayed neutrons were produced by irradiating uranium with neutrons from the Be+H reaction in the cyclotron, and detected by a boron ion chamber connected to a linear amplifier-oscillograph system. Measurements with and without cadmium and boron around the uranium during irradiation showed that under these conditions the effect is produced primarily by slow neutrons and approximately follows the $1/v$ law. Decay curves were made by placing 2.5 kg of U_3O_8 inside a paraffin cylinder together with the detection chamber, and observing the boron disintegrations, after the cyclotron was turned off.

Counts per five-second interval on the oscillograph record are shown as ordinates in Fig. 1. The decay curve seems best analyzed into two periods of about 45 seconds and 10–15 seconds.

The ratio of the delayed neutron emission cross section to the uranium fission cross section was also estimated. A smaller U_3O_8 plaque (450 g) was utilized to achieve better geometrical conditions and to minimize neutron absorption. First the number of delayed neutrons from the U_3O_8 plaque, detected by the boron chamber immediately after the irradiation, was measured. For calibration of the detector, a weak Rn−Be neutron source was substituted for the U_3O_8 plaque. If the effective number of neutrons per second per mC from the Rn−Be source was 15,000 the counting system had an over-all efficiency of 1 : 2400 for neutrons emitted from the U_3O_8. The number of fissions per second from a known amount of uranium in a second detection chamber was then determined under the same geometrical conditions. The ratio of the initial number of delayed neutrons per second to the total number of fissions per second produced in the plaque was thus found to be 1 : 60. An independent check on the uranium fission cross section[2] for slow neutrons gave about 3×10^{-24} cm², and the cross section for the delayed neutron emission must therefore be about 0.05×10^{-24} cm².[3]

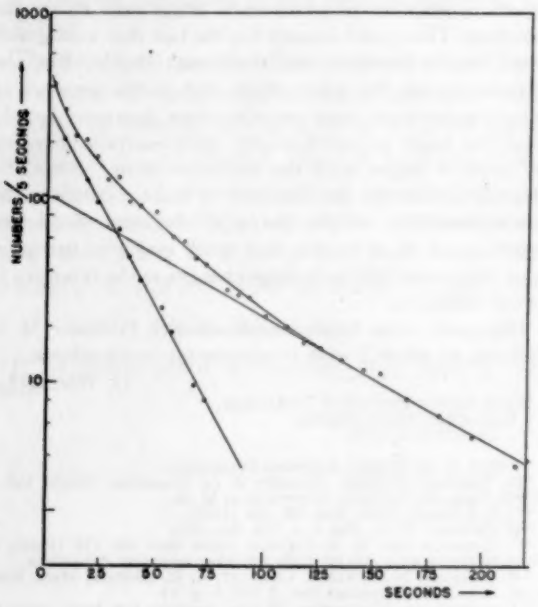

FIG. 1. Decay of delayed neutrons.

The gamma-rays emitted by uranium after neutron irradiation have also been studied. This decay curve can likewise be analyzed into periods of 10–15 seconds,[1] 40–50 seconds, together with some longer periods. Meitner, Hahn and Strassman[4] have reported beta-ray periods from uranium of 10 seconds and 40 seconds.

These observations seem to indicate that some of the fission fragments emit beta-rays with these periods and then are still sufficiently excited for the emission of gamma-ray quanta, or occasional "delayed" neutrons. It must be observed that these delayed neutrons are much less numerous than the neutrons more immediately following fissions as observed by other experimenters.[5, 6, 7]

E. T. BOOTH
J. R. DUNNING
F. G. SLACK

Department of Physics,
Columbia University,
New York, New York,
April 17, 1939.

[1] Roberts, Meyer and Wang, Phys. Rev. **55**, 510 (1939).
[2] Anderson, Booth, Dunning, Fermi, Glasoe and Slack, Phys. Rev. **55**, 511 (1939).
[3] Roberts, Hafstad, Meyer, Wang, Phys. Rev. **55**, 664 (1939).
[4] Meitner, Hahn and Strassmann, Zeits. f. Physik **106**, 249 (1937).
[5] von Halban, Joliot and Kowarski, Nature **143**, 470 (1939).
[6] Anderson, Fermi and Hanstein, Phys. Rev. **55**, 797 (1939).
[7] L. Szilard and W. H. Zinn, Phys. Rev. **55**, 799 (1939).

The Identification of Some of the Products of Uranium Cleavage

In a recent letter to the editor of the *Physical Review*[1] we announced the discovery of a number of antimony, tellurium and iodine isotopes formed through neutron activation of uranium. Among those active bodies was an eight-day iodine activity which was shown to be I^{131}. It was also suggested that a 70-minute tellurium body might be Te^{129}. The suggestion has been shown to be correct, and several other tellurium isotopes have been found which can be identified with known activities. These are shown in Table I.

The identification of the 70-minute body as Te^{129} rests on its half-life and on its beta-ray absorption curve. The absorption curves of the 70-minute bodies obtained by neutron activation of uranium and by deuteron activation of tellurium[2] were taken under identical geometrical conditions. The two curves were parallel over a factor of 100 in intensity. The same method was employed on the ten-hour bodies. Again the beta-ray absorption curves were found to be parallel over a factor of 100 in intensity. The parent of the ten-hour activity was isolated by separating antimony from activated uranium. Periodic tellurium extractions from the antimony showed that the half-life of the parent of the ten-hour body is 80 hours.

TABLE I.

ATOMIC WEIGHT	Sb	Te	I
131		30 hr. → 25 min.	8 days → 8 days
129	4.6 hr. → 82 hr.	70 min. → 10 hr.	
127			

A new piece of evidence confirms the assignment of the eight-day iodine body as I^{131}. It has been found here that the known I^{131} emits characteristic xenon x-rays. The eight-day iodine body produced from uranium likewise emits xenon x-rays.

Seaborg, Livingood and Kennedy[2] have assigned Te^{131} an isomeric pair of activities of which a 30-hour body is the higher state and a 25-minute body is the lower. These two bodies have been produced by neutron activation of uranium and their half-lives established through periodic quantitative iodine extractions from tellurium precipitated out of an activated uranium sample.

In our last communication[1] we made the following assignments of activities:

Te	I
40 min.	→ 54 min.
1 hr.	→ 22 hr.

This assignment, however, was qualified by the statement, "It is barely possible that the 22-hour activity and the 54-minute body are isomers with the 54-minute activity having the higher energy state." Further experiments now show that the 54-minute and the 22-hour bodies are not isomers and that the assignment made above is correct.

A more detailed account of these and previous experiments will be given in a paper which will appear soon. This work has been expedited by suggestions made by Dr. E. Segrè and Dr. G. T. Seaborg. I wish to express my thanks to Professor E. O. Lawrence for his interest in this experiment and to the Research Corporation for financial support.

PHILIP ABELSON

Radiation Laboratory,
University of California,
Berkeley, California,
April 11, 1939.

[1] P. Abelson, Phys. Rev. 55, 670 (1939).
[2] G. T. Seaborg, J. J. Livingood and J. H. Kennedy, Phys. Rev. 55, 794 (1939).

Search for Beta-Particles Emitted During Uranium Fission Process

The large energy release associated with the neutron induced uranium fission process[1] might suggest that very energetic beta-particles could be emitted during or shortly after the disintegration. We have made a search for such particles using two Geiger-Müller counters in a coincidence arrangement placed near 400 g of freshly purified U_3O_8 in which several thousand fissions per minute were being produced by irradiation with paraffin-slowed neutrons from a Ra—Be source. With 1.3 cm of aluminum between the counters no effect was observed; this is in agreement with the recent report by Heyn, Aten and Bakker[2] who found no beta-particles of energy exceeding 10 Mev.

An extension of the above type of experiment to include particles of lower energy would merely reveal the presence of recoil electrons from capture gamma-rays and the beta-particles from the short-lived activities which are known to be present. The possibility of the emission of beta-particles (of lower energies) *simultaneous* with the fission process is still interesting because such emission would lower the neutron excess in the primary products. That this process does not occur during the majority of the fissions is shown in the following experiment. A tube counter of the proportional type with a thin layer of U_3O_8 on the inner wall and an ordinary Geiger-Müller counter were placed side by side near a paraffin-encased neutron source and connected to a circuit designed to count coincidences between the very large "explosion" kicks in the one counter and beta-particles in the other. Extremely few real coincidences were observed; the intensity of the neutron source and the geometry employed were such that we can conclude that in at least 90 percent of the fissions no electrons of energy greater than 1 Mev are emitted within the resolving time of the coincidence circuit (about 10^{-6} sec.). That coincidences could have been counted by this method was proved by using the same circuits to record coincidences between the beta-particles of ThC and the immediately following alpha-particles from ThC' ($T\frac{1}{2}\sim10^{-11}$ sec.).

J. W. KENNEDY
G. T. SEABORG

Department of Chemistry,
University of California,
Berkeley, California,
April 17, 1939.

[1] O. Hahn and F. Strassmann, Naturwiss. 27, 11 (1939) and numerous subsequent reports.
[2] F. A. Heyn, A. H. W. Aten, Jr., and C. J. Bakker, Nature 143, 516 (1939).

Erratum: The Scattering of Alpha-Particles by Argon, Oxygen, and Neon

(Phys. Rev. 54, 1011 (1938))

Dr. M. M. Rogers has kindly called my attention to some errors in calculation of the nuclear radii given in the above paper. The value given for the oxygen nucleus should be $3.5(10^{-13})$ cm instead of $4.5(10^{-13})$ cm, and that given for the neon nucleus (Ne^{20}) should be $4.0(10^{-13})$ cm instead of $4.6(10^{-13})$ cm.

These were calculated from the Gamow penetration formula on the assumption that the penetrability of the barrier was about 10 percent at the lowest energy for which scattering anomalies were observed. The fact that the values obtained for the radii are so far from those to be expected indicates that this method of calculation is probably not valid, at least in the case of scattering at angles small compared to 180°.

GORDON BRUBAKER

Sloane Physics Laboratory,
Yale University,
New Haven, Connecticut,
April 4, 1939.

Nuclear Excitation of Indium with Alpha-Particles

It has been found that indium bombarded with neutrons,[1] protons,[2] or x-rays[3] becomes beta-radioactive and that this activity is due to In^{115*} which forms a metastable state and decays with a half-life period of 4.1 hours.

Barnes and Aradine[2] also tried to produce this excitation with 8.5 Mev alpha-particles but did not observe the 4.1-hour period.

Since we have 16 Mev alpha-particles available from our cyclotron, we have investigated this process again. After bombardment with about 0.03μA for periods of 30 to 90 minutes the 4-hour period was found with either the multiple counter[4] described recently, or a Dow metal counter of 0.004-inch wall thickness.[5] By exposing two identical layers of indium, one behind the other, it was found that the activity is not due to neutrons or x-rays, since only the piece in front directly exposed to the beam becomes active. Traces of antimony and tin were added to a a solution of activated indium and after chemical separation the 4-hour period was found with the indium precipitate. The number of counts is comparable with the intensity reported by other observers for the nuclear excitation process. Samples of indium obtained from Hilger and from the Indium Corporation of America gave the same results: we conclude therefore that impurities cannot be responsible for this activity.

In the Wilson chamber six hours after exposure only soft electrons can be observed. These electrons are absorbed in aluminum of approximately the thickness as reported by others.[6]

Besides the 4-hour period other weak activities of about one hour and a half day have been found which are being investigated now. Also a short period of about 5 minutes (due to a positron-emitter as shown by cloud chamber experiments) has been found. This period goes with the antimony-tin precipitate, and since only stable tin isotopes can be formed, it should be due to antimony.

It seems, therefore, that the nuclear excitation of In^{115} can also be produced by an (α, α) process.

K. Lark-Horovitz
J. R. Risser
R. N. Smith

Purdue University,
Lafayette, Indiana,
April 2, 1939.

[1] Goldhaber, Hill, Szilard, Phys. Rev. **55**, 47 (1939).
[2] Barnes and Aradine, Phys. Rev. **55**, 50 (1939).
[3] Collins, Waldman, Stubblefield, and Goldhaber, Phys. Rev. **55**, 506 (1939).
[4] How and Lark-Horovitz, Phys. Rev. **53**, 334 (1938).
[5] Risser, Phys. Rev. **52**, 768 (1937).
[6] See reference 1, p. 49.

Vibration-Rotation Energies in the Tetrahedrally Symmetric XY_4 Type of Molecule

The complete quantum-mechanical Hamiltonian for the oscillating-rotating XY_4 type molecule has been derived perfectly generally to second order of approximation and may be written $H=H_0+H_1+H_2$. In H_0 are contained the energy of a spherical top, $P/2A_0$, P being the total angular momentum operator and A_0 the equilibrium value of the moment of inertia, and the energies

$$\tfrac{1}{2}\Big[\sum_{i=1}^{3}(p_i^2+4\pi^2\nu_2^2q_i^2)+\sum_{k=4}^{6}(p_k^2+4\pi^2\nu_4^2q_k^2)+\sum_{j=7}^{9}(p_j^2+4\pi^2\nu_3^2q_j^2)+(p_0^2+4\pi^2\nu_1^2q_0^2)\Big]$$

of the molecule oscillating in its nine modes. H_1 contains the first-order centrifugal expansion terms, the potential energy terms cubic in the coordinates, and in particular the Coriolis interaction terms $(p_xP_x+p_yP_y+p_zP_z)/A_0$; the p_α are components along the axes of the molecule of the angular momentum arising from the oscillations and consist essentially of a sum of terms of the type

$$\zeta_{ij}\Big[\Big(\frac{\nu_i}{\nu_j}\Big)^{\frac{1}{2}}q_i\frac{\partial}{\partial q_j}-\Big(\frac{\nu_j}{\nu_i}\Big)^{\frac{1}{2}}q_j\frac{\partial}{\partial q_i}\Big],$$

ζ_{ij} being the modulus of the internal angular momentum vector. For the frequency ν_2, $\zeta_2=0$ and for ν_3 and ν_4 the relation $\zeta_3+\zeta_4=\frac{1}{2}$ is known to hold. H_2 contains the second-order centrifugal expansion terms, second-order Coriolis terms, terms quadratic in p_α and quartic terms of the potential energy. The zeroth-order wave equation is at once soluble and of the terms in H_1 only the Coriolis interaction terms where $\nu_i=\nu_j$ give first-order contributions to the energy. It is therefore convenient to transform H by a contact transformation, SHS^{-1} into $H_0+H_1'+H_2'$, so that to second approximation H_1' contains only the Coriolis interaction terms where $\nu_i=\nu_j$. This transformation facilitates the determination of the second-order energy corrections.

It has been possible to find linear combinations of the zeroth-order eigenfunctions such that the matrix of H_1' will be diagonal, for the states ν_1, ν_2, ν_3, ν_4, $2\nu_3$, $2\nu_4$, $\nu_1+\nu_3$, $\nu_1+\nu_4$, $\nu_2+\nu_3$, $\nu_2+\nu_4$, and $\nu_3+\nu_4$. For the state ν_3 (and ν_4) these combinations were found to be identical with those of Jahn[1] which lead to the eigenvalues of H_1': $-(J-1)\zeta_3\hbar^2/A_0$, $-\zeta_3\hbar^2/A_0$ and $J\zeta_3\hbar^2/A_0$. For the states $\nu_2+\nu_{3,4}$ and $\nu_1+\nu_{3,4}$ the eigenfunctions are respectively products of the functions

$$\Big(\frac{1}{2}\Big)^{\frac{1}{2}}\chi_{\nu_0=0}^{\nu_0=1}\pm\chi_{\nu_0=1}^{\nu_0=0}$$

and $\varphi(\nu_0=1)$ times the eigenfunctions of ν_3 and ν_4 and lead to the same eigenvalues of H_1'. The selection rules for J are the same as those found by earlier investigators.

For $\nu_3+\nu_4$ wave functions have been derived which give the matrix of H_1' as a step matrix, consisting of two single steps, two double steps and one triple step. The eigenvalues for this case are

$$J(\zeta_3+\zeta_4)(\hbar^2/A_0),\quad -(J-1)(\zeta_3+\zeta_4)(\hbar^2/A_0),$$
$$\tfrac{1}{2}\{(J-1)(\zeta_3+\zeta_4)\pm[(J+1)^2(\zeta_3-\zeta_4)^2+4\zeta_3\zeta_4]^{\frac{1}{2}}\}\hbar^2/A_0,$$
$$-\tfrac{1}{2}\{(J-2)(\zeta_3+\zeta_4)\pm[J^2(\zeta_3-\zeta_4)^2+4\zeta_3\zeta_4]^{\frac{1}{2}}\}\hbar^2/A_0$$

and those given by the cubic equation

$$0=\epsilon^3+2(\zeta_3+\zeta_4)\epsilon^2+[\tfrac{3}{4}(\zeta_3+\zeta_4)^2-(J^2-J-\tfrac{1}{4})(\zeta_3-\zeta_4)^2]\times\epsilon-J(J+1)(\zeta_3+\zeta_4)(\zeta_3-\zeta_4)^2$$

where $E^1=\epsilon\hbar^2/A_0$ and $\hbar=h/2\pi$. The selection rules are

$\Delta J = \pm 1, 0$ except for transitions from the ground state to the first two of the above eigenvalues where the selection rules are $\Delta J = -1,0$ and $\Delta J = -1,0$, respectively. This state of affairs seems to be more complicated than envisaged by other workers.[2]

The state $2\nu_3$ (and $2\nu_4$) has been investigated in the same manner and eigenfunctions have been obtained for H_1' which lead to the eigenvalues 0, $2J\zeta_3\hbar^2/A_0$, $(J-2)\zeta_3\hbar^2/A_0$, $-3\zeta_3\hbar^2/A_0$, $-(J+3)\zeta_3\hbar^2/A_0$ and $-2(J+1)\zeta_3\hbar^2/A_0$.

From these eigenfunctions the corrections to the rotation-vibration energy levels arising from H_3' have been evaluated for these states. A splitting up of the rotation levels was found quite generally. The term studied by Jahn is found to be important not only for ν_4, but for all overtone and combination bands of ν_4.

Complete details of these calculations and the values of the vibration-rotation energy levels and their dependence upon the potential energy constants will be published in this journal in the near future.

W. H. SHAFFER
H. H. NIELSEN
L. H. THOMAS

Mendenhall Laboratory of Physics,
The Ohio State University,
Columbus, Ohio,
April 6, 1939.

[1] H. A. Jahn, Proc. Roy. Soc. **A168**, 469 (1938).
[2] M. Johnston and D. M. Dennison, Phys. Rev. **48**, 868 (1935).

Progressive Breakdown in a Conducting Liquid

The impulsive electrical discharge through liquids has been investigated quite extensively.[1] In most of this work liquids with good insulating properties were studied, which necessitated the use either of small gap spacings or of high voltage. Under these conditions the actual breakdown process takes place in a very short time interval. Consequently, apparatus of high time-resolving power must be used to follow the various stages in the discharge. It is the purpose of this note to report some observations on a comparatively slow type of liquid breakdown.

The discharge takes place between Cu electrodes under the surface of a $CuSO_4$ solution contained in a special cell fitted with a viewing window. The high voltage electrode is conical, with the end rounded (about $\frac{1}{4}$ mm radius of curvature), and is mounted coaxially at a distance of 9 mm from the flat end of a 5-mm diameter rod, which serves as the grounded electrode. The low potential resistance of the solution between electrodes is 70 ohms. Impulsive voltage is applied to the gap from a 0.5 mf condenser through a series resistance of 75 ohms. The maximum voltage across the gap is 9.1 kv.

With the electrodes separated to such a distance that complete breakdown across the gap does not occur, luminosity appears at the conical electrode regardless of polarity. This is to be expected because of the high current density and high field at the point. Fig. 1a shows an ordinary photograph of this case with the point positive. The resemblance to electrical figures observed under insulating liquids is quite marked.[2] There is no noticeable

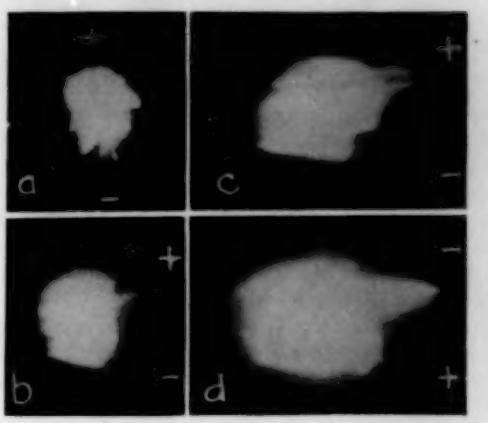

FIG. 1 (a) Stationary photograph of figure (point +); (b) rotating mirror photograph of complete discharge, point +; (c) same as (b) showing stepped progression; (d) rotating mirror photograph (point −).

difference in appearance between the positive and negative figures. It is well known that electrical figures in general have a rather definite rate of expansion under constant conditions.[3] Consequently, it would be expected that the formation of an ionized path between electrodes would be due to the extension of a figure of the type shown in Fig. 1a from the point to the plane electrode. Rotating mirror photographs show this to be the case.

Figure 1b is such a photograph with the point positive. The luminosity starts at the point and moves towards the grounded electrode at a rather constant rate (5.3×10^4 cm/sec.). After an ionized path bridges the gap, the luminosity increases suddenly. Fig. 1c shows a stepped type of extension with the same polarity (average speed 2.3×10^4 cm/sec.). This "stepping" is probably connected with the current and voltage limitation introduced by the supply circuit.

Figure 1d is a photograph with point negative. The speed of progression is 2.9×10^4 cm/sec. The average speed was found to depend upon the voltage applied to the gap for both positive and negative points.

The order of the various stages in this type of breakdown is the same as that observed in long sparks, surface discharges on liquids, and in long discharge tubes. The initial leader stroke (adapting Schonland's terminology) would normally be followed by a return stroke discharging the leader channel and this, in turn, followed by the discharge of the circuit as a whole. The return stroke is unresolved in these photographs, but the damped discharge of the circuit as a unit accounts for the great increase in luminosity after the leader has reached the grounded electrode.

L. B. SNODDY
J. W. BEAMS

Rouss Physical Laboratory,
University of Virginia,
Charlottesville, Virginia,
April 11, 1939.

[1] Nikuradse, *Das flüssige Dielektrikum* (J. Springer, 1934). Washburn, Physics **4**, 29 (1933).
[2] Pribram, Physik. Zeits. **32**, 481 (1931).
[3] Toepler, Ann. d. Physik **21**, 193 (1906). Pedersen, Ann. d. Physik **69**, 205 (1922).

Radioactive Halogens Produced by the Neutron Bombardment of Uranium and Thorium

We have looked for radioactive iodine in uranium and thorium after bombardment by deuteron-deuteron neutrons. Under the conditions of our experiments we did not find the iodine of 2.5-hour half-life recently reported[1] as a product of the uranium fission. However, the results indicate two radioactive iodine isotopes, of half-lives about 45 minutes and 12 hours, respectively, from both uranium and thorium, and also a radioactive bromine of about 40-minutes half-life from uranium.

Uranium in the form of uranium nitrate or ammonium uranate was irradiated with neutrons, with paraffin surrounding the uranium but not between the uranium and the neutron source. After two-hour irradiation the uranium salt was dissolved in dilute nitric acid, a small amount of iodine added and extracted with carbon tetrachloride. After thorough washing, the extracts were reduced with bisulfite and the iodide precipitated as silver iodide. This precipitate showed an activity the logarithmic decay curve of which fell rapidly at the start, then flattened out into a straight line of slope corresponding to about a 12-hour half-life. Analysis of the curve indicated that the initial rapid fall was due to a substance of about 45-minute half-life. In another experiment the iodide solution was divided into halves, one of which was precipitated immediately, the other standing for five hours. Small amounts of cesium, barium, and lanthanum nitrates were added to the second portion, a rapid stream of argon bubbled through for five minutes, and the iodide then precipitated with silver nitrate. The activity of the second precipitate agreed with the first to about 10 percent, and both decayed with a 12-hour half-life. We believe this to show that the long-lived substance is an iodine, and not the daughter of the 45-minute substance. It is to be observed that an I^{130} of 13-hour half-life has been reported.[2]

It has been shown[3] that the minute amounts of radioactive substance produced in artificial disintegrations behave in distribution processes quantitatively the same as if accompanied by larger amounts of "carrier." Thus the chemical behavior of the activities reported above did not exclude bromine, or even chlorine. To investigate these possibilities we added bromide to the iodide solution, separated the iodide by nitrite oxidation and extraction, then the bromide by permanganate oxidation and extraction. The iodide precipitate gave the composite decay curve previously obtained, the bromide precipitate was feebly active. When this experiment was repeated with bromine carrier in the initial extraction from the uranium solution the bromide precipitate showed a strong activity decaying with a 40-minute half-life; no longer-lived substance was found. The iodide precipitate was only feebly active, which we attribute to oxidation of the iodine by bromine to iodate which would not be extracted. When a small amount of iodate was added to the uranium solution after the bromine extraction, reduced, oxidized to iodine and extracted, the iodide gave the composite decay curve previously obtained. We believe that the completeness of the chemical separations precludes the possibility that the bromide activity was iodine contamination, likewise that the 45-minute iodine could be bromine contamination.

Similar, but less complete experiments have been performed with thorium. As in the case of uranium, two iodines, chemically separable from bromine were found. We do not have good evidence for a bromine from thorium, but it is not excluded by our results.

The activities obtained from the uranium when 100 to 400 g portions of uranium nitrate were irradiated were of the order of several thousand counts per minute. Comparable amounts of thorium gave activities of a few hundred counts per minute. Control experiments on unirradiated uranium and thorium gave zero activity in the halide precipitates.

Apparatus used in this research was constructed with the aid of a grant from the Research Corporation.

R. W. Dodson
R. D. Fowler

Chemical Laboratory,
The Johns Hopkins University,
Baltimore, Maryland,
April 3, 1939.

[1] P. Abelson, Phys. Rev. **55**, 418 (1939).
[2] J. J. Livingood and G. T. Seaborg, Phys. Rev. **54**, 775 (1938).
[3] D. C. Grahame and G. T. Seaborg, J. Am. Chem. Soc. **60**, 2524 (1938).

The Dispersion of Water for Electromagnetic Waves

Up to the present time no conclusive evidence of dispersion of water for electric waves has been found by observers in the region of wave-lengths of 50 to 100 cm or more. Drake, Pierce and Dow[1] working in the region from $\lambda = 391.8$ to 2547 cm found the refractive index to be 8.925 for water of low conductivity at 22°C. Other observers working in the same region found values of refractive index which were in good agreement. No definite dispersion was observed. Some observers working in the region below 50 cm have found a variation of the index of refraction of water with wave-length. However, Knerr[2] points out that the lack of precision in the methods used by these observers does not allow definite conclusions to be drawn about the dispersion in this region. From his own observations, Knerr quotes a value for the refractive index of 8.80 for water at 22°C with no conclusive evidence of dispersion in the region of $\lambda = 6.48$ to 20.44 cm.

The refractive index of water has been investigated using the method of standing waves inside a copper pipe with a concentrically placed wire. Actual dispersion of water was detected from wave-lengths of a meter to one-half meter by making simultaneous observations of waves of the first and second harmonics of a continuous wave oscillator. It was observed that with air in the pipe the two waves traveled with the same velocity since it was impossible to resolve the nodes of the standing waves; while with water in the pipe the wave of the second harmonic traveled with a velocity greater than that of the first. After the tenth node it was found that the positions of the nodes of standing waves could be separated, and actual measurements of wave-length were made for each harmonic. The observed values are: for $\lambda = 52.84$ cm, $n = 8.799$ and for

$\lambda = 105.68$ cm, $n = 8.839$, for water having a conductivity of 0.3×10^7 e.s.u. at 25°C. The probable error, calculated on the basis of deviations from the mean, was less than 0.01 percent in measuring wave-length in air and less than 0.04 percent in measuring wave-length in water. This is a variation of about (0.45 ± 0.07) percent and appears as conclusive evidence of dispersion in this region.

LESTER L. SKOLIL

The Brace Laboratory of Physics,
University of Nebraska,
Lincoln, Nebraska,
April 14, 1939.

[1] Drake, Pierce and Dow, Phys. Rev. **35**, 613 (1930).
[2] Henry W. Knerr, Phys. Rev. **52**, 1054 (1937).

Decay of Willemite and Zinc Sulphide Phosphors

The question has recently been raised[1] whether the luminescence of willemite (zinc orthosilicate) decays according to a bimolecular law, and indirect evidence from the shape of the curve of light output *vs.* current density during continuous electron bombardment has been cited in favor of this view. On this basis it has been suggested that the mechanism of decay in willemite is similar to that in zinc sulphide phosphors, and different from that in thallium-activated alkali halides, which show exponential decay characteristics. One purpose of this note is to call attention to direct measurements[2] of the phosphorescence of a sample of willemite after electron bombardment which show that the decay during the first 1/10 sec. is almost strictly exponential, and that the rate is independent of the current density, the electron energy, and the intervals of excitation and decay. Zinc sulphides, contrastingly, show under the same conditions a marked dependence of initial decay rate on current density.

Decay rates of these same samples and of several other typical phosphors, after excitation by ultraviolet light, have recently been measured The findings, summarized in Table I, again indicate that the silicates are in a different class from the sulphides. This difference also appears in the oscillographic curves of Schleede and Bartels.[3] The results with willemite are in accord with those of Fonda[4] in this laboratory. Fonda found, in fact, that the exponential decay rate is unchanged when the phosphor is taken to liquid-air temperature. The exponential decay is found only with "normal" willemites, synthesized for nearly optimum response to ultraviolet excitation. Willemites having high Mn content, or incompletely reacted, show anomalous decay characteristics. We have never found a sample with so abrupt an initial decay as Beese[5] reports.

In the later stages of decay of willemite the brightness declines at a much slower rate. The relative prominence of this long-lived component, unlike the rate of the initial exponential decay, varies markedly from sample to sample.

R. P. JOHNSON

Research Laboratory,
General Electric Company,
Schenectady, New York,
April 6, 1939.

[1] E. G. Ramberg and G. A. Morton, Phys. Rev. **55**, 409L (1939).
[2] R. B. Nelson and R. P. Johnson, Abstract No. 11, Washington Meeting Am. Phys. Society, Dec. 1938. An account of these experiments has been accepted for publication in the *Journal of Applied Physics*.
[3] A. Schleede and B. Bartels, Zeits. f. tech. Physik **19**, 364 (1938).
[4] G. R. Fonda, paper to appear in *Journal of Applied Physics*.
[5] N. C. Beese, J. Opt. Soc. Am. **29**, 26 (1939).

Remarks on the Anomalous Damping of Ultrasonic Waves

Recent experiments[1] have established the fact that the damping constant of ultrasonic waves in light gases exceeds the theoretical value by several hundred to two thousand percent. This anomalous effect seems to be independent of the intensity of the sound wave and occurs with equal order of magnitude also in purified He. There does not seem to exist a reasonable theoretical explanation for it.

The fact that the anomaly occurs in helium and is independent of the intensity eliminates attempts to ascribe it to turbulence phenomena or to conditions which are related to the molecular structure of the gas. We feel compelled to look for its cause in a universal phenomenon which can be present in all gases and are unable to picture any other cause but fluctuations in the gas.

It is obvious that such fluctuations would produce an additional absorption. It may perhaps be thought that such an effect would be hopelessly small since we know from the case of light that the opalescence in ideal gases is

TABLE I. *Decay characteristics of various phosphors.*

Phosphor	Luminescent color	Exciting agent	Decay law	Time constant (sec.)
$2ZnO \cdot SiO_2 \cdot Mn$ (Willemite)	Green	Electron beam	~Exponential	$\sim 13 \times 10^{-3}$
$2ZnO \cdot SiO_2 \cdot Mn$ (Willemite)	Green	Ne 740A	~Exponential	$\sim 13 \times 10^{-3}$
$2ZnO \cdot SiO_2 \cdot Mn$ (Willemite)	Green	Hg 2537A	~Exponential	$\sim 13 \times 10^{-3}$
Zinc-beryllium silicate	Yellow	Hg 2537A	~Exponential	$\sim 9 \times 10^{-3}$
Zinc-beryllium silicate	Pink	Hg 2537A	~Exponential	$\sim 7 \times 10^{-3}$
Cadmium silicate	Pink	Hg 2537A	~Exponential	$\sim 30 \times 10^{-3}$
Soda-lime glass	Yellow	Hg 2537A	~Exponential	$\sim 7 \times 10^{-3}$
ZnS·Ag	Blue	Electron beam	$L = \frac{a}{b+t}$	—
ZnS·Ag	Blue	Hg 2537A	$L = \frac{a}{b+t}$	—
ZnS·CdS·Ag	Yellow	Electron beam	$L = \frac{c}{(d+t)^2}$	—
ZnS·CdS·Ag	Yellow	Hg 2537A	$L = \frac{c}{(d+t)^2}$	—

scarcely observable and following a λ^{-4} law it should even be large compared with an acoustical effect on account of the large wave-length in this latter case. A closer study of the equation of hydrodynamics teaches on the other hand that the main effect is proportional to the *gradient* of the density-fluctuation and that the whole treatment has to be fundamentally modified because the "speed of fluctuation" is, in general, large compared with the sound frequency. Both effects tend to increase the absorption enormously. The appearance of the gradient alone adds a factor probably exceeding 10^8. The absence of the effect of the dielectric constant also adds a factor of approximately one million while the influence of the time-dependence of fluctuation cannot be estimated quite as easily but is seen to be large and acting in the right direction. The author intends to supplement these deliberations by a quantitative treatment.

O. HALPERN

Physics Department,
New York University,
University Heights, New York,
March 6, 1939.

[1] Cf., e.g., A. van Itterbeek and L. Thijs, Physica 5, 889 (1938).